GEOTECHNICAL SPECIAL PUBLICATION NO. 195

Performance Modeling and Evaluation of Pavement Systems and Materials

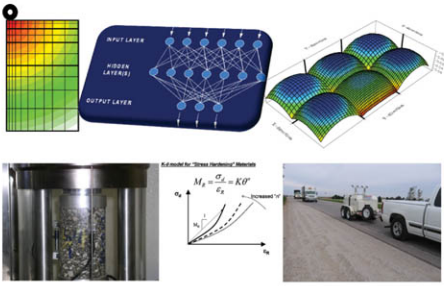

Edited by
Halil Ceylan
Kasthurirangan Gopalakrishnan
Xueyan Liu
Likui Huang

ASCE
GEO INSTITUTE

GEOTECHNICAL SPECIAL PUBLICATION NO. 195

PERFORMANCE MODELING AND EVALUATION OF PAVEMENT SYSTEMS AND MATERIALS

SELECTED PAPERS FROM THE 2009 GEOHUNAN INTERNATIONAL CONFERENCE

August 3–6, 2009
Changsha, Hunan, China

HOSTED BY
Changsha University of Science and Technology, China

CO-SPONSORED BY
ASCE Geo-Institute, USA
Asphalt Institute, USA
Central South University, China
Chinese Society of Pavement Engineering, Taiwan
Chongqing Jiaotong University, China
Deep Foundation Institute, USA
Federal Highway Administration, USA
Hunan University, China
International Society for Asphalt Pavements, USA
Jiangsu Transportation Research Institute, China
Korea Institute of Construction Technology, Korea
Korean Society of Road Engineers, Korea
Texas Department of Transportation, USA
Texas Transportation Institute, USA
Transportation Research Board (TRB), USA

EDITED BY
Halil Ceylan, Ph.D.
Xueyan Liu, Ph.D.
Kasthurirangan Gopalakrishnan, Ph.D.
Likui Huang

Published by the American Society of Civil Engineers

Library of Congress Cataloging-in-Publication Data

Performance modeling and evaluation of pavement systems and materials : selected papers from the 2009 GeoHunan International Conference, August 3-6, 2009, Changsha, Hunan, China / hosted by Changsha University of Science and Technology, China ; co-sponsored by ASCE Geo-Institute, USA … [et al.] ; edited by Halil Ceylan … [et al.].
p. cm. -- (Geotechnical special publication ; no. 195)
Includes bibliographical references and indexes.
ISBN 978-0-7844-1047-9
1. Pavements, Asphalt concrete--Design and construction--Evaluation--Congresses. 2. Pavements, Concrete--Design and construction--Evaluation--Congresses. I. Ceylan, Halil. II. Changsha li gong da xue. III. American Society of Civil Engineers. Geo-Institute. IV. GeoHunan International Conference on Challenges and Recent Advancements in Pavement Technologies and Transportation Geotechnics (2009 : Changsha, Hunan Sheng, China)

TE278.P447 2009
625.8--dc22 2009022665

American Society of Civil Engineers
1801 Alexander Bell Drive
Reston, Virginia, 20191-4400

www.pubs.asce.org

Any statements expressed in these materials are those of the individual authors and do not necessarily represent the views of ASCE, which takes no responsibility for any statement made herein. No reference made in this publication to any specific method, product, process, or service constitutes or implies an endorsement, recommendation, or warranty thereof by ASCE. The materials are for general information only and do not represent a standard of ASCE, nor are they intended as a reference in purchase specifications, contracts, regulations, statutes, or any other legal document. ASCE makes no representation or warranty of any kind, whether express or implied, concerning the accuracy, completeness, suitability, or utility of any information, apparatus, product, or process discussed in this publication, and assumes no liability therefore. This information should not be used without first securing competent advice with respect to its suitability for any general or specific application. Anyone utilizing this information assumes all liability arising from such use, including but not limited to infringement of any patent or patents.

ASCE and American Society of Civil Engineers—Registered in U.S. Patent and Trademark Office.

Photocopies and reprints.
You can obtain instant permission to photocopy ASCE publications by using ASCE's online permission service (http://pubs.asce.org/permissions/requests/). Requests for 100 copies or more should be submitted to the Reprints Department, Publications Division, ASCE, (address above); email: permissions@asce.org. A reprint order form can be found at http://pubs.asce.org/support/reprints/.

Copyright © 2009 by the American Society of Civil Engineers. All Rights Reserved.
ISBN 978-0-7844-1047-9 Manufactured in the United States of America.

Geotechnical Special Publications

1 *Terzaghi Lectures*
2 *Geotechnical Aspects of Stiff and Hard Clays*
3 *Landslide Dams: Processes, Risk, and Mitigation*
7 *Timber Bulkheads*
9 *Foundations & Excavations in Decomposed Rock of the Piedmont Province*
11 *Dynamic Response of Pile Foundations - Experiment, Analysis and Observation*
14 *Geotechnical Aspects of Karst Terrains*
15 *Measured Performance Shallow Foundations*
16 *Special Topics in Foundations*
17 *Soil Properties Evaluation from Centrifugal Models*
18 *Geosynthetics for Soil Improvement*
19 *Mine Induced Subsidence: Effects on Engineered Structures*
21 *Hydraulic Fill Structures*
22 *Foundation Engineering*
23 *Predicted and Observed Axial Behavior of Piles*
24 *Resilient Moduli of Soils: Laboratory Conditions*
25 *Design and Performance of Earth Retaining Structures*
27 *Geotechnical Engineering Congress*
28 *Detection of and Construction at the Soil/Rock Interface*
29 *Recent Advances in Instrumentation, Data Acquisition and Testing in Soil Dynamics*
32 *Embankment of Dams - James L. Sherard Contributions*
33 *Excavation and Support for the Urban Infrastructure*
34 *Piles Under Dynamic Loads*
35 *Geotechnical Practice in Dam Rehabilitation*
37 *Advances in Site Characterization: Data Acquisition, Data Management and Data Interpretation*
39 *Unsaturated Soils*
40 *Vertical and Horizontal Deformations of Foundations and Embankments*
41 *Predicted and Measured Behavior of Five Spread Footings on Sand*
42 *Serviceability of Earth Retaining Structures*
43 *Fracture Mechanics Applied to Geotechnical Engineering*
44 *Ground Failures Under Seismic Conditions*
45 *In Situ Deep Soil Improvement*
46 *Geoenvironment 2000*
47 *Geo-Environmental Issues Facing the Americas*
48 *Soil Suction Applications in Geotechnical Engineering*
49 *Soil Improvement for Earthquake Hazard Mitigation*
50 *Foundation Upgrading and Repair for Infrastructure Improvement*
51 *Performance of Deep Foundations Under Seismic Loading*
52 *Landslides Under Static and Dynamic Conditions - Analysis, Monitoring, and Mitigation*
53 *Landfill Closures - Environmental Protection and Land Recovery*
54 *Earthquake Design and Performance of Solid Waste Landfills*
55 *Earthquake-Induced Movements and Seismic Remediation of Existing Foundations and Abutments*
56 *Static and Dynamic Properties of Gravelly Soils*
57 *Verification of Geotechnical Grouting*
58 *Uncertainty in the Geologic Environment*
59 *Engineered Contaminated Soils and Interaction of Soil Geomembranes*
60 *Analysis and Design of Retaining Structures Against Earthquakes*
61 *Measuring and Modeling Time Dependent Soil Behavior*
62 *Case Histories of Geophysics Applied to Civil Engineering and Public Policy*
63 *Design with Residual Materials: Geotechnical and Construction Considerations*
64 *Observation and Modeling in Numerical Analysis and Model Tests in Dynamic Soil-Structure Interaction Problems*
65 *Dredging and Management of Dredged Material*
66 *Grouting: Compaction, Remediation and Testing*
67 *Spatial Analysis in Soil Dynamics and Earthquake Engineering*
68 *Unsaturated Soil Engineering Practice*
69 *Ground Improvement, Ground Reinforcement, Ground Treatment: Developments 1987-1997*
70 *Seismic Analysis and Design for Soil-Pile-Structure Interactions*
71 *In Situ Remediation of the Geoenvironment*
72 *Degradation of Natural Building Stone*
73 *Innovative Design and Construction for Foundations and Substructures Subject to Freezing and Frost*

74 *Guidelines of Engineering Practice for Braced and Tied-Back Excavations*
75 *Geotechnical Earthquake Engineering and Soil Dynamics III*
76 *Geosynthetics in Foundation Reinforcement and Erosion Control Systems*
77 *Stability of Natural Slopes in the Coastal Plain*
78 *Filtration and Drainage in Geotechnical/Geoenvironmental Engineering*
79 *Recycled Materials in Geotechnical Applications*
80 *Grouts and Grouting: A Potpourri of Projects*
81 *Soil Improvement for Big Digs*
82 *Risk-Based Corrective Action and Brownfields Restorations*
83 *Design and Construction of Earth Retaining Systems*
84 *Effects of Construction on Structures*
85 *Application of Geotechnical Principles in Pavement Engineering*
86 *Big Digs Around the World*
87 *Jacked Tunnel Design and Construction*
88 *Analysis, Design, Construction, and Testing of Deep Foundations*
89 *Recent Advances in the Characterization of Transportation Geo-Materials*
90 *Geo-Engineering for Underground Facilities*
91 *Special Geotechnical Testing: Central Artery/Tunnel Project in Boston, Massachusetts*
94 *Performance Confirmation of Constructed Geotechnical Facilities*
95 *Soil-Cement and Other Construction Practices in Geotechnical Engineering*
96 *Numerical Methods in Geotechnical Engineering: Recent Developments*
97 *Innovations and Applications in Geotechnical Site Characterization*
98 *Pavement Subgrade, Unbound Materials, and Nondestructive Testing*
99 *Advances in Unsaturated Geotechnics*
100 *New Technological and Design Developments in Deep Foundations*
101 *Slope Stability 2000*
102 *Trends in Rock Mechanics*
103 *Advances in Transportation and Geoenvironmental Systems Using Geosynthetics*
104 *Advances in Grouting and Ground Modification*
105 *Environmental Geotechnics*
106 *Geotechnical Measurements: Lab & Field*
107 *Soil Dynamics and Liquefaction 2000*
108 *Use of Geophysical Methods in Construction*
109 *Educational Issues in Geotechnical Engineering*
110 *Computer Simulation of Earthquake Effects*
111 *Judgment and Innovation: The Heritage and Future of the Geotechnical Engineering Profession*
112 *Soft Ground Technology*
113 *Foundations and Ground Improvement*
114 *Soils Magic*
115 *Expansive Clay Soils and Vegetative Influence on Shallow Foundations*
116 *Deep Foundations 2002: An International Perspective on Theory, Design, Construction, and Performance*
117 *Discrete Element Methods: Numerical Modeling of Discontinua*
118 *A History of Progress: Selected U.S. Papers in Geotechnical Engineering*
119 *Soil Behavior and Soft Ground Construction*
120 *Grouting and Ground Treatment*
121 *Probabilistic Site Characterization at the National Geotechnical Experimentation Sites*
122 *Sinkholes and the Engineering and Environmental Impacts of Karst*
123 *Recent Advances in Materials Characterization and Modeling of Pavement Systems*
124 *GeoSupport 2004: Drilled Shafts, Micropiling, Deep Mixing, Remedial and Specialty Foundation Systems*
125 *Current Practices and Future Trends in Deep Foundations*
126 *Geotechnical Engineering for Transportation Projects*
127 *Recycled Materials in Geotechnics*
128 *Soil Constitutive Models: Evaluation, Selection, and Calibration*
129 *Advances in Designing and Testing Deep Foundations*
130 *Advances in Pavement Engineering*
131 *Contemporary Issues in Foundation Engineering*
132 *Advances in Deep Foundations: In Memory of Michael W. O'Neill*
133 *Earthquake Engineering and Soil Dynamics*
134 *Soil Dynamics Symposium in Honor of Professor Richard D. Woods*
135 *Erosion of Soils and Scour of Foundations*

136 *Innovations in Grouting and Soil Improvement*
137 *Legal and Liability Issues in Geotechnical Engineering*
138 *Site Characterization and Modeling*
139 *Calibration of Constitutive Models*
140 *Slopes and Retaining Structures under Seismic and Static Conditions*
141 *International Perspectives on Soil Reinforcement Applications*
142 *Waste Containment and Remediation*
143 *Geomechanics: Testing, Modeling, and Simulation*
144 *Sinkholes and the Engineering and Environmental Impacts of Karst*
145 *Seismic Performance and Simulation of Pile Foundations in Liquefied and Laterally Spreading Ground*
146 *Asphalt Concrete: Simulation, Modeling and Experimental Characterization*
147 *Unsaturated Soils 2006*
148 *Advances in Unsaturated Soil, Seepage, and Environmental Geotechnics*
149 *Site and Geomaterial Characterization*
150 *Soil and Rock Behavior and Modeling*
151 *Advances in Earth Structures: Research to Practice*
152 *Ground Modification and Seismic Mitigation*
153 *Foundation Analysis and Design: Innovative Methods*
154 *Pavement Mechanics and Performance*
155 *Underground Construction and Ground Movement*
156 *Geomechanics II: Testing, Modeling, and Simulation*
157 *Computer Applications in Geotechnical Engineering*
158 *Contemporary Issues in Deep Foundations*
159 *Case Studies in Earth Retaining Structures*
160 *Dynamic Response and Soil Properties*
161 *Embankments, Dams, and Slopes: Lessons from the New Orleans Levee Failures and Other Issues*
162 *Problematic Soils and Rocks and In Situ Characterization*
163 *Geoenvironmental Engineering*
164 *Innovative Applications of Geophysics in Civil Engineering*
165 *Geosynthetics in Reinforcement and Hydraulic Applications*
166 *Educational Activities in Geotechnical Engineering*
167 *Geotechnics of Soil Erosion*
168 *Grouting for Ground Improvement: Innovative Concepts and Applications*
169 *Soil and Material Inputs for Mechanistic-Empirical Pavement Design*
170 *Probabilistic Applications in Geotechnical Engineering*
171 *Advances in Shallow Foundations*
172 *Soil Improvement*
173 *Advances in Measurement and Modeling of Soil Behavior*
174 *Designing Our Underground Space*
175 *Field Measurements in Geomechanics 2007*
176 *Analysis of Asphalt Pavement Materials and Systems: Emerging Methods*
177 *GeoCongress 2008: Geotechnics of Waste Management and Remediation*
178 *GeoCongress 2008: Geosustainability and Geohazard Mitigation*
179 *GeoCongress 2008: Characterization, Monitoring, and Modeling of GeoSystems*
180 *From Research to Practice in Geotechnical Engineering*
181 *Geotechnical Earthquake Engineering and Soil Dynamics IV*
182 *Pavements and Materials: Characterization, Modeling, and Simulation*
183 *Sinkholes and the Engineering and Environmental Impacts of Karst*
184 *Pavements and Materials: Modeling, Testing, and Performance*
185 *Contemporary Topics in Deep Foundations*
186 *Contemporary Topics in In-Situ Testing, Analysis, and Reliability of Foundations*
187 *Contemporary Topics in Ground Modification, Problem Soils, and Geo-Support*
188 *Advances in Ground Improvement: Research to Practice in USA and China*
189 *Characterization, Modeling, and Performance of Geomaterials*
190 *Asphalt Material Characterization, Accelerated Testing, and Highway Management*
191 *Road Pavement Material Characterization and Rehabilitation*
192 *Recent Advancement in Soil Behavior, In Situ Test Methods, Pile Foundations, and Tunneling*
193 *Material, Design, Construction, Maintenance, and Testing of Pavement*
194 *Soils and Rock Instrumentation, Behavior, and Modeling*

This page intentionally left blank

Preface

The papers contained in this Geotechnical Special Publication (GSP) entitled, Performance Modeling and Evaluation of Pavement Systems and Materials, cover research topics in the areas of hot-mix asphalt constitutive modeling, pavement responses under dynamic loading, moisture damage and permanent deformation in asphalt concrete, asphalt and Portland cement concrete evaluation, and pavement performance assessment. Analysis approaches include three-dimensional finite element modeling techniques, matter element modeling, Fuzzy complex matter element modeling, neural networks, Grey theory, and similarity analysis. Relationship between the loading surface and conductivity of smart asphalt concrete, analysis of crack resisting mechanism in asphalt macadam base, cohesive crack model based on bounding surface concept for asphalt concrete, mix design of pervious recycled concrete, development of a large algebraic solver for structural mechanics, etc. are also discussed. Infrastructure engineers working within transportation and geotechnical facilities with special interest in pavement constitutive modeling, performance and evaluation will find this publication of particular interest.

This page intentionally left blank

Contents

Pavement Performance Modeling and Evaluation

Review of the Back-Propagation Neural Network Method as a Basis for Pavement Performance Assessment **1**
Ming Li, Chao Lan, Hai-rui Mu, and Jun-min Song

Evaluation of PCCP Performance Based on Fuzzy Complex Matter Element Method **9**
Xiaoge Tian, Du Lin, and Wenbiao Wu

Asphalt Pavement Evaluation Based on Matter Element Model **18**
Kezhen Yan, Jinzhao Zhang, JianLiang Wu, and Luocheng Wu

Correlations among Pavement Surface Roughness, Moving Dynamic Vehicle Loads, and Concrete Pavement Performance **25**
Seong-Min Kim, Suk-Keun Rhee, Hee Beom Park, and Dong Ju Yun

Weights Comparison of Pavement Surface Distress Index in China and the US **32**
Ziping Chiang, Chine-Ta Chen, Po-Hsun Sung, and Jyh-Dong Lin

Studies on Risk Management of the Urban Infrastructure Projects Based on the BOT Financing Model **39**
Hanli Chen and Tao Qin

Analyzing the Cause of Asphalt Pavement Rut Damage of Heng-Zao Freeway **47**
Renjie Qin, Yuzhi Li, and Zhenke Li

Study on the Method to Calculate Rutting of Asphalt Pavement Based on the Dynamic Load Coupled between the Road and Vehicle **55**
Zhaoyi He, Zhaofeng Lu, and Hongxing Chen

Calibration of Roughness Measuring Instrument for Adopting the Performance Warranty System **62**
Deok-Soon An, Jeong-Hee Nam, and Soo-Ahn Kwon

Pavement Systems Modeling

Similarity Analysis of Rutting Test for Asphalt Pavement Based on Similarity Theory **68**
Zejiao Dong, Xiaoliang Cheng, Hao Zheng, and Yiqiu Tan

Three Integral Constant Determination Methods and Their Applications to Subgrade Settlement Grey Prediction Model **74**
Jian-san Zhao, Li-min Tang, Deng-pan Zhang, and Ping-ying Tang

Temperature Prediction Model for Flexible Pavements in Taiwan **82**
Chi-Chou Liao, Bo-Ruei Chen, Shun-Hsing Chen, and Wei-Hsing Huang

Parallel Direct Solver for Linear Systems Resulting from Constitutive Modeling of Pavement **90**
T. B. Jönsthövel, X. Liu, A. Scarpas, and C. Vuik

Dynamic Responses Model of Asphalt Pavement under Complex Vehicle Loads 96
Guoping Qian, Jianlong Zheng, and Honggang Zhang

Mix Design of Pervious Recycled Concrete..... 103
Jiusu Li

Pavement Materials Modeling

Influence of Water Saturated State on Moisture Susceptibility of Asphalt Mixture 109
Liang Zhou, Feicheng Chen, Jiang Yuan, and Xie Qi

Development and Verification of Creep Constitutive Model for Asphalt Mixture Based on Continuum Damage Theory..... 115
Jiupeng Zhang, Yuhui Pi, and Xiaoming Huang

On Dynamic Pore Pressure in Moisture Damage of Asphalt Pavement..... 122
Xin-zhuang Cui, Wei-dong Cao, Shu-tang Liu, and Lin-lin Dong

Influence of ATB on Pavement Performance..... 129
Jian-guo Wei and Jian-long Zheng

Characteristics and Prediction of Permanent Deformation in HMA 136
Ying Gao, Xiaoming Huang, Zhaohui Qi, and Jiupeng Zhang

Evaluation of Low-Temperature Properties of Long-Term-Aged Asphalt Mixtures..... 143
Ningli Li, Tiehu Li, Huaxin Chen, and Zhengqi Zhang

Mechanical Study of Steel Bridge Pavement with Composite Asphalt Materials 151
C. Y. Wu and Y. Li

A Cyclic Cohesive Crack Model Based on Bounding Surface Concept 158
Rongzong Wu and John T. Harvey

Research on the Relationship between the Loading and the Conductivity of Smart Asphalt Concrete 165
Feng Zhu, Cheung Lam Wah, and Zejiao Dong

Indexes

Author Index..... 171

Subject Index..... 173

Review of the Back-Propagation Neural Network Method as a Basis for Pavement Performance Assessment

Li Ming[1], Lan Chao[2], Mu Hai-rui[3] and Song Jun-min[4]

[1]Technical Superintendent, Pengfang Paving Engineering Research Co. Ltd., 10 Qiaonan Village, Banan District, Chongqing 400054, China; rehawli@163.com

[2]Director, Pengfang Paving Engineering Research Co. Ltd., 10 Qiaonan Village, Banan District, Chongqing 400054, China; chaol1996@sina.com

[3]Pengfang Paving Engineering Research Co. Ltd., 10 Qiaonan Village, Banan District, Chongqing 400054, China; cqmobing@126.com

[4]Xinjiang University, 21 Youhao Road, Urumqi 830008, China; songjm950720@126.com

ABSTRACT: The conventional methods of pavement performance assessment indices were established by statistical analyses based on single item and multiple linear regression techniques. These regression models have many deficiencies and are not able to truly reflect the inherent complex nonlinear relationships among the performance indices. However, the Back-Propagation (BP) neural network method with ca comprehensive nonlinear dynamic system is able to address some of these weaknesses. In this paper, the International Roughness Index (IRI), Damage Rate (DR), Structure Strength Index (SSI), Sideway Force Coefficient (SFC), and Rutting Depth (RD) were selected as the five index variables. These variables are considered as some of the most significant factors that affect pavement performance. Additionally, these indices were easily classified as non-dimensional quantities and became input data units in the application of the BP neural network. In the study, Pavement Management Index (PMI) was accordingly sub-divided into five groups representing five grades; namely (1) excellent, (2) good, (3) medium, (4) subordinated, and (5) inferior. In this paper, pavement performance assessment based on the BP neural network method and PMI is presented along with a practical application example; followed by a summary of findings and recommendations

1. INTRODUCTION

The assessment of asphalt pavement performance is the basis of a series of

pavement management works (such as prediction of performance, making a plan of maintenance or rebuilding, rational allocation of maintenance funds, etc.). Consequently, the authenticity of the assessment results constitutes a key factor in determining the success or failure of the whole pavement management decision. Additionally, it also influences the carryover effect of pavement management system directly. Therefore, it appears particularly important to research the assessment methodology for asphalt pavement performance management.

Currently, combining subject and object matters is a common way to establish a comprehensive assessment index system for pavement workability, which is achieved through statistics of single item and multiple linear regression techniques. This subsequently allows for the establishment of a connection between subjective scoring and objective measured data such as Present Serviceability Index (PSI) in AASHTO, Riding Comfort Index (RCI) in Canada, Maintenance Control Index in Japan, MCI, tc. (Li N. et al., 1997). This methodology has a certain application value. But the regression technique has its own deficiency; so it is difficult to truly reflect the internal complex nonlinear relationships through the specific regression relation established by this methodology. Furthermore, its adaptability is subject to certain restrictions.

Based on the foregoing, this paper explores the design of Back-Propagation (BP) neural network and the selection of pavement performance assessment indices as basis of assessing pavement performance. The paper also provides an example of applying the BP neural network for pavement performance assessment.

2. BACK-PROPAGATION NEURAL NETWORK

In the 80's of 20th century, headed by Rumelhart and McClelland, experts put forward the BP algorithm of Multilayer Feed forward Neural Networks (MFNN). It is a study process with supervision and also an application of Gradient Descent in MFNN (XU Li-na, 2003). BP networks excel at data modeling because of their superior function approximation capabilities (Meier and Tutumluer, 1998).

Artificial neural network (ANN), as a highly complex nonlinear dynamical system, has high-dimensionality. In recent successful applications, the use of ANNs was introduced for the analysis of jointed concrete pavement responses under dual-wheel and tri-tandem type aircraft gear loadings (Ceylan et al., 1998 and 2000). An ANN model was verified and validated with the results of the ILLI-SLAB finite element solutions, which were intended to enable pavement engineers to easily incorporate current sophisticated finite element methodology into routine practical design. As a result of this verification analysis, a simplified HMA |E*| prediction model was accordingly developed based on the ANN methodology (Gopalakrishnan et al., 2008).

3. BP NEURAL NETWORK DESIGN FOR PAVEMENT PERFORMANCE ASSESSMENT

3.1. The Selection of Pavement Performance Assessment Index

Pavement Performance is a synthesis concept, which characterizes the changing trends of pavement behavior and service function under traffic loading, environmental changes (i.e., moisture variations, temperature fluctuations, etc), and other influencing factors. In essence performance reflects the different degrees of pavement behavior meeting or adapting to the driving requirements including functional performance and structural performance. Based on the current and ever-growing heavy traffic spectrum in China including the traffic channelization and overloaded trucks, this paper will analytical determine the subentry indices that are considered more influential on the asphalt pavement assessment. These indices include International Roughness Index (IRI), Damage Rate (DR), Structure Strength Index (SSI), Sideway Force Coefficient (SFC), and Rutting Depth (RD).

3.2. Dimensionless Processing of Pavement Performance Assessment Indices

Based on the theoretical discussions above, it is clearly evident that comprehensive evaluation of asphalt pavement performance is affected by many factors. Due to the different dimensions of the subentry indices and different types of dimensions, there is no general or common characteristic of these indices and it is practically difficult to compare them directly when analyzing them. For this reason, it is often recommended to normalize these subentry indices to some similar dimensionless interval with a common utility function so as to enable comprehensive analysis and obtain accurate results. In this paper, the linear dimensionless method-extremum method was selected and utilized to calculate the pavement performance indices.

Comparing to PMI, SSI and SFC belong to the direct index grouping, which means that a larger index in terms of magnitude is better. The IRI, CR, and RD on the other hand belong to the inverse group of indices, which means that the smaller index in magnitude is the better the result in terms of pavement performance. On this basis, different models were adapted to conduct the dimensionless processing in this paper (JIN Cong, 2001).

3.3. Design of BP Neural Network

The three-layer BP neural network designed in this paper is as follow: Input layer is the input variable of the BP network. For comprehensive assessment of freeway asphalt pavement performance, the designed number of input cells was five,

which corresponded to the five factors affecting comprehensive pavement performance assessment (i.e., IRI, CR, RD, SSI, and SFC). These are shown in Figure 1. For accurate results, each neural network input index should be processed with a dimensionless method.

In this paper, the neural network contains only one hidden layer. The number of hidden layer cells is determined by Experiential Formula (Wang Ai-min et al., 2006). The number of hidden layer cells in BP neural network designed in this paper is shown in Table 1. In this table, the corresponding suggested values are put forward.

The output layer is the output variable of the neural network. The index for pavement performance comprehensive assessment referred in this paper is the Pavement Management Index (PMI). In accordance with the degrees of pavement conditions, five grades representing five pavement comprehensive performance conditions were utilized (i.e., excellent, good, medium, subordinated, and inferior). Therefore, in the design of the BP neural network, the desired output of output layer is indicated by five output variables, namely excellent, good, medium, subordinated, or inferior, which correspond to the orthogonal vectors: Ⅰ={1 0 0 0 0}，Ⅱ={0 1 0 0 0}，Ⅲ={0 0 1 0 0}，Ⅳ={0 0 0 1 0}， Ⅴ={0 0 0 0 1}. The BP neural network structure for asphalt pavement performance comprehensive evaluation is accordingly shown in Figure 1.

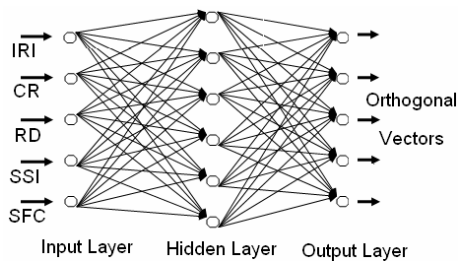

FIG. 1. BP neural network structure diagram for pavement performance assessment

Table 1. The Construction of Neural Network

BP neural network	number of input layer cells “m”	number of hidden layer cells “p”	suggested values “p”	Number of output layer cells “n”
asphalt pavement	5	3-12	6	5

Learning rate is a variable indicator of the quantitative power value produced in every circuit of the BP network in terms of training time. Larger learning rate may cause unsteadiness of the system; smaller learning rate may cause longer training time and slower the convergence pace. However, a smaller learning rate tends to minimize network errors due to trough confinement. As a result, a smaller learning rate would generally be desired to ensure system steadiness and error minimization. Thus, a learning rate of 0.01-0.8 was recommended for this study.

4. THE REALIZATION OF PAVEMENT PERFORMANCE ASSESSMENT BASED ON BP NEURAL NETWORK

Here in this paper, “Microsoft Visual Basic” Visual was adapted as the programming language for the BP neural network modes for pavement performance comprehensive assessment. Figures 2 and 3 show specific learning training parameters interface and assessment application interface, respectively.

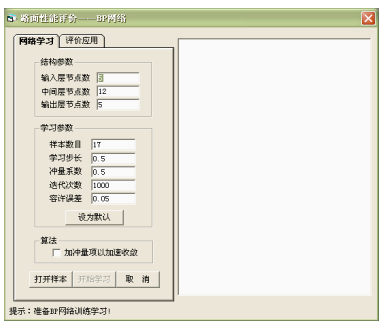

FIG. 2. Learning training interface of BP neural network

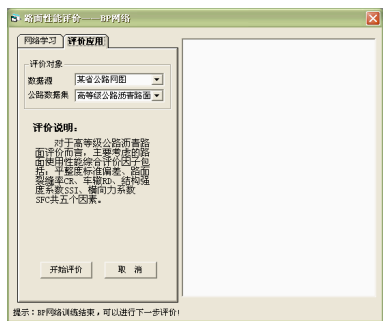

FIG. 3. Assessment and application interface of BP neural network

5. THE APPLICATION OF PAVEMENT PERFORMANCE COMPREHENSIVE ASSESSMENT METHODOLOGY BASED ON BP NEURAL NETWORK

Pavement performance comprehensive index-Pavement Management Index is mathematically obtained by assigning scores based on the assessed pavement performance. The specific method applied in this study uses a 5-point approach and assigns excellent, good, medium, subordinated, and inferior grades to characterize the different pavement performances; with 1 point for each grade. Specific assessment grades and interrelated maintenance management measures are shown in Table 2.

Table 2. Maintenance Criteria of PMI Index

	Assessment Grade				
	inferior	**subordinated**	**medium**	**good**	**excellent**
PMI	(0,1]	(1,2]	(2,3]	(3,4]	(4,5]
Maintenance Measures	Heavy Repair	Medium Repair	Minor Repair	No need repair	

Based on Yin et al's pavement performance data (Wang Yin et al., 2000), typical groups of data were selected as training and verification samples for the BP neural network evaluated in this paper. With this data, comprehensive assessment of other f pavement sections in the BP neural network was accomplished.

Furthermore, 12 groups of data for the examination of the BP neural network assessment effect were utilized. Additionally, other indices such as Pavement Quality Index (PQI) and Pavement Service Index (PSI) were also included in the analysis for comparison purposes. Based on this comparison, the application effect of the BP neural network was - demonstrated. The assessment result of the BP neural network is shown in Figure 4. As shown in Figure 4, the network assessment result was satisfactory, which was consistent with the actual pavement performance condition observed in the field

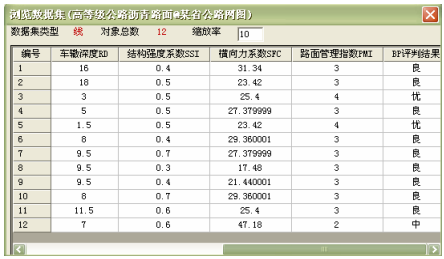

FIG. 4. Interface of BP Network Assessment Results

6. SUMMARY

For the pavement performance comprehensive assessment, the combination of BP neural network and Pavement Management Index (PMI) were analytically investigated in this paper. Analytical results indicated that BP neural network and PMI can successfully be utilized to formulate maintenance strategies as regards to pavement performance assessment.

Application of artificial neural network is a relatively new technology to the road industry, which exhibits greater promising potential and application value for pavement performance assessment. The unprecedented capability of the BP neural network technique in handling and processing nonlinear problems undoubtedly makes it even more attractive for pavement performance assessment applications. This being a relatively new method, more research is recommended for continued improvement including model refinement and verification with different array of data sets.

7. REFERENCES

Ceylan, H., Tutumluer, E., and Barenberg, E.J. (1998). “Artificial Neural Networks as Design Tools in Concrete Airfield Pavement Design.” *ASCE International Air Transportation Conference*, Austin, Texas, pp. 447-465.

Ceylan, H., Tutumluer, E., and Barenberg, E.J. (2000). “Artificial Neural Networks for Analyzing Concrete Airfield Pavements Serving the Boeing B-777 Aircraft.” *Journal of the Transportation Research Board*, Transportation Research Record 1684, pp. 110-117.

Gopalakrishnan, K., Kim, S., and Ceylan, H. (2008). “Advanced Approaches to

Hot-mix Asphalt Dynamic Modulus Prediction." *Canadian Journal of Civil Engineering*, Vol. 35(7) : 699-707.

Jin, Cong (2001). "A Model of Synthetic Evaluation for Economic Benefit Based on Hamming Neural Networks." *System Engineering-Theory & Practice*, (2) : 108-112.

Li, N., Haas, R., and Xie, W.-C. (1997). "Development of a new asphalt pavement performance prediction model." *Canadian Journal of Civil Engineering*, Vol. 24(4) : 547-559.

Meier, R. and E. Tutumluer (1998). "Uses of Artificial Neural Networks in the Mechanistic-Empirical Design of Flexible Pavements." Proceedings of *the International Workshop on Artificial Intelligence and Mathematical Methods in Pavement and Geomechanical Engineering Systems*. Florida International University, Florida, pp. 1-12.

Wang, Ai-min, Song Qiang, et al. (2006). "The Forecast Model and Emulating of the Compositions of Sinter Ore Basing on the BP Neural Network." *Microcomputer Information.* Vol. 22(9) : 243-245.

Wang, Yin, Hu, Chang-bin, et al. (2000). "Study on Comprehensive Performance Evaluation for Freeway Asphalt Pavement." *Journal of Shenyang Architectural and Civil Engineering Institute*, Vol. 16(4) : 264-268.

Xu, Li-na (2003). "Artificial Neural Network Control." Publishing House of Electronics Industry, Beijing, pp. 27-41.

+

Evaluation of PCCP Performance Based on Fuzzy Complex Matter Element Method

Tian Xiaoge[1], Lin Du[2], and Wu Wenbiao[3]

[1]School of Transportation Engineering, Changsha University of Science and Technology, Changsha Hunan, P.R.China, 410076
[2]China Communications 2nd Highway Survey and Design Institute, Wuhan Hubei, P.R.China, 430101
[3]Tongji University, Shanghai, P.R.China, 200092

ABSTRACT : The performance evaluation of Portland cement concrete pavement (PCCP) is the key step in its maintenance, rehabilitation and overlay. A new evaluation index system was put forward considering the needs of PCCP overlay, based on the traditional evaluation index system, whose aim is mainly at maintenance. A systematic pavement performance evaluation model was established by using the fuzzy complex matter element method, and the weight of each factor was determined considering its objective and subjective weights, determined from Analytic Hierarchy Process (AHP) method and entropy method respectively. Finally, the pavement performance of a test road was evaluated using this method, and the evaluation result agrees with the actual pavement condition.

INTRODUCTIONS

The PCCP maintenance technical specifications (China, JTJ 073.1-2001) evaluate the PCCP performance from four parts, including damaged status, bearing capacity, running quality and slippery resist capacity of the PCCP. Pavement condition index (PCI) and ratio of broken plate (DBL) are used to evaluate the pavement damaged status. The load transfer capacity of the joint (K_j) and the voids under the plate are used to evaluate the bearing capacity of the pavement structure layer. Running quality index (RQI) is used to evaluate running quality of the pavement. The sideway force coefficient (SFC) or slippery resist value (SRV) and texture depth are used to evaluate the anti-slide capacity. This evaluation system has two deficiencies: ①it only puts forward the index, lacks classification standards in the structural capacity evaluation. Even more, there is not any index on the bearing capacity of the base course and foundation; ②it cannot put forward a comprehensive evaluation index or method, so the different section of the highway cannot be compared, and it is difficult to optimize the decision-making of the scheme of the maintenance.

The evaluation of PCCP performance is a multi-factor synthetic judgment, and

there are subjective judgments of the investigator, which can cause certain personal error, and the boundary of light and medium, medium and serious is fuzzy.

A set of index system and classification standard was put forward, based on the PCCP maintenance specifications, to reflect the structural and functional damage status of the pavement, and the fuzzy complex matter element method was used to evaluate the PCCP performance.

EVALUATION INDEX SYSTEM of PCCP PERFORMANCE

The damage in PCCP is generally classified into structural and functional. Through analyzing the evaluation index systems at home and abroad, and the development of the detecting technology, a new evaluation index system was put forward in this paper includes two parts:

(1) Evaluation index of PCCP functional performance

For a PCCP, PCI was adopted to reflect its damage status, and RQI was adopted to evaluate its running quality, International Friction Index (IFI) was adopted to evaluate its capacity of slippery resistance, as for IFI can unite all the kinds of slippery-resist test methods and equipments.

(2) Evaluation index of PCCP structural status

Because the thickness, strength and modulus of elasticity of the plates are comparative stable with time, the base course and the joints are the marked influential factors for the life and structural response of the pavement, so the four indexes, DBL, K_j, the resilience modulus of base course Et, and the ratio of voided plates (T) were put forward to evaluate the structural status of PCCP in this paper. When the deflection character parameter of FWD was adopted to calculate E_t, the standard of classification can refer to the literature (Zengsheng, 2003). Therefore, the evaluation index system and standard of classification of PCCP were put forward in this paper as following:

Table 1. Evaluation index system and classification standards

Target	Index	Evaluation factor	Grade of evaluation			
A	B	C	Good	Medium	Inferior	Bad
A: Pavement Performance	B1: functional performance	C1: PCI	100~70	69~55	54~40	40~20
		C2: RQI	10~7.0	6.9~4.5	4.4~2.0	2.0~0
		C3: IFI	0.322~0.257	0.256~0.154	0.153~0.012	0.011~0
	B2: structural status	C4: DBL	0~5	5~10	10~20	20~40
		C5: E_t	>295	265~295	215~265	<215
		C6: K_j	>80	56~80	31~55	0~30
		C7: T	0~5	5~10	10~20	20~40

EVALUATION OF PAVEMENT PERFORMANCE USING FUZZY COMPLEX MATTER ELEMENT

The main idea of the matter element analysis method is describing the thing with three factors, thing, character and value. The matter element is the ordered pair of these three factors. If the value is fuzzy, then it is called fuzzy matter element.

The general status of PCCP is determined from the actual measurement values of different factors. This is a identify problem, which is composed with the value of

survey, evaluation index and classification standard. So the fuzzy matter element analysis method can be used to establish a multi-index evaluation model of PCCP.

(1) procedures of evaluation using Fuzzy complex matter element

① calculating the degrees of membership, $\mu_j(x_{1i})$ (j=1,2,⋯,m; i=1,2,…,n) for n character (evaluation index) of m things (standard of grade).

② determining the relevancy coefficient K_{ji} according to the function of degree of membership, $\mu(x_{ji})$. Then the fuzzy complex matter element R_{mn} is founded.

③ calculating the relevancy coefficient K_{ij}, and relevancy coefficient weight vector W of the corresponding standard of grade of each evaluation index according to the operation mode $M(\cdot,+)$, then getting the relevancy degree of the corresponding standard of different grades, and establishing the relevancy degree fuzzy complex matter element.

④ evaluating the corresponding grade of the pavement performance according to the principle of the largest degree of relevancy.

(2) Determination of the analysis parameter in the Fuzzy complex matter element

① Degree of membership

The measured values of classified parameters are dispersion, so these values can be considered as a normal distribution for the same index when the times of measurement is more. So,

$$\mu(x) = \exp[-(\frac{x-p}{q})^2] \tag{1}$$

Where, $p = \frac{a+b}{2}$, $q = \frac{|a-b|}{1.665}$, and a, b is the boundary value of the complex matter element (a, b).

② Relevancy coefficient

In the condition that classical domain is coincide with node domain, the relevancy function and the degree of membership is equal, and can be exchanged. So relevancy coefficient K_{ji} can be determined from membership degree function $\mu(x_{ji})$:

$$k_{ji} = \mu_{ji} = \mu(x_{ji}),\ (j = 1,2,...,m;\ i = 1,2,...,n) \tag{2}$$

Where, K_{ji} is the relevancy coefficient between standard thing M_o and compared thing M_j of the character i. μ_{ji} or $\mu(x_{ji})$ is the membership degree of xji.

③ Relevancy degree

The relevancy degree is a measurement of the relevancy between two things. It can be determined from the weighted average of the relevancy coefficient. i.e.,

$$K_{oj} = W * k,\quad j = 1,2,...,m \tag{3}$$

Where, K is the relevancy coefficient vector between standard thing M_o and compared thing M_j of the character i, W is the relevancy coefficient weight vector between standard thing M_o and compared thing M_j of the character i.

④ Weight

It is very important to determine the weights of every index in evaluating the performance of pavement with the synthetically evaluation method, and it will often influence the objectivity of the evaluative results. Considering that the evaluation of

PCCP includes not only the subjective factor based on the knowledge, experience and value from experts, but also the objective information from the actual detecting data, so the weights determined from Analytic Hierarchy Process (AHP) method and entropy method were combined to determine the weight of each index. So the weight can reflect the important of each evaluation index and the actual condition of the problem more comprehensively and more objectively.

If the subjective weight given by AHP method is W_i', and the objective weight given by entropy method is W_i'', then the final weight W_i can be determined as following,

$$W_i = \frac{W_i' \cdot W_i''}{\sum_{i=1}^{n} W_i' \cdot W_i''} \tag{4}$$

CASE ANALYSIS

Based on the evaluation index system of PCCP performance founded foregoing, a case pavement was evaluated using the fuzzy complex matter element method.

(1) Determining the Fuzzy complex matter element of the pavement performance

According to the detecting data, the actual value of evaluation factors of the pavement is as shown in table 2.

Table 2. The actual value of evaluation factors

C_1: PCI	47
C_2: RQI	6.1
C_3: IFI	0.261
C_4: DBL	15
C_5: E_t	249
C_6: K_j	65.8
C_7: T	17

Taking the actual values and corresponding gradational boundaries into equation (1), the degree of membership in the fuzzy complex matter element matrix can be determined as in table 3.

Table 3. The degree of membership $\mu(x_{ji})$ for each evaluation factor

Evaluation Factor	Good	Medium	Inferior	Bad
C1	0.0117	0.0518	1.0	0.1349
C2	0.1696	0.9471	0.0300	0.0
C3	0.5869	0.4471	0.0128	0.0
C4	0.0	0.002	1.0	0.2103
C5	0.2335	0.0518	0.9141	0.2835
C6	0.0173	0.9873	0.0900	0.0004
C7	0.0	0.0	0.8950	0.3100

Then the fuzzy complex matter element $R_{7\times4}$ of the pavement condition can be obtained.

$$R_{7\times4}=\begin{bmatrix} & \text{Good} & \text{Medium} & \text{Inferior} & \text{Bad} \\ PCI & 0.0117 & 0.0518 & 1.0 & 0.1349 \\ RQI & 0.1696 & 0.9471 & 0.0300 & 0.0 \\ IFI & 0.5869 & 0.4471 & 0.0128 & 0.0 \\ DBL & 0.0 & 0.0020 & 1.0 & 0.2103 \\ \mathrm{E}t & 0.2335 & 0.0518 & 0.9141 & 0.2835 \\ K_j & 0.0173 & 0.9873 & 0.0900 & 0.0004 \\ T & 0.0 & 0.0 & 0.8950 & 0.3100 \end{bmatrix} \quad (5)$$

(2) Determining the weight of every index

Weight of AHP method

The hierarchical chart of pavement performance evaluation index is shown in picture 1.

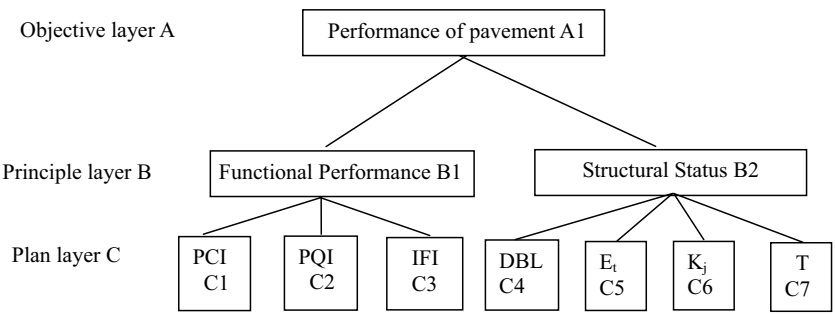

Figure 1. The hierarchy chart of pavement performance evaluation index

The weight of each evaluation factor can be calculated as in table 4.

Table 4. AHP weights of each evaluation factor

Evaluation Factor	B1: Functional Performance	B2: Structural Status	Weight
	0.750	**0.250**	$W_i' = \sum_{j=1}^{m} B_j . C_{nj}$
C1	0.163	-	0.12225
C2	0.540	-	0.4050
C3	0.297	-	0.22275
C4	-	0.118	0.0295
C5	-	0.564	0.1410
C6	-	0.055	0.01375
C7	-	0.263	0.06575

Entropy method

Carrying on normal processing on the degree of membership $\mu(x_{ji})$ of each evaluation factor in table 2, and y_{ij} of each index can be determined as in table 5.

Table 5. y_{ij} of each evaluation factor

Evaluation Factor	Good	Medium	Inferior	Bad
C1:	0.0098	0.0432	0.8344	0.1126
C2:	0.1479	0.8259	0.0262	0.0000
C3:	0.5607	0.4271	0.0122	0.0000
C4:	0.0000	0.0016	0.8249	0.1735
C5:	0.1575	0.0349	0.6164	0.1912
C6:	0.0158	0.9016	0.0822	0.0004
C7:	0.0000	0.0000	0.7427	0.2573

As for the evaluation value M is classified into four classes, so,

$$k = \frac{1}{\ln m} = 0.72135$$

According to the value of K and the data of y_{ij} in table 5, the entropies of C_1 to C_7, corresponding deviations h_i, and the weight W_i of each evaluation factor can be calculated, as shown in table 6.

Table 6. Entropy weight of each evaluation factor

Evaluation Factor	$e_i = -k\sum_{i=1}^{m} y_{ij} \ln y_{ij}$ Entropy:	$h_i = 1 - e_i$	$W_i'' = \frac{h_i}{\sum_{i=1}^{n} h_i}$
C1:	0.4170	0.5830	0.1493
C2:	0.3867	0.6133	0.1570
C3:	0.5349	0.4651	0.1191
C4:	0.3412	0.6588	0.1687
C5:	0.7378	0.2622	0.0671
C6:	0.2651	0.7349	0.1882
C7:	0.4113	0.5887	0.1507

Calculating the synthesis weights

The synthesis weight of each evaluation index can be determined through its AHP weight W_i' and entropy weight W_i'' according to equation 4. The results are listed in table 7.

Table 7. Synthesis weights of each evaluation index

Evaluation Factor	Weight		
	AHP Method	Entropy Method	Synthesis Weight
C1	0.12225	0.1493	0.1349
C2	0.4050	0.1570	0.4700
C3	0.22275	0.1191	0.1961
C4	0.0295	0.1687	0.0368
C5	0.1410	0.0671	0.0699
C6	0.01375	0.1882	0.0191
C7	0.06575	0.1507	0.0732

(3) Evaluation of pavement performance by Fuzzy complex matter element

The complex matter element of weight R_w can be composed from the synthesis weight W_i of each evaluation index, as shown in table 7.

$$R_W = \begin{bmatrix} & PCI & RQI & IFI & DBL & Et & K_j & T \\ W & 0.1349 & 0.4700 & 0.1961 & 0.0368 & 0.0699 & 0.0191 & 0.0732 \end{bmatrix} \quad (6)$$

Carrying out $M(\bullet, +)$ operation, i.e. carrying out multiplication operation first and then carrying out addition operation, on the fuzzy complex matter element $R_{7\times4}$ in

the equation (5) and complex matter element of weight R_W in the equation (6), the relevancy degree fuzzy complex matter element of the pavement performance can be obtained, as in equation (7).

$$R = \begin{bmatrix} & \text{Good} & \text{Medium} & \text{Inferior} & \text{Bad} \\ K & 0.2130 & 0.5624 & 0.3194 & 0.0685 \end{bmatrix} \tag{7}$$

Where, K is the relevancy degree of the corresponding evaluation value to the different grades for the case pavement performance.

It can be seen from the equation (7) that the relevancy degree to "Medium" pavement performance is the biggest, the value is 0.5624, and the relevancy degree to "Inferior" is the second biggest, the value is 0.3194. So, it can be deduced that the performance of the case pavement belongs to "Medium Inferior" grade according to the principle of the most relevancy degree, which agrees with the fact.

CONCLUSIONS

(1) A new evaluation index system was put forward considering the practical needs of overlay, base on the Technical Specifications of Cement Concrete Pavement Maintenance for Highway (JTJ 073.1-2001).

(2) The determination of the weights combined the weights using Analytic Hierarchy Process (AHP) method and entropy method simultaneously, which can reflect the importance of each evaluation index and the actual condition of the problem more comprehensively and more objectively.

(3) Finally, a new method, fuzzy complex element method based on synthesis weight, to synthetic evaluation of PCCP performance was founded. And the result of the case study indicates that the new method is feasible.

REFERENCES

Ministry of Communications (2001). Technical Specifications of Cement Concrete Pavement Maintenance for Highway (JTJ 073.1-2001). Beijing: People's Communications Press.

Institute of Road Science (1998), Ministry of Communications. Standard of International Roughness Index (IRI). Beijing: Institute of Road Science, Ministry of Communications.

American Society for Testing and Material (1999). Terminology Relating to Traveled Surface Characteristics Annual Book of ASTM Standards.

PIARC (1995), International PIARC Experiment to Compare and Harmonize Texture and Skid Resistance Measurements.

James, C, J. J.Hecuy (2002). Evaluation of IFI Calibration Procedures for New and Existing Devices. Canada: Transportation Development Centre.

Zengsheng (2003). Research on the Analysis Method and Evaluation of PCC Pavement Performance: [doctorate dissertations of central south university].

Caiwen (1994). Matter Element Model and Application the 1st edition Beijing:

technology literature press.
Xiao, Chunfang (1999). Research on Fuzzy Matter Element Analysis and Application, Intensity and Environment, (2).
Chen, Shouyu (1998). Theory and Application of Project Fuzzy Collection. Beijing: National Defense Industry Press.
Negoita, C.V. (1999). Applications of Fuzzy Sets to Systems Analysis. Applied Economics Letters, 4.

Asphalt Pavement Evaluation Based on Matter Element Model

Yan Kezhen[1]; Zhang Jinzhao[2] ; Wu JianLiang[3] and Wu Luocheng[4]

[1] Hunan University, Changsha 410082, China; E-mail: yankz2004@163.com.
[2]The First highway survey &design institute of, China, Xi' an 710064, China; 616zhang@vip.163.com
[3]Hunan University, Changsha 410082, China; E-mail: gl02@chd.edu.cn
[4]Hunan University, Changsha 410082, China; E-mail: wlcwillcg2006@yahoo.com.cn.

ABSTRACT: Pavement performance evaluation is one of the most important problems in pavement management system. In traditional methods for pavement performance evaluation, the weights of evaluation indexes are hard to determine and mainly depended on subjective judgment. The paper get the evaluation indexes by employing the concept of entropy and the weights of the evaluation indexes are obtained from surveying data. The matter element model for pavement evaluation is established. By calculating the dependence degree of the matter element model, the pavement evaluation is obtained. The results show that the matter element model has good ability to evaluate the pavement performance.

INTRODUCTION

The evaluation of pavement performance is an important process in pavement management system (PMS). There are usually two kinds of models including systematic analysis and regression modeling analysis. The analytical hierarchy process (AHP) and fuzzy mathematics analysis methods belong to the systematic analysis. Lu (1992) developed an AHP method to get the weights of evaluation indexes, and evaluated the pavement performance by fuzzy mathematics method. According to gray theory, Zhang and Jia (2005) determined subordinate function of evaluation indexes by means of triangle whitenization weight function and evaluated the asphalt pavement by grey cluster. However, these two models rely more on experienced judgment. Regression modeling analysis is used to establish a function between the pavement performance and its main influencing factors for surveying data. The Regression model is restrained by the territory condition. In this paper, the entropy is employed to measure the weights of evaluation indexes, and the matter element model is developed to evaluate the performance of the flexible pavement.

ENTROPY WEIGHT

The Concept of Entropy

The concept of entropy comes from thermodynamics, standing for the heat that does not make work, which can be calculated from heat divided by the change of temperature. Later the entropy concept is absorbed in information theory. In information theory, the value of entropy indicates the disorder of system. From the concept of entropy we can know that the larger the entropy of one index, the more uncertain the value of the index. In other words, this index can provide more information to describe the thing. The index with the larger entropy is more important to characterize this kind of thing.

Supposing the number of evaluating indexes is *n,* and *m* is the number of evaluating objects**,** the value for object *i* ,and the value of index *j* is c_{ij} ,and an original indexes value matrix $C_{ij(m\times n)}$ can be obtained. For evaluation index c_j, the entropy E_i and weight B_i can be obtained as follow:

$$c'_{ij} = \frac{c_{ij} - c_{\min}}{c_{\max} - c_{\min}} + 1 \tag{1}$$

$$P_{ij} = \frac{c'_{ij}}{\sum_{i=1}^{m} c'_{ij}} \tag{2}$$

$$E_j = \frac{-\sum_{i=1}^{m} P_{ij}.L_i.Ln(P_{ij})}{Ln(\sum_{i=1}^{m} L_i)} \tag{3}$$

$$B_j = \frac{1 - E_j}{n - \sum_{j=1}^{n} E_j} \tag{4}$$

Where $c_{\max}$, $c_{\min}$ are the maximum and minimum value of C_{ij}, L_i stands for the quantity of object *i*.

The Evaluation Indexes and Its Weights

The plateau of Qinghai-Tibet locates at high altitude region. Asphalt pavements are constructed on permafrost district which combined with the strong solar radiation in Qinghai-Tibet plateau. The asphalt pavements are very easy to crack in this area and the frost soils is likely to thaw. Under those conditions, asphalt pavements are frequently suffered from distress of cracking, rutting, bleeding, raveling, and so on.

In this paper, the indexes are selected for evaluation the performance of pavement in Qinghai-Tibet plateau as Tab 1. The data obtained from 37 locations with a total length of 219.1 Km in Qinghai-Tibet high are used to determine the weights of evaluation indexes. Applied equations (1), (2), and (3), with the L_i stand

for the length of *i*th local, the weights are obtained and shown in Tab 1.

Table 1. The Weights of Indexes

index	long crackingC_1	transverse crackingC_2	block crackingC_3	ruttingC_4	subsidenceC_5	shovingC_6
entropy	0.097	0.093	0.205	0.071	0.135	0.12
index	potholeC_7	ravelingC_8	heave and boilC_9	bleedingC_{10}	repairC_{11}	
entropy	0.087	0.098	0.0824	0.069	0.07	

MATTER- ELEMENT MODEL FOR ASPHALT PAVEMENT EVALUATION

The extension evaluation method based on matter-element theory and extension set theory can be used to determine the degree which something may belong to a set according to the value of the corresponding character. The use of the dependent degree can make the accurate evaluation, which has provided a new way to solve the problem of pavement performance evaluation.

Determination of Class Field, Limited Field and Matter-Element for Appraising

(1) Class field

$$R_{0j}=(N_{0j},C,V_{0j})=\begin{pmatrix} N_{0j}, & c_1, & V_{0j1} \\ & c_2, & V_{0j2} \\ & ..., & ... \\ & c_n, & V_{0jn} \end{pmatrix}=\begin{pmatrix} N_{0j}, & c_1, & \langle a_{0j1},b_{0j1}\rangle \\ & c_2, & \langle a_{0j2},b_{0j2}\rangle \\ & ..., & ... \\ & c_n, & \langle a_{0jn},b_{0jn}\rangle \end{pmatrix} \tag{5}$$

Where, N_{0j} is the classified level of pavement performance $(j=1,2,...,m)$, c_i is the character of the pavement performance level N_{0j}, i.e. the main factors influencing pavement performance $(i=1,2,...,n)$, V_{0ji} is the range of N_{0j}.

(2) Limited field

$$R_p=(P,C,V_p)=\begin{pmatrix} P, & c_1, & V_{p1} \\ & c_2, & V_{p2} \\ & ..., & ... \\ & c_n, & V_{pn} \end{pmatrix}=\begin{pmatrix} P, & c_1, & \langle a_{p1},b_{p1}\rangle \\ & c_2, & \langle a_{p2},b_{p2}\rangle \\ & ..., & ... \\ & c_n, & \langle a_{pn},b_{pn}\rangle \end{pmatrix} \tag{6}$$

(3) Matter -Element for appraising

For evaluating pavement performance, the expression of given by matter-element can be express as follow：

$$R = (p, C, V_p) = \begin{pmatrix} P, & c_1, & v_1 \\ & c_2, & v_2 \\ & \cdots, & \cdots, \\ & c_n, & v_n \end{pmatrix} \tag{7}$$

Where p is the pavement performance for appraising, v_i is the value of p with respect to c_i.

Determination of the Dependent Degree for Pavement Performance

According to the dependent function of the extension set, the dependent degree of the matter-element for appraising is:

$$K_j(p) = \sum_{i=1}^{n} a_i K_j(v_i) \tag{8}$$

$$K_j(v_i) = \frac{\rho(v_i, V_{0ji})}{\rho(v_i, V_{pi}) - \rho(v_i, V_{0ji})} \tag{9}$$

$$\rho(v_i, V_{0ji}) = \left| v_i - \frac{1}{2}(a_{0ji} + b_{0ji}) \right| - \frac{1}{2}(b_{0ji} - a_{0ji}) \tag{10}$$

$$\rho(v_i, V_{pi}) = \left| v_i - \frac{1}{2}(a_{pi} + b_{pi}) \right| - \frac{1}{2}(b_{pi} - a_{pi}) \tag{11}$$

Where $K_j(p)$ is the dependent degree of the pavement performance. The weights for the characters c_k are denoted by Λ. The weight for the characters $c_i (i \neq k)$ are denoted by α_i.

Evaluating Pavement Performance

The pavement performance for appraising p must be satisfied:

(1) If $v_k \notin V_{0jk}$, then it is indicated that p is no longer in the range of the stability levels classified and new value has appeared. Thus the class field and limited field must be re-determined.

(2) If $v_k \in V_{0jk}$, then $K_j(p)$ can be calculated according to equation (8).

Normalizing the dependent degree of the pavement performance in the range of [-1, 1]. Selecting the maximum value from the normal dependent degree to recognize the pavement performance. That is if

$$K_{j_0} = \max_{j_0 \in \{1,2,\ldots,m\}} K_j(p) \tag{12}$$

Then the pavement performance for appraising p, belongs to the level j_0.

APPLICATION EXAMPLE

Classification Standard of Pavement Performance Evaluation

The pavement performance is classified into 5 levels, ie. excellent (A_1), good (A_2), common (A_3), inferior (A_4) and bad (A_5). The matter element of pavement performance can be described as follow:

$$R_{A_1}=\begin{bmatrix} N_{A_1} & c_1 & \langle 85,100\rangle \\ & \cdots & \cdots \\ & c_{11} & \langle 85,100\rangle \end{bmatrix} \qquad R_{A_2}=\begin{bmatrix} N_{A_2} & c_1 & \langle 70,85\rangle \\ & \cdots & \cdots \\ & c_{11} & \langle 70,85\rangle \end{bmatrix}$$

$$R_{A_3}=\begin{bmatrix} N_{A_3} & c_1 & \langle 55,70\rangle \\ & \cdots & \cdots \\ & c_{11} & \langle 55,70\rangle \end{bmatrix} \qquad R_{A_4}=\begin{bmatrix} N_{A_4} & c_1 & \langle 40,55\rangle \\ & \cdots & \cdots \\ & c_{11} & \langle 40,55\rangle \end{bmatrix} \qquad R_{A_5}=\begin{bmatrix} N_{A_5} & c_1 & \langle 0,40\rangle \\ & \cdots & \cdots \\ & c_{11} & \langle 0,40\rangle \end{bmatrix}$$

The limited field of the level of pavement performance can be given as:

$$R_{0A}=(N_{0A} \quad C \quad V_0)=\begin{bmatrix} N_{0A} & c_1 & \langle 0,100\rangle \\ & \cdots & \cdots \\ & c_{11} & \langle 0,100\rangle \end{bmatrix}$$

Table 2. Marks of Pavement Condition

index	mark	index	mark	index	mark
Long cracking	30	subsidence	43	heave and boil	87
Transverse cracking	58	shoving	38	bleeding	76
Blocking cracking	31	pothole	72	repair	84
rutting	80	raveling	84		

Evaluation Example

The original pavement condition data obtain from one section of Qinghai-Tibet highway. The marks of pavement condition are shown in Table 2. The matter-element for appraising of the pavement performance is obtained as Table 3. With the various classified standards as the class field and equations (9)-(11), the dependent degree of the pavement performance for appraising and the various classification standards can be obtained. Normalizing the dependent degree, the result of calculation is given as follow:

$$K_j(p) = [-1.000, -0.583, -0.865, -0.821, -0.509]$$

From the result it can be seen that the maximum dependent degree of matter-element is obtained when j=5, indicating that the level of the pavement performance belongs to bad level. The result achieved in this paper is consistent with the distress condition of pavement.

Table 3. Evaluation Matrix

kind	A1	A2	A3	A4	A5
Long cracking	-0.647	-0.571	-0.455	-0.25	0.5
Transverse cracking	-0.39	-0.222	0.077	-0.067	-0.3
Blocking cracking	-0.635	-0.576	-0.436	-0.225	0.409
rutting	-0.22	0.33	-0.33	-0.556	-0.677
subsidence	-0.494	-0.385	0.218	0.075	-0.065
shoving	-0.552	-0.457	-0.309	-0.05	0.056
pothole	-0.317	0.077	-0.067	-0.377	-0.533
raveling	-0.059	0.067	-0.467	-0.644	-0.733
heave and boil	0.182	-0.133	-0.567	-0.711	-0.783
bleeding	-0.273	0.333	-0.2	-0.467	-0.6
repair	-0.059	0.067	-0.467	-0.644	-0.733

CONCLUSIONS

The evaluation of pavement performance is a complicated problem. In this paper, entropy is used to represent the importance of evaluation indexes, which can determine the weights of evaluation indexes. The evaluation method based on the matter-element theory and the extension set theory has provided a new way to solve the problem of pavement performance evaluation. The result evaluated by this method can reflect the pavement condition, and can be used in practical engineering.

REFERENCES

Lu, Y. X. (1992). "The AHP-Fuzzy method of comprehensively evaluation the condition of flexible pavement distress." *Journal of Chong Qing Jiao Tong Institute*., Vol. 11 (22): 81-88.

Zhang, Y.Q. and Jia, S.Y. (2005). "Evaluation method for asphalt pavement performance of freeway." *Journal of Chang'An University (Natural Science Edition)*., Vol. 25 (2); 11-15.

Zou, Z.H. and Yun, Y.S. (2003). "Jing-nan Entropy method for determination of weight of evaluating in fuzzy synthetic evaluation for water quality assessment indicators." *Journal of Environmental Science*, Vol.18 (5): 1020-1023.

Chao, K.H., Ho, S.H., and Wang, M.H. (2006). "Modeling and fault diagnosis of a photovoltaic system. " *Electric Power Systems Research*, Vol. 78: 97-105.

Xun, Z.Y. and Shen, J. H. (2003). "Appraisal matter-element analysis theory for appraising damaged degree in building industry." *China Civil Engineering Journal*, Vol.36 (9): 100-105.

Kenji, T., Ichiro, T., Hirohiko, I.K., Ma, Y.M., and Hu, Z.Y. (2003). "Surface energy budget and closure of the eastern Tibetan Plateau during the GAME-Tibet IOP 1998 ." *Journal of Hydrology*, Vol.283 : 169–183.

Correlations among Pavement Surface Roughness, Moving Dynamic Vehicle Loads, and Concrete Pavement Performance

Seong-Min Kim [1], Suk-Keun Rhee [2], Hee Beom Park [3], and Dong Ju Yun [4]

[1]Associate Professor, Department of Civil Engineering, Kyung Hee University, 1 Seocheon, Kiheung, Yongin, Kyunggi 446-701, Korea; seongmin@khu.ac.kr
[2]Professor, Department of Civil Engineering, Kyung Hee University, 1 Seocheon, Kiheung, Yongin, Kyunggi 446-701, Korea; skrhee@khu.ac.kr
[3]Graduate Research Assistant, Department of Civil Engineering, Kyung Hee University, 1 Seocheon, Kiheung, Yongin, Kyunggi 446-701, Korea; bambams@khu.ac.kr, Corresponding author, Presenter
[4]Graduate Research Assistant, Department of Civil Engineering, Kyung Hee University, 1 Seocheon, Kiheung, Yongin, Kyunggi 446-701, Korea; yowaa@khu.ac.kr

ABSTRACT: The dynamic loads imposed by moving vehicles have variations in load magnitude due to the surface roughness of the pavement system and larger dynamic loads than the design loads can affect the pavement performance and life. The purpose of this study was to find the relationships among the pavement surface roughness, variations in moving dynamic vehicle loads, and the performance of the concrete pavement system. The artificial pavement profiles of triangular amplitude variation were developed first to use in the analysis to find the effects of the wavelength and amplitude of the surface roughness on the moving dynamic vehicle loads. The analysis was performed and the relationships between the surface roughness elements and the load magnitude, the load frequency, and the phase between the front- and rear-axle loads, of the moving tandem-axle loads were found. To obtain the pavement responses to moving arbitrary vehicle loads, formulations were developed in the transformed field domain using a triple Fourier transform in time, space, and moving space. Based on the analysis results of this study, the correlations among the surface roughness, dynamic vehicle loads, and the pavement performance could be obtained.

INTRODUCTION

If a pavement surface has roughness, the loads imposed by moving vehicles will have variations in the magnitude due to the surface roughness. These load variations are directly related to both the pavement life and users' perception because the pavement stresses are dependent on the load magnitude and users' perception is dependent on the

vehicle vibration. Currently, studies related with the pavement surface profile become more important because of those reasons (Ceylan et al., 2007; McGhee and Gillespie, 2007; Papagiannakis et al., 2007). Therefore, it is suitable to use dynamic loading caused by surface roughness as an indicator to predict the pavement response and corresponding pavement performance.

In this study, the aspects of the effects of the surface roughness elements such as the wavelength and amplitude on the moving dynamic vehicle loads were examined first by creating artificial pavement profiles. Then, the dynamic vehicle loads were analyzed considering the real pavement profiles and the stress responses subjected to those dynamic loads were obtained using the formulation developed in the transformed field domain using a triple Fourier transform in time, space, and moving space. Finally, the pavement remaining life was predicted using the AASHTO load equivalency factor. From the analysis results of this study, the correlations among the surface roughness, dynamic vehicle loads, and the concrete pavement performance could be obtained, and details of the study are presented in this paper.

SURFACE ROUGHNESS ASPECTS ON DYNAMIC LOADING

To investigate the effects of parameters, such as wavelength and amplitude of roughness and vehicle speed, on the moving dynamic load, the artificial profile data has been made and used for the dynamic analysis. The wavelengths of 1.2, 2.4, 6, and 12m, the roughness amplitudes of 5, 10, 15, and 20 mm, and the vehicle speeds of 32, 64, 96, and 128 km/h have been considered. Many sets of the artificial profile data have been assembled by combining different roughness amplitudes and wavelengths. The artificial profiles used for the parametric study are shown in Figure 1. To predict the dynamic tandem-axle loads, a computer program developed for the TxMLS project was used (Center for Transportation Research, 1992; Kim et al., 1995).

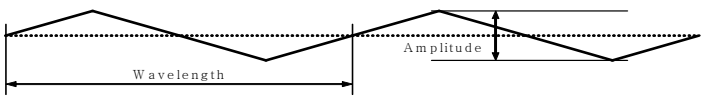

FIG. 1. Artificial profiles.

The time histories of the dynamic loads on the front- and rear-axle tires are investigated first when the vehicle moves on the artificial profile consisting of 1.2m wavelength and 5mm roughness amplitude. When the vehicle speed is 32km/h, as shown in Figure 2(a), the dynamic loads on the front-axle tires show more fluctuations and the maximum dynamic load occurs on the rear-axle tires although the maximum dynamic loads on the front- and rear-axle tires are very close. When the vehicle speed is 96km/h (Figure 2(b)), the fluctuations of the dynamic loads on the front- and rear-axle tires are very similar, but the maximum dynamic load occurs on the front-axle tires. Therefore, the location where the maximum dynamic load occurs depends on the vehicle speed and profile data.

The effect of the roughness amplitude on the maximum dynamic load has been investigated and the results are shown in Figures 3 and 4. The maximum dynamic load increases as the roughness amplitude increases for a given wavelength and a vehicle speed. When the speed is 32km/h, as shown in Figure 3, the different wavelengths do not clearly affect the maximum dynamic load. For higher speeds, on the other hand, shorter wavelengths (1.2 and 2.4m) of the profile yield higher maximum dynamic loads. In other words, the maximum dynamic load is not affected by the vehicle speed when the profile has a larger wavelength, as shown in Figures 4(c) and (d).

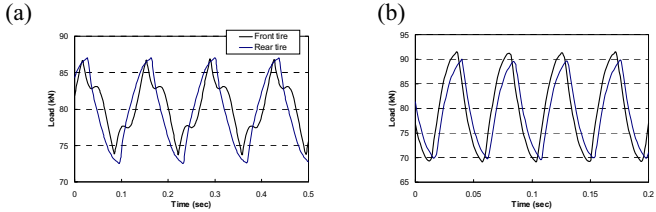

FIG. 2. Load time histories on front- and rear-axle tires when vehicle speed is (a) 32 and (b) 96km/h.

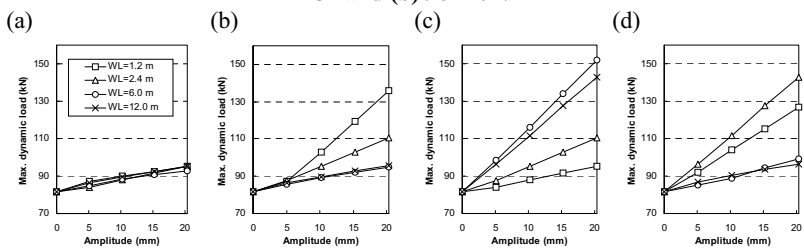

FIG. 3. Effect of roughness amplitude on dynamic loading for a vehicle speed of (a) 32, (b) 64, (c) 96, and (d) 128km/h.

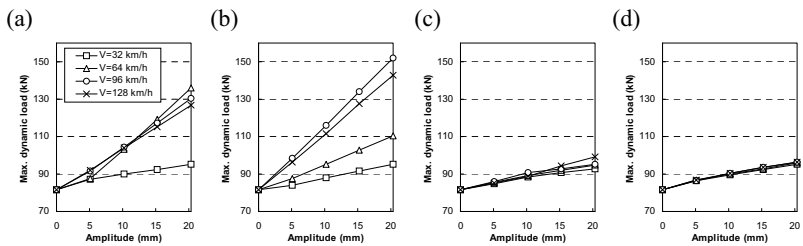

FIG. 4. Effect of roughness amplitude on dynamic loading for a roughness waveleght of (a) 1.2, (b) 2.4, (c) 6, and (d) 12m.

The effect of the wavelength of the profile on the maximum dynamic load was also investiagted. Except for the vehicle speed of 32km/h, higher dynamic loads could be observed when the wavelengths are 1.2 and 2.4m.

The effect of the vehicle speed on the maximum dynamic load is shown in Figures 5 and 6. As the vehicle speed increases, the maximum dynamic load tends to increase initially and then becomes almost constant when the speed is higher than a certain level that depends on the wavelength and amplitude of the profile.

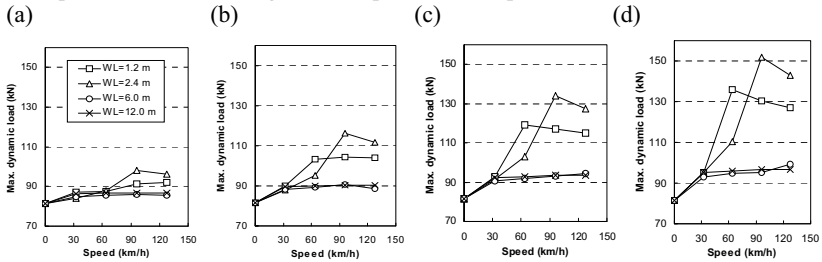

FIG. 5. Effect of vehicle speed on dynamic loading for a roughness amplitude of (a) 5, (b) 10, (c) 15, and (d) 20mm.

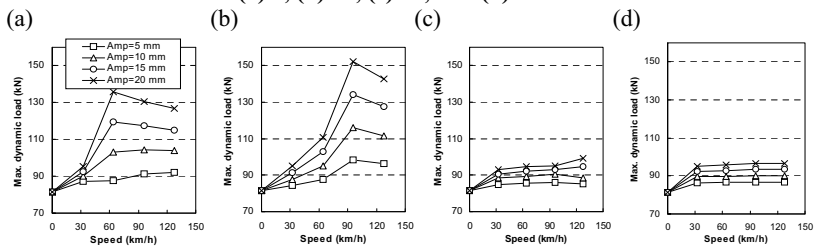

FIG. 6. Effect of vehicle speed on dynamic loading for a roughness waveleght of (a) 1.2, (b) 2.4, (c) 6, and (d) 12m.

From this study, it has been found that the dynamic load can be significantly larger than the static load when the wavelength of the profile is short (smaller than about 4.5m) and the vehicle speed is high (higher than about 48km/h). The roughness amplitude has an almost linearly proportional relationship to the maximum dynamic load and the slope of the linear relationship depends on the vehicle speed and the roughness wavelength.

SURFACE ROUGHNESS EFFECT ON PAVEMENT PERFORMANCE

As investigated previously, the loads imposed by the moving vehicles have variations in the load magnitude because of the surface roughness of the pavement. Since the

maximum magnitude of the dynamic load is normally larger than the static load, the pavement life will be reduced from the design life that is obtained based on the static load. For instance, the load on the perfectly smooth pavement surface is the same as the static load, but the maximum load becomes higher as the present serviceability index (PSI) value increases (Figure not shown). The maximum dynamic load on the PSI 2.0 pavement is about 40% larger than the static load.

The responses of the pavement systems subjected to moving dynamic loads can be obtained using several different methods. In this study, the transformed field domain analysis has been used based on the Fourier transforms in the time, space, and moving space (Kim and Roesset, 1998). The time histories of the pavement stresses under the rear-axle tires are shown in Figure 8. The shapes of the stress time histories are very similar to those of the load time histories. The maximum stress increases as the PSI value decreases. The maximum stress on the PSI 2.0 pavement is about 40% larger than the stress on the perfectly smooth pavement, which is very close to the increment amount in the dynamic load as mentioned previously.

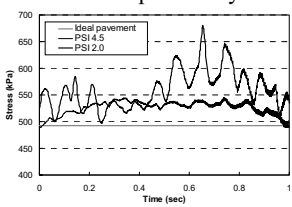

FIG. 7. Stress time history under rear-axle tires for different surface profiles

Once the pavement stresses are obtained, the pavement remaining life can be calculated by means of the AASHTO load equivalency factor that may be approximated by the fourth power law as follows:

$$LEF_i = \left(\frac{Stress\ due\ to\ axle\ load\ i}{Stress\ due\ to\ 18\ kip\ axle\ load}\right)^4 \quad (1)$$

where LEF_i is the load equivalency factor of an axle load i. If the stress time histories shown in Figure 7 are considered, the load equivalency factors can be obtained as shown in Figure 8(a). The remaining life of the pavement is inversely proportional to the load equivalency factor and can be defined by

$$Pavement\ Remaining\ Life = 1 / LEF \quad (2)$$

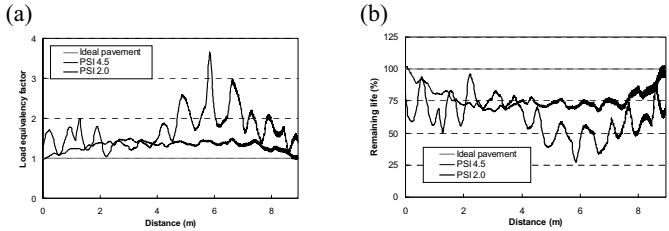

FIG. 8. (a) Load equivalency factor, (b) Remaining life

Figure 8 shows the remaining life of the pavement corresponding to the load equivalency factor shown in Figure 8(a). The remaining life of the PSI 2.0 pavement near the distance of 6m is about 25% of the design pavement life as shown in Figure 8(b). It is noted that the dynamic load factor can be substituted for the stress ratio in the load equivalency factor because the ratio of the stress is very close to the ratio between the dynamic load and the static load.

CONCLUSIONS

- The surface roughness affects the moving dynamic vehicle loads and as the surface roughness increases, the dynamic loads become much larger than the static loads.
- The magnitude of the dynamic loading is almost linearly proportional to the surface roughness amplitude and increases significantly compared with the static load when the roughness wavelength is short and the vehicle speed is high.
- The method to find the relationship between the surface roughness and the pavement performance was proposed and the remaining life of pavement can significantly be reduced as the surface profile becomes rougher.

ACKNOWLEDGMENTS

The research described in this paper was sponsored by Korea Institute of Construction and Transportation Technology Evaluation and Planning, and was part of a study on the standardization of construction criteria based on performance.

REFERENCES

Center for Transportation Research. (1992). *Structural dynamic simulation for MLS*, Computer Program, The University of Texas at Austin.

Ceylan, H., Kim, S., Gopalakrishnan, K., and Wang, K. (2007). "Environmental effects on deformation and smoothness behavior of early-age jointed plain concrete pavements." *Transportation Research Record – J. Transportation Research Board*,

National Academies, Vol. 2037: 30-39.

Kim, S.M. and Roesset J.M. (1998). "Moving loads on a plate on elastic foundation." *J. Engineering Mechanics*, ASCE, Vol. 124 (9): 1010-1017.

Kim, S.M., Roesset, J.M., White, T. D., and Hugo, F. (1995). "Dimensional analysis of the Mobile Load Simulator action on pavements." *Report 2914-1F*, Center for Transportation Research, The University of Texas at Austin.

McGhee, K.K., Gillespie, J.S. (2007). "Value of pavement smoothness." *Transportation Research Record – J. Transportation Research Board*, National Academies, Vol. 2040: 48-54.

Papagiannakis, A.T., Zelelew, H.M., and Muhunthan, B. (2007). "Wavelet analysis of energy content in pavement roughness and truck dynamic axle loads." *Transportation Research Record – J. Transportation Research Board*, National Academies, Vol. 2005: 153-159.

Weights Comparison of Pavement Surface Distress Indexes in China and the US

Ziping Chiang[1], Chine-Ta Chen[2], Po-Hsun Sung[3], and Jyh-Dong Lin[4]

[1]Assistant Professor, Department of Logistics and Marketing Management, Leader University, No.188, Sec. 5, Anjhong Rd., Tainan 709, Taiwan (R.O.C.); ziping@mail.leader.edu.tw
[2]Ph.D Candidate, Department of Civil Engineering, National Central University, No.300, Jhongda Rd., Jhongli, Taoyuan 320, Taiwan (R.O.C.); u9039400@cc.ncu.edu.tw
[3]Ph.D Candidate, Department of Civil Engineering, National Central University, No.300, Jhongda Rd., Jhongli, Taoyuan 320, Taiwan (R.O.C.); 963402007@cc.ncu.edu.tw
[4]Professor, Department of Civil Engineering, National Central University, No.300, Jhongda Rd., Jhongli, Taoyuan 320, Taiwan (R.O.C.); jyhdongl@ncu.edu.tw

ABSTRACT: Different pavement surface distress indexes have been developed in different regions in order to meet different engineering demands. Thus, a special pavement distress index can show the unique characteristics of a specific region. In this paper, we analyze and compare the weights of distress types for the PCI (Pavement Condition Index), the PCR (Pavement Condition Rating), and for the pavement condition index that was developed in Mainland China (PCI_MC). In order to estimate the weights of the PCI distress types, the integral method is used to calculate the area using a deduct value curve. Based on a normalization method, we set the M level of Alligator Cracking as a basic unit and show the distress type sequence for the PCI, PCR, and the PCI_MC. The descriptive statistics indicating the severity of the distress types for the three indexes are shown. Engineers who want to develop a new pavement distress index specific to the special demands of a particular region should consult the differences among these three indexes.

INTRODUCTION

The pavement surface distress index is one of the most important key performance indicators in pavement management systems. The administrators of road management in transportation organizations set the threshold of pavement surface distress indexes in order to provide data for pavement life cycle analysis. Thus, an optimal strategy for costs and benefits can be planned based on many mathematical algorithms. Many pavement surface distress indices have been developed by scholars. One of the most famous indices is the Pavement Condition Index (PCI) which was proposed by the U.S. Army Corps of Engineers. The PCI is based on a visual survey of the pavement and also on a numerical rating of the pavement condition that ranges from 0 to 100, with 0 being the worst possible condition, and 100 being the best

possible condition. The PCI is widely used in transportation and civil engineering, and is a statistical measure that requires a manual survey of the pavement. (Darter and Shahin 1980, Shahin et al. 1987, Shahin et al. 2003, and Shahin 2005) The process of a PCI survey involves the following 5 steps: (ASTM-D6433 1999)
Step 1: Divide the total pavement section into sample units.
Step 2: Based on the number of sample units in the total section, a certain number of these units are selected for testing.
Step 3: The type, extent and severity of pavement distress in each section are recorded using the ASTM Standard D 6433-99 method.
Step 4: The PCI of each tested sample unit is calculated using the method defined in the standard. In summary, this involves calculating the distress quantities and the distress densities for each tested unit. These values are used to determine a deduct value, and this deduct value is subtracted from 100 to give the PCI value.
Step 5: The PCI of the total section is then determined based on the sample values.

Many regions measure the performance of pavement by the PCI and formulate the road maintenance schedule based on this calculation. But in other regions, the road administrators use their own methods to estimate the scores of pavement surface distress conditions. For example, the Pavement Condition Rating (PCR) was developed and used in the Ohio Department of Transportation. (Saraf 1998) The steps for calculating the PCR are similar to that of the PCI, but the PCR uses a fixed deduct value instead of deduct value curves, as shown in figure 1. Based on figure 1, it can be seen that the distress types for the PCR and PCI are different. The function of the PCR can be shown as equation 1:

$$PCR = 100 - \sum_{i=1}^{n} Deduct_i, \tag{1}$$

where n is number of observable distresses, and
$Deduct_i$ is the product of *ith* weight for distress, severity, and extent.

Mainland China has also developed its own calculating process for pavement condition indexes. [7] In order to discriminate between the PCIs that are described in ASTM D6433-99, we labeled the PCI calculating process for Mainland China as PCI_MC. The PCI_MC is calculated by the Distress Rating (DR). The function of the PCI_MC can be shown as equation 2:(JTJ-073.2 2001)

$$PCI\_MC = 100 - 15 \cdot DR^{0.412}, \tag{2}$$

$$DR = \sum_{i=1}^{19} \sum_{j=1}^{3} (D_{ij} \cdot K_{ij} / A),$$

where D_{ij} is the distress area (m^2) for *ith* distress type, *jth* severity level;
K_{ij} is the transformed coefficient for *ith* distress type, *jth* severity level, and
A is the road sample area (m^2).

Section: _____ Date: _____

Log mile: _____ to_____ **FLEXIBLE** Rated by: _____

Sta: _____ to_____ _____

PAVEMENT CONDITION RATING FORM

DISTRESS	DISTRESS WEIGHT	SEVERITY WT.*			EXTENT WT.**			DEDUCT POINTS***
		L	M	H	O	F	E	
RAVELING	10	0.3	0.6	1	0.5	0.8	1	
BLEEDING	5	0.8	0.8	1	0.6	0.9	1	
PATCHING	5	0.3	0.6	1	0.6	0.8	1	
POTHOLES/DEBONDING	10	0.4	0.7	1	0.5	0.8	1 ✓	
CRACK SEALING DEFICIENCY	5	1	1	1	0.5	0.8	1	
RUTTING	10	0.3	0.7	1	0.6	0.8	1 ✓	
SETTLEMENT	10	0.5	0.7	1	0.5	0.8	1	
CORRUGATIONS	5	0.4	0.8	1	0.5	0.8	1	
WHEEL TRACK CRACKING	15	0.4	0.7	1	0.5	0.7	1 ✓	
BLOCK AND TRANSVERSE CRACKING	10	0.4	0.7	1	0.5	0.7	1 ✓	
LONGITUDINAL JOINT CRACKING	5	0.4	0.7	1	0.5	0.7	1	
EDGE CRACKING	5	0.4	0.7	1	0.5	0.7	1	
RANDOM CRACKING	5	0.4	0.7	1	0.5	0.7	1 ✓	
							TOTAL DEDUCT =	
							SUM OF STRUCTURAL DEDUCT (✓) =	
							100 - TOTAL DEDUCT = PCR =	

*L = LOW **O = OCCASIONAL

M = MEDIUM F = FREQUENT

H = HIGH E = EXTENSIVE

*** DEDUCT POINTS = DISTRESS WEIGHT X SEVERITY WT. X EXTENT WT.

REMARKS:

FIG. 1. The pavement condition rating form. (Saraf 1998)

The distress types for PCI_MC include Alligator Cracking, Irregular Cracking, Longitudinal Cracking, Potholes, Transverse Cracking, Raveling, Depression, Rutting, Swell, Bleeding, and Patching. The above pavement surface distress indexes, which have been developed in many areas, have different calculating methods based on dissimilar location characteristics or because of different considerations on the part of the road managers. The differences between the PCR and the PCI_MC can be estimated easily because of their similar calculating processes. However, the PCI is difficult to compare with other pavement surface distress indexes. Thus, we show a method to combine the deduct value curves into a single value.

THE WEIGHTS OF DISTRESS TYPES OF PCI

Based on the ASTM D6433, Shahin et al. (1987), and Shahin (2005), the weight of PCI distress types are hidden in the Deduct Value Curves (DVC). However, it is hard to measure the objective comparison by the curves of distress types. Thus, we use integral method to calculate the area using the deduct value curves. For example, the deduct value curves for alligator cracking are shown in figure 2. We set three areas under the L level (i), M level (i+ii), and H level (i+ii+iii) curves.

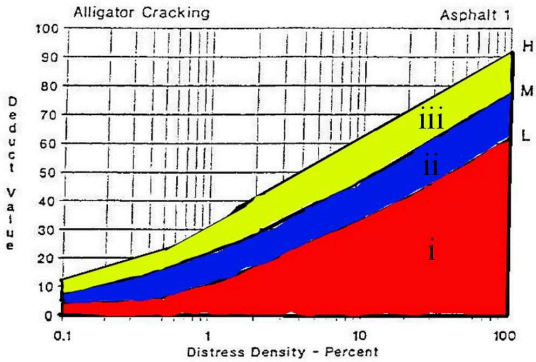

FIG. 2. The deduct value curves of alligator cracking.

We got the DVC functions from the MicroPAVER system and calculated the areas using Mathematica software. The areas of the three levels (L, M, and H) of alligator cracking are 167.4, 241.1, and 315.3, respectively. Based on this process, the areas of all distress types can be shown as table 1.

Table 1. The Areas of Deduct Value Curves

Distress Type	L Level		M Level		H Level	
	Area	Ratio	Area	Ratio	Area	Ratio
Alligator Cracking	167.4	0.69	241.1	1.00	315.3	1.31
Bleeding	23.7	0.10	65.6	0.27	124	0.51
Block Cracking	44.1	0.18	81.8	0.34	149.7	0.62
Bumps and Sags	50.5	0.21	124.4	0.52	235.5	0.98
Corrugation	72.7	0.30	197.7	0.82	318.4	1.32
Depression	102.1	0.42	151.2	0.63	216	0.90
Edge Cracking	26.8	0.11	63.1	0.26	103.5	0.43
Joint Reflection Cracking	32.8	0.14	81.9	0.34	157.3	0.65
Lane/Shoulder Drop-Off	18.6	0.08	31.3	0.13	53.5	0.22
Longitudinal/Transverse Cracking	40.7	0.17	85.2	0.35	174.7	0.72
Patching and Utility Cut Patching	51.9	0.22	114.7	0.48	192.5	0.80
Polished Aggregate	21.8			0.09		
Potholes	257.9	1.07	359.6	1.49	443	1.84
Railroad Crossing	36.4	0.15	112.5	0.47	204.3	0.85
Rutting	126.6	0.53	206.1	0.85	285.9	1.19
Shoving	66.4	0.28	121.2	0.50	185.2	0.77
Slippage Cracking	118.6	0.49	187.5	0.78	279.3	1.16
Swell	29.7	0.12	88.4	0.37	145.3	0.60
Weathering and Raveling	27.9	0.12	101.1	0.42	105.1	0.44

The distress types for PCI_MC include Alligator Cracking, Irregular Cracking, Longitudinal Cracking, Potholes, Transverse Cracking, Raveling, Depression, Rutting, Swell, Bleeding, and Patching. The above pavement surface distress indexes, which have been developed in many areas, have different calculating methods based on dissimilar location characteristics or because of different considerations on the part of the road managers. The differences between the PCR and the PCI_MC can be estimated easily because of their similar calculating processes. However, the PCI is difficult to compare with other pavement surface distress indexes. Thus, we show a method to combine the deduct value curves into a single value.

In order to make a comparison of the PCR and the PCI_MC, we set the ratio of the M level of Alligator Cracking as 1, and the distress types in each level are shown in the ratio column in table 1.

ANALYSIS AND DISCUSSIONS

Based on table 1, we have the distress weights for each severity level of the PCI. We multiply the weight for distress by the weight of the severity level of the PCR and also set the ratio of the M level of Wheel Track Cracking (Alligator Cracking) as 1. The product is shown as table 2.

Table 2. The Ratios of Each Severity Level of PCR

Distress Type	L Level Ratio	M Level Ratio	H Level Ratio
Raveling	0.29	0.57	0.95
Bleeding	0.38	0.38	0.48
Patching	0.14	0.29	0.48
Potholes/Debonding	0.38	0.67	0.95
Cracking Sealing Deficiency	0.48	0.48	0.48
Rutting	0.29	0.67	0.95
Settlement	0.48	0.67	0.95
Corrugations	0.19	0.38	0.48
Wheel Track Cracking	0.57	1.00	1.43
Block and Transverse Cracking	0.38	0.67	0.95
Longitudinal Joint Cracking	0.19	0.33	0.48
Edge Cracking	0.19	0.33	0.48
Random Cracking	0.19	0.33	0.48

Based on table 1, table 2 and the *K* factor of the PCI_MC, we know the following:

1. The considered distress types of three indexes are quite different. For example, only the PCI considers Railroad Crossing; the PCR and the PCI_MC do not include this distress type.
2. The PCI distress type sequence (from important to inconsequential) are Potholes, Alligator Cracking, Rutting, Corrugation, Slippage Cracking, Depression, Bumps and Shoving, Patching and Utility Cut Patching, Railroad Crossing, Longitudinal/Transverse Cracking, Block Cracking, Joint Reflection Cracking,

Swell, Weathering and Raveling, Bleeding, Edge Cracking, Lane/Shoulder Drop-Off, and Polished Aggregate.

3. The PCR distress type sequence (from important to inconsequential) are Wheel Track Cracking, Settlement, Potholes/Debonding, Block and Transverse Cracking, Rutting, Raveling, Cracking Sealing Deficiency, Bleeding, Corrugations, Longitudinal joint Cracking, Edge Cracking, Random Cracking, and Patching.
4. The PCI_MC distress type (from important to inconsequential) are Swell, Sags, Potholes, Alligator Cracking, Edge Cracking, Depression, Depression, Rutting, Bumps, Shoving, Peeling, Polished Aggregate, Longitudinal Cracking, Irregular Cracking, Transverse Cracking, Raveling, Weathering, Bleeding, and Patching.
5. We assume that the distribution of the three severity levels (L:M:H) are 1:2:1. The descriptive statistics for the three pavement surface distress indexes are quite different. The results can be shown as table 3.

Table 3. The Descriptive Statistics of Distress Types' Severity of the PCI, PCR, and the PCI_MC

	PCI	PCR	PCI_MC
Mean	0.54	0.52	0.71
Variance	0.11	0.04	0.14
Skewness	2.14	0.58	-0.99
Kurtosis	1.28	0.91	-0.31
Range	1.38	0.70	1.13
Minimum	0.09	0.30	0.13
Maximum	1.47	1.00	1.25
Observations	19.00	13.00	19.00

CONCLUSIONS

Pavement surface distress indexes are key factors with regard to the planning and scheduling of pavement maintenance. Many different indexes have been developed for solving different engineering issues in different regions. In this paper, we analyze and compare the weights for PCI, PCR, and PCI_MC distress types. For the purpose of estimating the weights of the distress types for the PCI, the integral method is used to calculate the area of using the deduct value curve. We obtain the PCI, PCR, and the PCI_MC distress type sequences, and finally, the descriptive statistics for the severity of the distress types for the three indexes are shown.

ACKNOWLEDGMENTS

The authors appreciate the support of the NSC 97-2221-E-426 -009.

REFERENCES

ASTM-D6433. (1999). *Standard Practice for Roads and Parking Lots Pavement Condition Index Surveys*, American Society for Testing and Materials.

Darter, M.I., and Shahin, M.Y. (1980). "Pavement Rehabilitation: Identifying the Need." *Journal of Transportation Engineering*, Vol. 106 (1), 1-10.

JTJ-073.2. (2001). *Technical Specifications for Maintenance of Highway Asphalt Pavement* China Communications Press, Beijing. (In Chinese)

Saraf, C. L. (1998). *Pavement Condition Rating System Review of PCR Methodology*, Ohio Department of Transportation, Columbus.

Shahin, M.Y. (2005). *Pavement Management for Airports, Roads, and Parking Lots*, Springer US, New York.

Shahin, M.Y., Burkhalter, J.A., and Wilken, G.A. (2003). *Micro PAVER Version 5.1 User Manual*, Construction Engineering Research Laboratory, US Army Corps of Engineers.

Shahin, M.Y., Nunez, M.M., Broten, M.R., Carpenter, S.H., and Sameh, A. (1987). "New Techniques for Modeling Pavement Deterioration." *Transportation Research Record*, Vol. 1123, 40-46.

Studies on Risk Management of the Urban Infrastructure Projects Based on the BOT Financing Model

Hanli Chen[1] and Tao Qin[2]

[1] Central South University, School of Civil and Architectural Engineering, Tel: (86)13787210114; chenhanli2008@sina.com.cn

[2]Hunan Party School and Hunan Administration School, Tel: (86)15873146128; Qintao5cn@sina.com.cn

ABSTRACT: With the acceleration of urbanized advancement in China, governments' high investment and low efficiency in urban infrastructure projects have already become a worldwide problem. The BOT financing model can be combined with government policy supports, investor's abundant fund and advanced management. The BOT financing model in urban infrastructure projects has greater risks, so their risk management is of great significance. The paper establishes risk evaluation index system of urban infrastructure projects on the BOT financing model, and sets up the risk evaluation model by use of Analytic Hierarchy Process (AHP) and Fuzzy Mathematics. We partially modify weight of AHP, by Fuzzy Cluster Analysis. Next, we establish the risk allocation model of urban infrastructure projects. Finally, we carry empirical analysis about the risk problem of an urban infrastructure project. Through comparing with result of model evaluation and measure of the risk allocation, empirical analysis indicates that the evaluation result of the model can reflect the risk situation of project thoroughly and objectively.

KEYWORDS: urban infrastructure projects; BOT financing model; risk analysis; fuzzy comprehensive evaluation; allocation of risks

INTRODUCTION

Recent years, with China's rapid economic development and the acceleration of urbanization, the existing urban infrastructure projects have been far from satisfying the development needs of the national economy. At the same time, the Government’s

high input, low efficiency and high consumption of resources have become a worldwide problem in urban infrastructure construction. The BOT financing model can be combined with government policy supports, private investors' abundant capital and advanced management mode, and now has been better applied in China's urban infrastructure construction. Because urban infrastructure projects Under the BOT model have long duration, the large amount of investment, complex relationship between rights and obligations, their projects face great risks and their risks have been core issues, which are common interest issues by the various participants.

1. ESTABLISHING RISK EVALUATION INDEX SYSTEM IN BOT FINANCING MODEL OF THE EXPRESSWAY PROJECTS

BOT, which is Build－Operate－Transfer, is model in developed countries which is developed a model of foreign investment or domestic private capital in infrastructure construction. The BOT financing model for urban infrastructure construction have their own advantages in national policy support, private investors will and practical experience. So the application of BOT financing model to urban infrastructure projects has its unique applicability. The risk of urban infrastructure projects under the BOT financing model those uncertain events throughout the life cycle which may have uncertain impacts on project's financing, construction, operation, or likely lead to loss or damage of urban infrastructure projects and the failure of the project at last. In BOT financing model, besides the same characteristic as general projects' risks, urban infrastructure projects' risks also have short-term, complex, long cycle characteristics. Because the cross impacts exist between the various risks factors with outside world, risks have diversity and the multilevel nature. In this paper, according to risk factors and urban infrastructure projects' relationship, we classify risks of urban infrastructure projects and establish risk evaluation index system.

2. ESTABLISHING RISK ASSESSMENT MODEL BASED ON FUZZY COMPREHENSIVE EVALUATION METHOD

Fuzzy comprehensive evaluation method enables all parties involved in the project to apply its corresponding risk assessment results and to realize how many project commitment risk, to all parties involved in the project provide theoretical basis for the decision-making. According To the BOT project risk assessment structure, the risk assessment will use two-stage fuzzy comprehensive evaluation methods.

2.1 Determining Factors and their Levels

BOT projects have nine major risk factors, which are recorded as X_P (P = 1, 2, … , 9). Indicators of risk factors set are X = (X_1, X_2, X_3… X_p), whose corresponding weight set is A = (a_1, a_2, a_3… a_p), in which a_K (K = 1, 2… P) denote proportion of X_K in the X, and $\Sigma\, a_K = 1$.

2.2 The Use of Fuzzy Clustering Analysis to Establish a Weight Set of Modification Index

First, after we treat data by analytic hierarchy process, we can get weight matrix as follows:

$$W = \begin{bmatrix} W_{11} & W_{12} & \cdots & W_{1n} \\ W_{21} & W_{22} & \cdots & W_{2n} \\ \cdots & \cdots & W_{ij} & \cdots \\ W_{m1} & W_{m2} & \cdots & W_{mn} \end{bmatrix} \tag{1}$$

Where W_{ij} is that the ith expert judge j to the jth indicator‘s importance after AHP treatment, m denotes the number of experts, n denotes the number of indicators. Second, in order to determine discrete level of experts’ weight in judge matrix, similarity coefficients between weights are calculated, and thus similar coefficient matrix is formed. Similar coefficient R_{ij} and similar coefficient matrix R are as follows:

$$R_{ij} = 1 - \sqrt{\frac{1}{n}\sum_{k=1}^{n}(W_{ik} - W_{jk})^2} \tag{2}$$

$$R = \begin{bmatrix} R_{11} & R_{12} & \cdots & R_{1m} \\ R_{21} & R_{22} & \cdots & R_{2m} \\ \cdots & \cdots & R_{ij} & \cdots \\ R_{m1} & R_{m2} & \cdots & R_{mn} \end{bmatrix} \tag{3}$$

Where R_{ij} is similar degree of weight results between the ith expert and the jth expert. The smaller the R_{ij} , the smaller the similar degree.

After eliminating divorced large degree’s weight, we can use cluster analysis approach:

$$P_i = \sum_{j=1}^{n} R_{ij} \tag{4}$$

$$P = (P_1, P_2, \cdots P_n)^T \tag{5}$$

P_i is the sum of similar matrix's every row, which denotes the degree of deviation between the ith expert's weight opinion and other experts' weight opinion. P is a line which is the sum of a row in similar matrix.
Finally, we use the degree of deviation's quantitative indicators to measure the views of various experts, and determine the degree of deviation through Eq. (6). In other words, when D_i is larger than a certain threshold, this view should be ruled out.

$$D_i = \frac{P_{\max} - P_i}{P_{\max}} \times 100\% \tag{6}$$

Where D_i is the degree of deviation of the ith expert's similar coefficient and the greatest similar coefficient. P_{max} is the maximum in the similar coefficient matrix.

2.3 Establishment of Evaluation Set

Through the evaluation set to give the benchmark, evaluation set can be expressed as $V = (V_1, V_2, V_3 \ldots V_n)$, in which V_j (j = 1, 2… n) shows the jth possible results of indicators of risk factors evaluation.

2.4 Establishment of Fuzzy Evaluation Matrix

Choose some experts to form risk assessment team. According to the given evaluation benchmark they can evaluate the risk of the project. This evaluation is a fuzzy mapping. Even (if) to the same risk's assessment, different assessment experts can make different assessment, so these assessment results can only be expressed as the possible degree of the ith factor to the jth evaluation scale. The kind of possible degree is called degree of subjection, denoted as M_{ij}.
So the fuzzy evaluation matrix from the X_K to evaluation set v is:

$$M = \begin{bmatrix} M_{11} & M_{12} & \cdots & M_{1m} \\ M_{21} & M_{22} & \cdots & M_{2m} \\ \cdots & \cdots & M_{ij} & \cdots \\ M_{m1} & M_{m2} & \cdots & M_{mn} \end{bmatrix} \tag{7}$$

Where M_{ij} (i = 1, 2… m; j = 1, 2… n) is the membership degree that is the risk factors of the indicators X_{ki} to the j-level remarks.

2.5 Fuzzy Comprehensive Evaluation

First, we do fuzzy matrix operations for the evaluation matrix R_k of the risk factors of indicators X_{ki}, and can get membership vector B_K of major risk factors index X_K to evaluation set V, in which $B_K=A_K \times R_K=$（b_{k1}，b_{k2}，…b_{km}）:

$$B_K = \begin{pmatrix} B_1 \\ B_2 \\ \\ \cdots \\ B_m \end{pmatrix} = \begin{pmatrix} b_{11} & b_{12} & \cdots & b_{1n} \\ b_{21} & b_{22} & \cdots & b_{2n} \\ & & & \\ \cdots & \cdots & \cdots & \cdots \\ b_{m1} & b_{m2} & \cdots & b_{mn} \end{pmatrix} \tag{8}$$

Next, to do fuzzy matrix calculation for R, we can get membership vector B_K of aim layer index X to evaluation set V: When $\Sigma\, b_j \neq 1$, assume $b_j' = b_j / \Sigma\, b_j$, we can get : $B' = (b_1', b_2' \cdots b_n')$.B' is membership vector B_K of aim layer index X to evaluation set V. and b_1', b_2'… b_n' respectively denote X to reviews V_1, V_2… V_n 's membership degree. Finally, a final conclusion is made by the largest degree of membership or the weighted average statutory principles.

$$B = A \times B_K = (a_1\ a_2 \cdots a_p) \begin{pmatrix} B_1 \\ B_2 \\ \cdots \\ B_P \end{pmatrix} = (b_1\ \ b_2 \cdots b_n) \tag{9}$$

2.6 Quantitative Evaluation

When we determine evaluation criteria, standard rank should be quantified as possible, i.e. use numerical value to express various grades' risk. So it is easy to judge and value relative share risks to all participants in the project.

The final value of risk assessment results are as follows:

$$U = B \times V \tag{10}$$

Its evaluation values can more clearly measure the risk extent and results can be compared.

3. RISK-SHARING OF URBAN INFRASTRUCTURE PROJECTS' BOT FINANCING MODEL

Suppose there are n project participants, which are respectively numbered 1, 2… n. The project has a total of m kinds of risks, which are respectively numbered 1, 2… m. We use $r_i^j \ (1 \le i \le n, 1 \le j \le m)$ to express the ith project participant's the jth kind of risk.

The cost and revenue of risk is closely connected. If any one wants to achieve gains, he will have to pay certain price. In general, the income and the price are positively related, that is, t he higher the cost, the higher the expected income.

The ith project participant's yield $y_i = y_i\left(r_i^1, r_i^2, \cdots, r_i^m\right) \quad i = 1,2,\cdots,n$

The ith project participant's cost $c_i = c_i\left(r_i^1, r_i^2, \cdots, r_i^m\right) \quad i = 1,2,\cdots,n$

Various participants in the project are willing to take risks, because their projects can bring benefits to them and the yield of project is bigger than the cost of project. Use $p_i=y_i-c_i$ to denote the satisfaction of the ith project. Risk-sharing's goal is to make risk-sharing projects' overall satisfaction to the greatest satisfaction under certain preconditions. In any case, the most suitable party to undertake the risk should be starting point which participants of BOT projects deal with the risk-sharing issue. Only in this way, can the degree of overall satisfaction achieve the greatest degree of overall satisfaction, so that the project participants can maximize their interests.

4. EMPIRICAL ANALYSIS OF RISK MANAGEMENT BASED ON BOT FINANCING MODEL'S URBAN INFRASTRUCTURE PROJECTS

4.1 Use of AHP and Fuzzy Clustering Analysis to Determine the Index's Weight

Taking an expressway BOT financing project in China as an example. Six experts were invited to compare and grade indicators. The obtained index weight matrix which is disposed by AHP. The evaluation index weight of the target level can also be obtained by the same methods:

W=(0.115，0.164，0.124，0.065，0.201，0.121，0.062，0.038，0.110)

4.2 Establishing Membership Matrix and Performing Fuzzy Comprehensive Evaluation from the Project Operator

20 experts are invited to score the risk indicators, according to the results of the risk

factors and the weight of the project measure risk. Evaluation results are shown in Table 1.

According to the datum in the table 1, fuzzy comprehensive evaluation set Bi of the risk indicators can be gained:

$$B_1 = A_1 R_1 = (0.0222 \quad 0.1938 \quad 0.2902 \quad 0.3170 \quad 0.1778) \tag{11}$$

Passing the fuzzy evaluation matrix of target layer obtain risk evaluation set B_{yy}.

$$B_{yy} = AB_K = (0.046467 \quad 0.164770 \quad 0.246457 \quad 0.403413 \quad 0.138906) \tag{12}$$

Table 1 Risk Fuzzy Evaluation of an Expressway BOT Project

Evaluation factors and weights		**Evaluation ratings and membership degrees**				
The first rank factors and weight	Second rank factors and weights	Project operators				
		V_1	V_2	V_3	V_4	V_5
Political risks X_1 (0.115)	National sovereignty risk X_{11}(0.222)	0.1	0.6	0.2	0.1	0
	State legal risks X_{12}(0.219)	0	0.1	0.3	0.5	0.1
	The state's tax risk X_{13}(0.147)	0	0.1	0.5	0.3	0.1
	Government confiscation of risk X_{14}(0.240)	0	0.1	0.3	0.3	0.3
	Risk of unstable political environment X_{15}(0.173)	0	0	0.2	0.4	0.4
※Taking political risk as an example.						

4.3 Comprehensive Assessment of the Parties Involved in the Project

In order to more intuitively assess the risk size of the parties involved in the project, the evaluation can be converted into a specific set of values, for all parties involved in the project so that it is easy to compare its size of borne risks.

Operators' comprehensive risk evaluation U_{yy}:

$$U_{yy} = B_{yy} \cdot V = 4.152 \tag{13}$$

Government departments' comprehensive risk evaluation: $U_{zf} = 3.602$.

Contractor's comprehensive risk evaluation: $U_{cb} = 6.430$

Investors comprehensive risk evaluation: $U_{tz} = 4.518$

From the results above, we can see that the largest risks of the expressway project in China are borne by the contractor, the second largest risks are borne by the investors, and smallest risks are borne by the operators and government departments.

CONCLUSIONS

In the project, the project company and the general contractor signed a fixed-period, fixed-price "turnkey" contract. The project's risk will be completely shifted from the project company to the project contractors, and the higher value result based on the contractor's risk assessment precisely confirms such a situation.

To sum up, the project's risk-sharing measures are more reasonable and successful. This model can more comprehensively and objectively reflect the project risks, thus providing a theoretical basis for the risk decision-making and risk management of the parties involved in the project.

ACKNOWLEDGMENTS

The author is very grateful to Peter Moles and Patrick T for their work on the original version of this paper.

REFERENCES

Jonathan P. Doh and Ravi Ramamurti (1999). "Reassessing Risk in Developing Country Infrastructure." *Long Range Planning*, 36:337-353.

Peter Moles, and Geoffrey Williams (1995). "Privately funded infrastructure in the UK: participants' risk in the Skye Bridge project." *Transport Policy*, 2(2):129-134.

Patrick, T. I. Lam (2004). "A sartorial review of risks associated with major infrastructure projects." *International Journal of Project Management*, 17:77-87.

Analyzing the Cause of Asphalt Pavement Rut Damage of Heng-Zao Freeway

Renjie QIN [1], LI Yuzhi[1] and LI Zhenke[1]

[1]School of Traffic and Transportation Engineering,Changsha University of Science and Technology, Changsha, Hunan, 410076, P.R.China, e-mail: rjqin@126.com.

ABSTRACT: Asphalt mixture is a viscous-elastic-plastic material, its performance changes with the conditions of the environment temperature and traffic loading. Although lots of measures have been taken from design to construction to control asphalt pavement early damages, such as selecting raw material and asphalt cementation material, mixture gradation, mixture mechanics capability, construction technology, and testing standards. But most freeways in China have still suffered early damages. In south regions, rut and water damages are the main problem because of the rainy climate and high environment temperature. According to the investigations of the existing traffic of Heng-Zao freeway in Hunan province and the axle-load condition, rut depth, on-site core samples, extracting test, thickness, field sampling and indoor rut test, the paper firstly analyzes the present condition, evaluates the pavement performance and construction technology, then analyzes the gradation type, finally summarizes all the possible causes of serious rut of the freeway. These can provide the references for the pavement design and construction in south regions.

INTRODUCTION

With the development of social economy, road traffic volume is increasing rapidly, especially the use of the heavy vehicle and high pressure tyre, rut damage of asphalt pavement is getting worse and worse and has become one of the most main damage in high-temperature areas. Freeway asphalt pavement rut in China is a quite common damage, especially during the period of continuous high temperatures in 2003, which happens once every 50 years. As an example, Beijing-Zhuhai freeway in Hubei province, with a total length of 339km, which opened to traffic in 2002, has been suffering from the very heavy rut damage this time, and the maximum rut depth is over 10cm (Huang, 2007) because of the heavy traffic, overloading and particularly the continuous high temperature. As the pavement performance has been damaged badly, it has to be repaved along the whole route that year.

Most high-grade highway in China is semi-rigid base asphalt pavement. Pavement rut mainly comes from the permanent deformation of asphalt concrete layers. Rutted pavements have poor smoothness, safety and service quality, and serious rut damage may destroy pavement structure, which shortens the pavement

service life greatly (Su, 2007). The main factors that affect rut depth are two: the internal factors are the asphalt pavement structure and asphalt concrete performance; the external factors include the climate, traffic volume, and traffic composition.

RUT CAUSES INVESTIGATION OF HENG-ZAO FREEWAY

Heng-Zao freeway, which opened to traffic in December 2003, starts from the Hongshi entrance of Xiangtan-Leiyang freeway, vias Hengyang, Yongzhou, and ends at Zaomupu which borders on Guangxi province. The total length is 185.427 kilometers, and nearly 83 kilometers were paved with asphalt material. The pavement structure is: 4cm modified SMA-13 +5cm AC-20I +6cm AC-25I +20cm Cement Stabilized Gravel+18cm Cement Stabilized Grit +18cm Cement Stabilized grit.

Traffic Investigation

In order to obtain the axle-load condition of the freeway, we have investigated the vehicle axis load of the toll stations along the main route for 24hours continuously. Firstly vehicles are classified by their different axle type (show in Table 1), then we select some axle loads randomly to get the ratio of different axle load (including the front axle, medial axle, rear axle). Based on the actual traffic volume data, Axle Load Spectrum is shown in Fig.1 finally:

Table 1. Classification of Vehicles In Traffic Investigation

Large class of vehicle	Vehicle classification	Axle number
Passenger car	Mini-bus	single-front axle +single-rear axles
	large and medium bus	single-front axle +single-rear axles
Freight car	minivan	single-front axle +single-rear axles
	large and medium truck	single-front axle +single-rear axles
		single-front axle + double-rear axles
	semi-trailer	single-front axle+ single-medial axle + single-rear axles
		single-front axle+ single-medial axle +double-rear axles
		single-front axle+ double-medial axle +double-rear axles
		single-front axle+ double-medial axles +three-rear axles

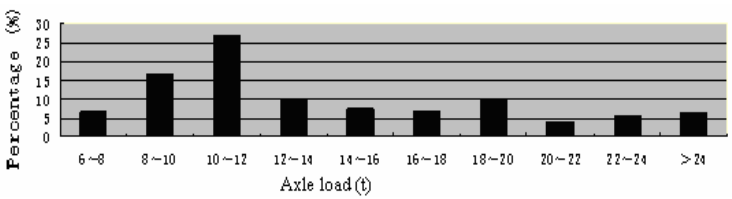

Fig.1. Axle Load Spectrum of Heng-Zao Freeway

The annual average growth rate of traffic volume of Heng-Zao freeway reaches to 1.6% actually, and the measured daily average axle load of design lane is 18578 times

per day in 2006.

Rut Survey

According to the current criterion, rut depths were measured with 3m straight ruler and road smoothness measuring equipment on the typical section of Heng-Zao freeway. The test data shows in Table 2.

Table 2. Average Rut Depths and Average IRI of typical pavement

Section	Stake number	Average rut depths(mm)		Average IRI	
		left range	right range	left range	right range
Heng-Zao Freeway	K65+000～K66+000	10.53	9.42	1.58	1.49
	K66+000～K67+000	11.69	11.46	1.81	1.55
	K67+000～K68+000	9.98	9.57	1.46	1.45
	K68+000～K69+000	11.63	11.63	1.73	1.70
	K69+000～K70+000	9.05	9.30	1.43	1.64
	K70+000～K71+000	8.05	8.66	1.67	1.45
	K71+000～K72+000	5.69	12.74	1.46	1.67
	K72+000～K73+000	8.50	11.18	1.44	1.84
	K73+000～K74+000	13.01	10.37	1.32	3.10
	K74+000～K75+000	11.10	7.91	1.47	2.01
	K75+000～K76+000	11.38	10.92	—	—
	K76+000～K77+000	10.85	15.38	—	—
	K77+000～K78+000	8.96	11.71	—	—

Drill Field Core Samples

Core samples position were distributed to the vehicle lanes and the hard shoulders reasonably, 4core samples from the vehicle lanes (2 samples in wheel paths and 2 in the bulging ruts), and 4 from hard shoulders. Fig. 2 shows the 8 cores positions.

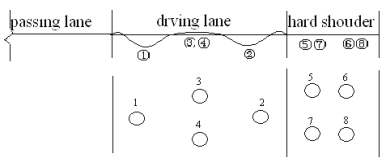

Fig. 2 Schematic Drawing of the Samples Positions

The thickness of each layer was obtained from the samples, and it was compared with the design thickness. The result shows in Table3.

Table 3. Thickness of Pavement with Deeper Rut and Lower Rut

No.	Measured Thickness (cm)				Design thickness(cm)				D-value(cm)				Measured Rut depths (mm)
	Upper layer	Mid layer	Lower layer	total	Upper layer	Mid layer	Lower layer	total	Upper layer	Mid layer	Lower layer	total	
9-1	3.2	4.7	5.4	13.3	4	5	6	15	-0.8	-0.3	-0.6	-1.7	12
9-2	3.1	4.7	5.4	13.2	4	5	6	15	-0.9	-0.3	-0.6	-1.8	
9-3	3.7	4.9	6.2	14.8	4	5	6	15	-0.3	-0.1	0.2	-0.2	
9-4	3.4	5.1	5.9	14.4	4	5	6	15	-0.6	0.1	-0.1	-0.6	
9-5	3.7	5.3	5.5	14.5	4	5	6	15	-0.3	0.3	-0.5	-0.5	
9-6	4.0	5.0	5.6	14.6	4	5	6	15	0.0	0.0	-0.4	-0.4	
9-7	3.9	5.0	5.8	14.7	4	5	6	15	-0.1	0.0	-0.2	-0.3	
9-8	4.0	5.1	5.6	14.7	4	5	6	15	0.0	0.1	-0.4	-0.3	
11-1	3.2	4.9	6.1	14.2	4	5	6	15	-0.8	-0.1	0.1	-0.8	6
11-2	3.3	4.8	5.9	14.0	4	5	6	15	-0.7	-0.2	-0.1	-1.0	
11-3	3.7	5.2	6.0	14.9	4	5	6	15	-0.3	0.2	0.0	-0.1	
11-4	3.5	5.1	6.2	14.8	4	5	6	15	-0.5	0.1	0.2	-0.2	
11-5	3.4	5.4	6.0	14.8	4	5	6	15	-0.6	0.4	0.0	-0.2	
11-6	3.5	5.3	5.9	14.7	4	5	6	15	-0.5	0.3	-0.1	-0.3	
11-7	3.4	5.0	6.3	14.7	4	5	6	15	-0.6	0.0	0.3	-0.3	
11-8	3.5	5.0	6.2	14.7	4	5	6	15	-0.5	0.0	0.2	-0.3	

Tests Result of Asphalt Aggregate Ratio

The aggregate gradation of each asphalt layer is checked and their asphalt content is tested by using samples, the results show in Table 4 and Table 5.

Table 4. The Test Results of Asphalt Aggregate Ratio (%)

Section / Ratio	Upper-Layer		Mid-Layer		Lower-Layer	
	Deeper rut SMA-13	Lower rut SMA-13	Deeper rut AC-20I	Lower rut AC-20I	Deeper rut AC-25I	Lower rut AC-25I
Design	6.2	6.2	4.1	4.1	3.8	3.8
Measured	6.2	6	4.7	4.5	4.5	4.2

Table 5. The Test Data and the Design Data of the Mineral Aggregate Gradation

Aggregate Gradation	Size(Mm)	31.5	26.5	19	16	13.2	9.5	4.75	2.36	1.18	0.6	0.3	0.15	0.08
SMA-13 deeper rut	test	-	-	100.0	100.0	95.9	72.8	33.9	23.2	19.6	15.8	13.9	11.7	8.8
	Design	-	-	100.0	100.0	97.3	59.4	24.5	21.4	17.5	15.3	13.3	12.3	10.0
SMA-13 lower rut	Test	-	-	100.0	100.0	96.8	75.1	35.2	23.2	19.5	16.7	14.4	12.1	8.6
	Design	-	-	100.0	100.0	97.3	59.4	24.5	21.4	17.5	15.3	13.3	12.3	10.0
AC-20I deeper rut	Test	-	100.0	98.3	91.0	84.7	70.9	43.7	33.8	24.7	17.7	14.0	9.9	5.6
	Design	-	100.0	96.9	84.8	71.8	59.0	41.5	31.1	23.8	16.4	12.4	8.9	6.5
AC-20I lower rut	Test	-	100.0	98.3	95.4	83.4	66.4	43.3	32.3	22.8	15.3	12.2	9.2	5.7
	Design	-	100.0	96.9	84.8	71.8	59.0	41.5	31.1	23.8	16.4	12.4	8.9	6.5
AC-25I deeper rut	Test	100.0	100.0	94.7	88.7	80.6	63.5	40.6	32.8	23.8	15.6	12.0	8.6	4.6
	Design	100.0	99.8	79.1	67.4	60.0	49.4	36.1	26.8	20.9	14.9	10.9	8.2	5.4
AC-25I lower	Test	100.0	100.0	90.5	85.7	75.7	64.4	43.3	26.7	18.5	12.7	10.2	7.8	5.0
	Design	100.0	99.8	79.1	67.4	60.0	49.4	36.1	26.8	20.9	14.9	10.9	8.2	5.4

The Dynamic Stability Tests Results of the Combined Samples of Upper-Layer and Mid-Layer

Strip samples are obtained (combined samples of upper layer or upper-layer and mid-layer), and dynamic stability tests are finished in laboratory. Table 6 shows the test results.

Table 6. The Deformation of Mid-Layer Combined Samples about Deeper Rut

Measured Samples	upper layer test thickness (mm)			Maximum depression (mm)	
	left	right	Deepest rut	Upper layer	boundary of upper-layer and mid-layer
From upper-layer and mid-layer with deeper rut	32.3	32.4	31.7	1.0	5.2

ANALYSIS OF THE RUT CAUSE OF HENG-ZAO FREEWAY

According to the survey data, using the method of designing and checking aggregate gradation of asphalt mixture that developed by Sha (Sha, 2005), the paper analyzes the asphalt mixture aggregate gradation of Heng-Zao freeway.

Introduce of VCA_{DRF} Method

According to the VCA_{DRF} method, aggregate gradation is composed of three parts of the coarse aggregate, fine aggregate and filling. However, there still have bitumen and air or pore for asphalt concrete besides the three parts. The boundary size of the coarse aggregate and fine aggregate is 4.75 mm. That is the largest size scope of coarse aggregate is Dmax~4.75mm; fine aggregate is 4.75 mm~0.075mm and filling is less than 0.075mm.

The basic thought of VCA_{DRF} method is to fill the coarse aggregate voids, for different dense and solid aggregates, available void ratio VCA_{DRU} value is the difference of the void ratio VCA_{DR} of the dry coarse aggregate density (dry solid density, generally density and loose density) and the one of the air voids Va, and it is filled by the volume VOLmaB of fine aggregate bitumen. The density of coarse aggregate is the GCA_{DRC} in dry solid condition when testing the dense and solid framework aggregate gradation.

Checking the lower layer AC-25I gradation

Basalt was used for paving upper layer asphalt pavement of Heng-Zao Freeway, and limestone was used for mid layer and lower layer. Table 7 shows the gross bulk density of different material layer.

Table 7. Parameter Values of Different Size about Each Layer Material

Size (mm)	31.5	26.5	19	16	13.2	9.5	4.75	2.36	1.18	0.6	0.3	0.15	0.075
AC-25I G_b(g/cm^3)	2.717	2.700	2.69	2.69	2.68	2.68	2.68	2.67	2.58	2.57	2.56	2.55	2.54
AC-20I G_b(g/cm^3)	/	2.700	2.69	2.69	2.68	2.68	2.68	2.67	2.58	2.57	2.56	2.55	2.54
SMA-13 G_b(g/cm^3)	/	/	/	2.74	2.73	2.72	2.71	2.66	2.65	2.63	2.62	2.59	2.58

The aggregate of lower layer is limestone, if VCA_{DRC}=40%, V_a=4.0% and G_B=1.0334g/cm^3, $G_{a,fi}$ =2.725g/cm^3, then volume parameters can be calculated as shown in Table 8.

Table 8 The Volume Parameters of Lower Layer AC-25I

Project		P_b	P_{ca}	P_{fa}	P_{fi}	GCA_{DRC}	$G_{b,ca}$	$G_{b,fa}$	VCA_{DRU}	$VOL_{ma,B}$
Measured	Deeper rut	4.5	59.4	36	4.6	1.60955	2.68258	2.58961	13.2857	19.9443
	Lower rut	4.2	56.7	38.3	5	1.60993	2.68321	2.61245	12.6789	20.5597
Design		3.8	63.9	30.7	5.4	1.61111	2.68519	2.59769	14.2783	17.4770

The data in Table 8 indicates that, the available void ratio VCA_{DRU} of all the gradations are less than the volume $VOL_{ma,B}$ of asphalt mortar remarkably. The coarse aggregate suspends up in asphalt mortar. This shows it is not the type of dense and solid framework aggregate gradation obviously.

Checking the mid layer AC-20I gradation

The mid layer aggregate material is limestone, if VCA_{DRC}=40%, V_a=4.0% and G_B=1.0334g/cm^3, $G_{a,fi}$ =2.725g/cm^3, then the volume parameters can be calculated, shows in Table 9.

Table 9. The Volume Parameters of Mid Layer AC-20I

Project		P_b	P_{ca}	P_{fa}	P_{fi}	GCA_{DRC}	$G_{b,ca}$	$G_{b,fa}$	VCA_{DRU}	$VOL_{ma,B}$
Measured	Deeper rut	4.7	56.3	38.1	5.6	1.60924	2.68206	2.59325	12.5948	21.2951
	Lower rut	4.5	56.7	37.6	5.7	1.60908	2.68180	2.59803	12.6855	20.9188
Design		4.1	58.5	35	6.5	1.60954	2.68257	2.59801	13.0844	19.8246

Analyzing the data in Table 9, it shows the same results as Table 8 between the VCA_{DRU} and the $VOL_{ma,B}$. Coarse aggregate also suspends up in asphalt mortar.

Checking the upper layer SMA-13 gradation

The mid layer material is basalt, if VCA_{DRC} =40%, Va=4.0% and GB=1.0334g/cm3, Ga,fi =2.725g/cm3, then the volume parameters can be calculated as shown in Table10.

Table 10. The Volume Parameters of Upper Layer

Project		P_b	P_{ca}	P_{fa}	P_{fi}	GCA_{DRC}	$G_{b,ca}$	$G_{b,fa}$	VCA_{DRU}	$VOL_{ma,B}$
Measured	Deeper rut	6.2	66.1	25.1	8.8	1.63025	2.71708	2.63661	14.5965	18.7488
	Lower rut	6.0	64.8	26.6	8.6	1.63008	2.71679	2.63621	14.3110	19.0523
Design		6.2	75.5	14.5	10	1.63055	2.71758	2.62950	16.6692	15.1837

The data indicates that the VCA_{DRU} of two measured gradations are less than the $VOL_{ma,B}$ remarkably, coarse aggregate suspends up in asphalt mortar. Absolutely they are not the same type. On the contrary, the design VCA_{DRU} is slightly greater than the design $VOL_{ma,B}$, but the actual value Va is much greater to 7.2%.

CONCLUSIONS

1) One of the main causes of rut is the heavy axle load (only 25% axle loads less than 100KN) and the high-temperature in south moist hot areas.
2) Asphalt content was controlled inaccurately in the phase of construction (especially when paving mid and lower layers, mid layer content is higher 9.75%~14.63% than design value while lower layer is 10.53%~18.42%), which is the other main cause.
3) According to thickness measuring data of each layer, the thickness is not controlled strictly, upper layer is thin and lower layer is thick, which is also the factor that causes rut damage.
4) Gradation of asphalt mixture isn't controlled strictly, which is the key factor that causes pavement rut. According to the latest research, nearly all the design gradation does not meet the test of dense and solid framework basically. Therefore, in condition of heavy traffic, high temperature and high asphalt content, rut damage appears inevitable.

ACKNOWLEDGMENTS

The authors appreciate the support of the National Science Foundation of China (50778025) and the Natural Sciences Foundation of Hunan Province of China (07JJ6090).

REFERENCES

Huang, Xiaoming, et.al. (2007). Investigation and test of expressway asphalt pavement high-temperature performance. Journal of highway and transportation research and

development. Vol 24, No 5. pp.16-20.
Su, Kai, et.al. (2007). Mechanics Analysis of Loads and Pavement Structure Type to Asphalt Pavement Rutting by 3D Finite Element Method. Journal of Tongji University (Natural Science). Vol 35, No.2. pp. 187-192.
Sha, Qinlin. (2005). The Design and Construction of The Series of Stone Asphalt Concrete SAC. *Beijing: China Communications Press*. pp. 113-190.

Study on the Method to Calculate Rutting of Asphalt Pavement Based on the Dynamic Load Coupled Between the Road and Vehicle

He Zhaoyi[1], Lu Zhaofeng[2], Chen Hongxing[3]

[1]Professor, Chongqing Jiaotong University, Chongqing, 400074, China;heyzwb@cquc.edu.cn
[2]Doctor, Chongqing Jiaotong University, Chongqing, 400074, China;zhaofeng.lu@yahoo.com
[3]Master, Chongqing Jiaotong University, Chongqing, 400074, China; chx8787@yahoo.com.cn

ABSTRACT: By measuring the roughness of high-grade asphalt pavement，the time domain model of roughness based on international roughness index (IRI) was established by Inverse Discrete Fourier Transform(IDFT), which realizes the simulation of road roughness. The multiple-degree-of-freedom (MDOF) vehicle model was founded making use of the Dynamic Simulation software ADAMS. And with the time domain model, dynamic load spectrums for different grade pavements and different speeds were obtained by calculating dynamic load. Based on mathematical statistical analysis for load spectrums at different speeds and the influence of vehicle's actual loading condition and intermissive time, dynamic load models for different grade pavements were obtained. Combined finite element technology and the visco-elastic-plastic theory of asphalt mixture with the software ANSYS, the two-dimensional finite model of pavement structure was established. Considering the material characteristic of nonlinear, the method of calculating asphalt pavement rutting was put forward. The error is less than 10% between theoretical value and practical measurement rutting data of Handan-Changzhi highway. The result indicates that the method of rutting prediction, which based on the time domain model of roughness and the dynamic load coupled between pavement and vehicle is reasonable and reliable.

INTRODUCTION

Asphalt concrete pavement, which has advantages such as convenient for construction, ride comfort and smooth, low noise and easy to repair and so on, was widely used in high-grade highway. However, with the growth of traffic volume and axle load and the enhancement of channel traffic, the early damage on the asphalt pavement becomes more and more serious. Rutting has become a major early defect form. A mass of rutting not only seriously affect the performances of the asphalt pavement and reduced the service life, but also caused threat to the traffic security.

Dynamic loads of vehicle and visco-elastic-plastic of asphalt mixture are main reasons among factors resulting in rutting. It is not difficult to conclude that rutting calculation is remaining on the basis of semi-empirical and semi-theoretical currently, which has certain limitations. While in numerical theory solution, the traffic load is seen as the static and continuous load without interval of time, thus the accuracy of calculation is affected greatly. The development of FEM technology and visco-elastic-plastic theory made dynamic FEM calculation become the main development direction of rutting calculation. This paper is to seek an effective method of calculating asphalt pavement rutting, using time-domain model of pavement roughness and road-vehicles coupling model, and finite element analysis software as well.

1 THE ESTABLISHMENT OF TIME-DOMAIN MODEL of PAVEMENT ROUGHNESS

The pavement roughness can be obtained through test methods or converting the pavement power spectral density to pavement roughness. The first method needs work load and is affected by the sample precision. The second method has been paid close extensive attention recently. Through studying the definition of IRI and road power spectral density (PSD), the relationship between the two is as below:

$$IRI = \frac{\sqrt{2}}{\pi\sqrt{v^3}}\left[\int_0^\infty w^2 \left|H_s(w)\right|^2 G_q(n)dw\right]^{1/2} \qquad (1)$$

Where $H_s(w)$ is frequency response function of sprung mass and $G_q(n)$ is pavement power spectral function, which can be fitted by equation (2) provided by criterion of GB7013-86.

$$G_q(n) = G_q(n_0)(\frac{n}{n_0})^{-w} \qquad (2)$$

Where n_0 is spatial reference frequency and $n_0 = 0.1m^{-1}$; $G_q(n_0)$ is the value of pavement power density corresponding with spatial reference frequency, which is named as pavement roughness coefficient; w is frequency index and normally be chosen as 2, Choosing standard vehicle parameters and 0.5 ~ 50 m wavelength range of pavement roughness (corresponding space frequency range is $0.02 \sim 2\,m^{-1}$), the equation (1) can be converted into

$$IRI = 0.78a_0\sqrt{G_q(n_0)} \qquad (3)$$

The equation (3) is the simple relationship between IRI and PSD.So the IRI value measured by equipment can be directly used in pavement roughness time-domain model establishment by equation (3).

There are many methods to establish time-domain model of pavement roughness. Because the simulation method of DFT has the advantages of precision in mathematical relations, clear coherent and higher simulation accuracy, it is applied to establish time-domain model of pavement roughness in this paper. Most of road grades in China lie in levels of A, B and C based on statistics value(Yu Zhisheng,2001) and corresponding changing scopes of IRI are shown in table 1:

Table 1 The IRI value of corresponding each grade pavement

Pavement grade		A	B	C
$G_q(n_0)$ ($10^{-6}m^3$)	lower limit	8	32	128
	upper limit	32	128	512
IRI	lower limit	2.21	4.42	8.84
	upper limit	4.42	8.84	17.64

By MATLAB program, the A-class pavement was simulated and accuracy validated as show in figure1 and figure 2:

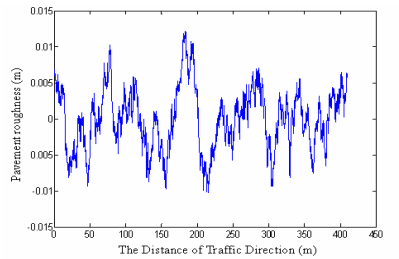

Figure 1 Time domain curves of A-class pavement roughness

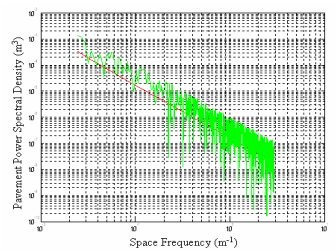

Figure2 Power spectrum comparison of A-class pavement between estimate value and theoretical value

It can be seen from figure 2, the power spectrum of pavement roughness obtained by IDFT can be better in accord with the expected spectrum. Therefore, when the measured pavement roughness in practice need being simulated, the result can be gained through measuring IRI and equation (3).

2 The establishment of vehicle dynamic load model

The vehicle model was established by using multi-body dynamics simulation software ADAMS. As is shown in Figure 3, the model has 434 freedom degrees and can better simulate vehicle characteristics, so the load attained by simulation has high precision.

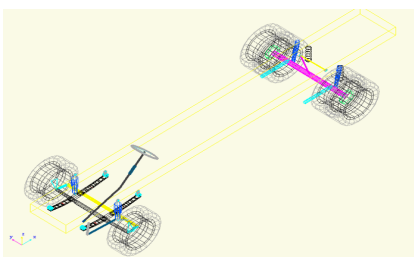

Figure 3 Vehicle simulation model

Owing to the limit of article length, only the dynamic loads contrast of A-class road in different speed and dynamic load at 60km/h rate in different level pavements are listed, which are shown in figure 4 and figure 5.

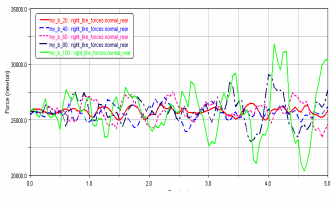

Figure 4 Dynamic load change of A-class road in different speed

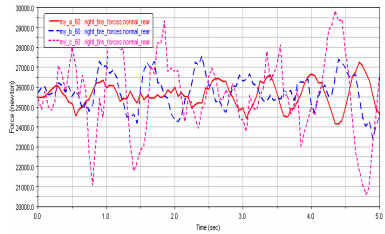

Figure5 Dynamic load change at 60km/h rate in different class pavements

It can be seen clearly from figure 4 and figure 5 that, with the speed increasing and pavement grade lowing, the additional dynamic load also increases and the dynamic load peak approximately lies in the same location. The dynamic loads changed with different speed and different pavement grade are shown in table 2:

Table 2. Vehicle dynamic load changes

speed / road grade	20（km/h）		40（km/h）		60（km/h）		80（km/h）		100（km/h）	
	Max (KN)	Av (KN)	Max (KN)	Av (KN)	Max (KN)	Av (KN)	Max (KN)	Av (KN)	Max (KN)	Av (KN)
A	26094	25534	26520	25594	27254	25627	26959	25630	27617	25659
B	26479	25767	27024	25590	27568	25786	27648	25841	31818	25878
C	27661	25538	29302	25645	29836	25646	34323	26254	34344	27435

Through the statistical analysis of vehicles speed and the dynamic load sum-up at different speed ,and considering the interval effects of vehicle load, the dynamic load models in different class pavement were obtained as show in figure 6:

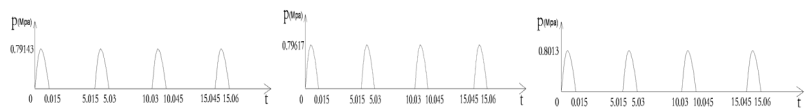

Figure 6 Road dynamic load model of A、B and C class

4 Rutting calculation

With the parameters of Handan-Changzhi highway in Hebei Province of China, the

rutting calculation was carried through. Road structure and its parameters are shown in Figure7 and Table 3.

Table 3 Different layer parameters of semi-rigid asphalt pavement

pavement structure	thickness (cm)	elasticity module (Mpa)	Poisson's ratio	internal friction angle (°)	cohesive force (KPa)	density (kg/m^3)
AC-13C	4	1400	0.25	-	-	2600
AC-20C	5	1200	0.25	-	-	2500
AC-25C	6	1000	0.25	-	-	2500
water stability macadam	19	1500	0.25	-	-	2400
lime-fly-ash macadam	19	1400	0.25	-	-	2000
lime stability soil	20	550	0.35	22	55	1930
foundation	500	48	0.4	16	30	1900

After establishing the model and calculating, it can be found that if the load mode with time interval is used, 3-D finite element model cannot be calculated for excessive computation. Therefore, 2-D finite element model was established in this paper. Combining the information available (Liao Jingmei et al.,2003; Liu Li'an ,2002; Zhong Wu ,2001), when the model sizes are bigger than 6 m × 5.73m, the geometry change almost has no impact on the calculation results, so the model sizes is selected as 6 m × 5.73m. The cell type used in surface layer of asphalt mixture is PLANE182, while in the base and foundation is PLANE42. The finite element grid model is shown in Figure 8:

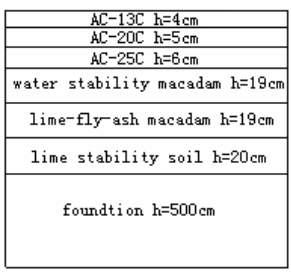

Figure7 pavement structure

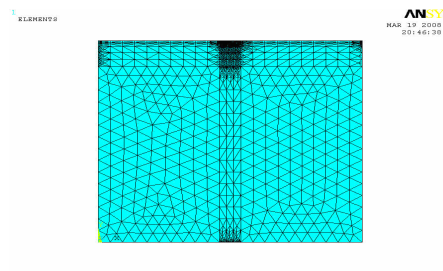

Figure8 Finite element grid model

Surveying the traffic on the test road and calculating the equivalent axle load number, the cumulative effect equivalent axle load number of up- and down-direction traffic is respectively 180,600 and 408,500 times. The test road was newly built and had good evenness. Measured by IRI，most section of the road was A-road and other was

B-road. So，the corresponding load method of A-road was used in rutting solving.

The permanent deformation of test road in the upstream direction is shown in figue9:

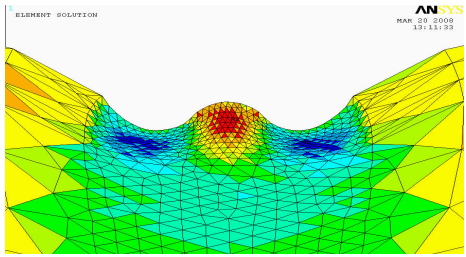

Figure 9 The Magnified Deformation

From the road cross-section, the rutting theoretical results and the practical results are shown in figue10~13.

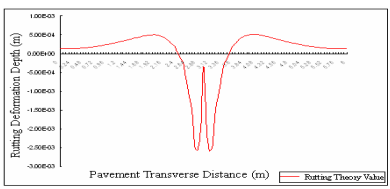

Figure10 Average theoretical rutting

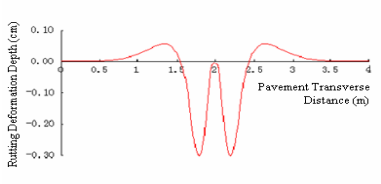

Fig11 Average practical rutting

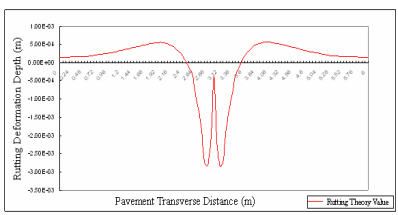

Figure12 The deepest theoretical rutting

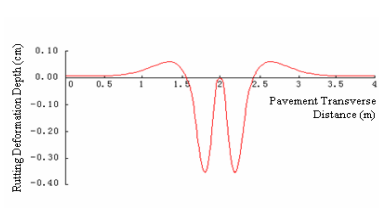

Figure13 The deepest practical rutting

Although the practical measurement rutting data only covers 4m in cross-sectional area, yet the theoretical value and practical value were very close from the shape and depth of rutting deformation, and the former is slightly less than the latter. Compared the deepest rutting value between theoretical and practical, it can be found that its discrepancy is slightly larger than that of rutting average. Because the tested road is new and has good evenness, the additional dynamic load of vehicle vibration is small

and the peak difference between dynamic load and static load is not large, the deepest rutting is little affected by the load. The quality of pavement construction and the uniformity of asphalt mixture are also the reasons of poor performance of anti-rutting. So the rutting practical values are slightly larger than the rutting theoretical values.

CONCLUSIONS

(1) Through theoretical analysis, the time-domain model of road roughness based on the IRI was obtained, which was verified with the theory of the discrete Fourier Transform with MATLAB simulation software.
(2) The vehicle model was established by ADAMS dynamic simulation software. The dynamic load spectrums at different speeds and different road grades were obtained. Through the mathematical statistic analysis of speeds, the dynamic load models were established.
(3)The method of rutting calculation based on the time-domain model of road roughness, the dynamic load spectrum and the dynamic load models in different road grades is reasonable and feasible.

ACKNOWLEDGMENTS

The work described in the paper was funded by National Nature Science Foundation of China. Valuable help was also provided by the laboratory of Construction and Maintenance Technique of Mountain Road, Chongqing Jiaotong University. All support is gratefully acknowledged.

REFERENCES

Liao, Jingmei; Lu, Yang; Zhou, Yongjiang. Analysis of Visco-Elastoplastic Deformation of Asphalt Pavement with Semi-Rigid Base Course [J].highway, 2003.6, .pp.61-65.

Liu, Li'an. Structural Response of Asphalt Pavement under Dynamic Loading [D]. Xi'an: chang'an university, 2002.1.

Yu, Zhisheng. Automobile theory [M].Beijing: China Machine Press, 2001.

Zhong, Wu，Finite Element Simulation of Rutting on Superpave Pavements, Ph.D dissertation, KANSAS STATE UNIVERSITY，2001.

Calibration of Roughness Measuring Instrument for Adopting the Performance Warranty System

Deok-Soon An[1], Jeong-Hee Nam[2], and Soo-Ahn Kwon[3]

[1]Researcher, Highway Facility Research Division, Korea Institute of Construction Technology, dsan@kict.re.kr
[2]Senior Researcher, Highway Facility Research Division, Korea Institute of Construction Technology, archnam@kict.re.kr
[3]Research Fellow, Highway Facility Research Division, Korea Institute of Construction Technology, sakwon@kict.re.kr

ABSTRACT: Most pavement construction in Korea today is conducted by following prescriptive specifications. The construction must be done according to the standard specifications and the contractor is responsible for any defects where the pavement quality does not meet the minimum requirements written in the specification. Adopting new materials and innovative construction technologies is limited under the current system. Many European countries have adopted the performance warranty systems to improve long-term pavement performance since the 1960's. In the performance warranty system, a specification defines a certain level of pavement performance as the minimum requirement. Examples of performance indices might include: rutting, roughness, cracking, skid resistance, etc. The prescriptive specification is no longer used in the performance warranty system. Instead, the contractor must satisfy the performance specifications of each index. One of the most important performance indices is the roughness of pavement. The method for evaluating the pavement roughness is essential in order to prevent conflict where there is a disagreement for evaluating results between the contractor and the client. The primary objective of this paper is to present a guideline for the calibration of the roughness measuring instrument of pavement by semi-manual and automatic methods in the performance warranty system.

INTRODUCTION

Most of the pavement constructions in Korea follow standard specifications. A general contractor constructs pavement based on specifications provided by the client. Under the current system, the contractor has only two-year limited responsibility following the completion of construction. The client, however, is solely in charge of the construction quality control in this circumstance. As a result, the contractor has

relatively less responsibility than under a performance-based contract. There are also the problems of premature pavement failures prior to the end of the design life. In many countries such as the United States and Japan, the performance-based contract system has been adopted to improve on pavement performance and to save on maintenance costs. The intent of the performance warranty system is to impose the maintenance responsibility on the contractor to sustain the pavement performance for a certain period of time after the completion of construction.

Currently, many research institutes are studying about the performance-based contract system. Some of the factors that affect the pavement performance are roughness, rutting, cracking, skid resistance, etc.. An evaluation of roughness is critical in a performance-based contract system because there is a chance of disagreement with the evaluation and its result between client and contractor; the method of evaluation should be agreeable to both of them. In Korea, a 7.6m long profilometer is used to measure pavement roughness, while other countries use a different measuring instrument that automatically determines the pavement condition. But the profilometer is difficult to apply to roads in service. Therefore a move towards an automatic device is inevitable.

Based on research that deals with roughness measurement, a field test was conducted to measure road roughness—one of the primary factors in evaluating pavement performance.

The primary objective of the study reported herein is to analyze the field data and to suggest how to calibrate the road roughness measuring instrument.

ROUGHNESS

Roughness is defined by the sense of comfort perceived by a driver on the road. The following list indices of roughness:

(1) Profilograph Index (PrI)
(2) International Roughness Index (IRI)
(3) Half-car Roughness Index (HRI)
(4) Ride Number (RN)
(5) Ride Quality Index (RQI)

IRI Calculation

The IRI is officially used throughout the world. The IRI is calculated from a quarter-car simulation as follows:

Data Input (raw data)

Moving average filter: filtering to apply to a 1/4 car model (250mm sample interval)

Quarter-car simulation at driving speed of 80km/h (Fig. 1): sums up absolute displacement between sprung mass (Euler's integral) and unsprung mass (Taylor series)

Accumulator: accumulates displacement

IRI calculation

Roughness Measurement in Korea and Other Countries

The roughness measurement in Korea is prescribed in KS (KS F 2373: Test Method for Measuring Pavement Roughness with 7.6m long Profilometer). In this method, the measuring instrument is operated by hand, which takes a substantial amount of time. This is impracticable and exposes the need in Korea for the introduction of an automatic measuring instrument. According to KS F 2373, the absolute value of the unevenness wave is summed up that it is located 5mm outside the range of the upper and lower cable at an interval of 150m. This value is used to calculate the profile, and the roughness index is represented by the PrI value.

In the United States, the roughness measurement is prescribed in ASTM (ASTM E 950: Standard Test Method for Measuring the Longitudinal Profile of Traveled Surfaces with an Accelerometer Established Inertial Profiling Reference). ASTM E 950 requires that a calibration is conducted prior to the test and that the speed is over 25km/h for measurement.

In Japan, the roughness measurement is prescribed in Pavement Test Manuals 6-2 (Pavement Performance Evaluation: Method for Measuring Roughness of Pavement Surface). The manuals suggest using either a 3m profilometer or an automatic instrument.

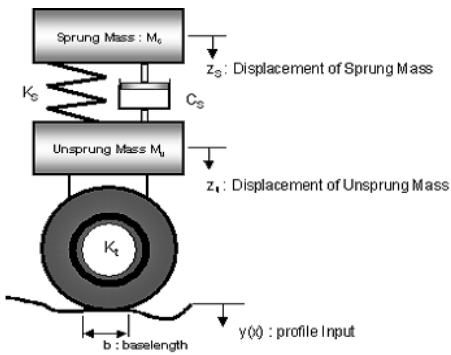

FIG. 1. Quarter-Car Simulation

Calibration of the Roughness Measuring Instrument

Many countries today use an instrument that automatically checks the pavement condition. This measuring instrument is especially beneficial when it is used for roads in service because: (a) it saves time and money, and (b) it ensures traffic safety. To measure pavement roughness more effectively, the following four steps present the most effective method for calibrating the roughness measuring instrument: M/n Road, ASTM E 950, Colorado, Florida.

(1) Calibration Information: Information necessary for a field test needs to be recorded

prior to calibration. This should include: date, time, driver, number of tests, measuring speed, and lane.

(2) Pre-test: Prior to the field test, the tire pressure, accelerometers, and sensors of the measuring instrument need to be checked. An instrument manufacturer should check the aforementioned components in order to ensure the accuracy in measuring distance and the perpendicular distance of the sensors.

(3) DMI (Distance Measuring Instrument) Verification: DMI is an instrument to measure the traveling distance of the roughness measuring instrument. DMI inspection is used to verify the accuracy of the actual distance measured and the distance that the vehicle travels. Generally, the criteria require that the distance is 1km or 1.6km, and the tolerance is within 0.2% or ±0.1% of the actual distance.

(4) Field Test and Data Analysis: This is the most important step in the calibration of the roughness measuring instrument. For data analysis, the reference value of roughness must be compared to the measured roughness of the instrument. It is suggested that it covers 160-200m of the road excluding the acceleration and deceleration areas. Additionally, several other factors need to be considered that include: repetitive measurement accuracy (within ±3.2km/h of the average speed), measurement in the wheel path area, and measuring speed over 25km/h(15mph). To analyze the data, it is necessary to compare the relationship between measured average IRI, reference IRI and repeatedly measured IRI.

Field Test by the Roughness Measuring Instrument

The field test was conducted to verify DMI for the 1km long section and measured IRI using a semi-manual and an automatic instrument for the 160m long section (Figure 2).

(a) manual **(b) semi-manual** **(c) automatic**

FIG. 2. Roughness Measurement using Different Methods

DMI Verification

The 1km section was measured five times with an identical instrument. All results fell within the tolerance range of 0.02% to 0.05%. The average tolerance was 0.03%, which verifies that the DMI was sufficiently accurate (Table 1).

Table 1. DMI Measurement Results

Time	1	2	3	4	5	Average
Distance (m)	1000.316	1000.426	1000.108	1000.316	1000.183	1000.270

IRI Verification

A semi-manual (Dipstick) and an automatic instrument were employed for reference and comparison of the 160m long section, respectively. The measuring speeds of automatic instrument were set at 40km/h, 60km/h, and 80km/h. Figure 3 shows the IRI-distance relationship for each measuring speed and the dipstick value. It is notable that both instrument measurements show very similar IRI values between 50m and 110m, whereas the deviation becomes wider as the distance increases. In regards to the measuring speed, the measurement at 60km/h shows the closest results between the two instruments.

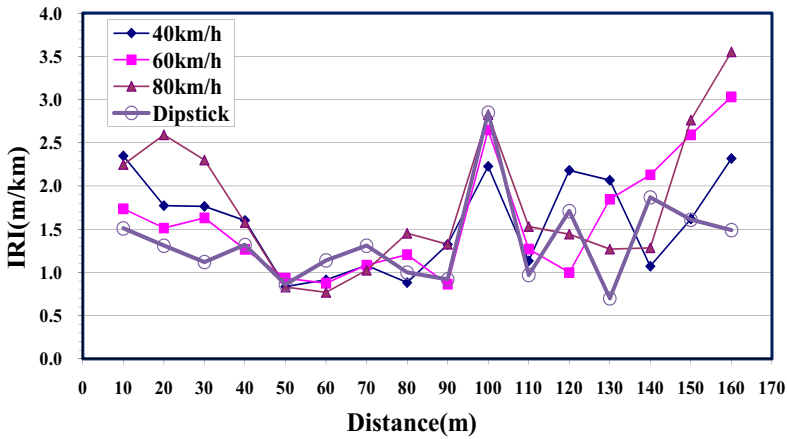

FIG. 3. IRI value of Dipstick and automatic Instruments under Different Measuring Speeds

CONCLUSIONS

The presented research work suggests that the calibration of the roughness measuring instrument should be done prior to the field test. The variables of field test were based on the data provided by researches conducted in Korea and other countries for various measuring instruments and calibrations. A dipstick was used as a reference instrument and an automatic instrument was used to measure the pavement condition. A field test

was conducted to verify the DMI and the IRI for the purpose of instrument calibration. In the case of the DMI, the actual distance and the measured distance were nearly the same. For the IRI, the measured value was closest to the dipstick value at the speed of 60km/h. A single field test was carried out for this research and it is suggested that extensive research follow up with repeated test data for further analysis.

ACKNOWLEDGEMENTS

This research paper is based on the Standardization Project of Construction Criteria provided by Performance in Regard to Construction and Transportation R & D, Policies and Infrastructure ('06~'11).

REFERENCES

American Association of State Highway and Transportation Officials (2005), "Determination of International Roughness Index (IRI) to Quantify Roughness of Pavements", AASHTO PP 37-40.

American Society of Testing and Materials, "Standard Test Method for Measuring Pavement Roughness Using a Profilograph", ASTM E 1274-1303, Annual Book of ASTM Standards.

American Society of Testing and Materials (2000), "Measuring the Longitudinal Profile of Traveled Surfaces with an Accelerometer Established Inertial Profiling Reference", ASTM E 950, Annual Book of ASTM Standards.

Florida Method of Test for Measuring Pavement Longitudinal Profiles Using a Laser Profiler (2001).

Similarity Analysis of Rutting Test for Asphalt Pavement Based on Similarity Theory

Dong Zejiao[1], Cheng Xiaoliang[2], Zheng Hao[3] and Tan Yiqiu[4]

[1]Doctor, School of Transportation Science & Engineering, Harbin Institute of Technology, No.202 Haihe Road, Nangang District, Harbin 150090, China; hitdzj@hit.edu.cn
[2]Master, School of Transportation Science & Engineering, Harbin Institute of Technology, No.202 Haihe Road, Nangang District, Harbin 150090, China; xiaoliang1985412@163.com
[3]Master, School of Transportation Science & Engineering, Harbin Institute of Technology, No.202 Haihe Road, Nangang District, Harbin 150090, China; zhenghao19870906@126.com
[4]Professor/Doctor, School of Transportation Science & Engineering, Harbin Institute of Technology, No.202 Haihe Road, Nangang District, Harbin 150090, China; yiqiutan@163.com

ABSTRACT: Generally, the performance of asphalt pavement at high temperature is evaluated by rutting test. However, few researches focusing on the mechanical similarity between the rutting test specimen and the actual asphalt pavement structure has been carried out. As a result, based on Similarity Theory, the mechanical similarity between rutting test specimen and typical asphalt pavement structure through using three-dimensional finite element simulation was analyzed. At first, the similarity parameters were derived based on the Similarity Theory. Then, the loading types, boundary conditions and material parameters of finite element models were listed here. Finally, typical mechanical states in an actual pavement structure and rutting test were compared and analyzed. The result indicates that there are some differences in the distribution of stress and strain field between the two cases due to the different boundary conditions and object sizes studied. However, it can be made up with a proper design to the specimen and loading area in rutting test.

INTRODUCTION

In recent years, the phenomenon that rutting occurs on asphalt pavement in a short time after construction becomes more and more popular, resulting in a bad influence (Shen Jinan, 2001). To solve premature rutting of asphalt pavement, first of all, deformation of asphalt mixture at high temperature should be evaluated accurately. It is noted that rutting test has become a primary laboratory method in evaluating rutting resistance of asphalt mixture (Cooley *et al*, 2000). It has some advantages: loading mode is similar to that of the actual pavement, and equipment is relatively cheaper and easier to operate (Williams *et al*, 2003). However, some asphalt mixtures whose dynamic stabilities meet the specifications, still cause premature rutting (Sun Lijun,

2005). It shows that rutting test is different from the actual mechanical state within the pavement structure at high temperature. Therefore, the similarity between the two cases based on Similarity Theory and finite element simulation was studied, aiming at providing useful suggestion for solving rutting problems.

SIMILARITY THEOREM

If N different physical parameters in one system have a certain function relationship:

$$F\left(\mathrm{X}_1, \mathrm{X}_2, ..., \mathrm{X}_N\right) = 0 \tag{1}$$

In $\mathrm{X}_i (i = 1, 2, 3, ..., N)$, if M physical parameters are independent from each other, then (1) can be expressed in the following form:

$$F\left(\pi_1, \pi_2, ..., \pi_{N-M}\right) = 0 \tag{2}$$

Where $\pi_j (j = 1, 2, 3, ..., N - M)$ are N-M different non-dimensional parameters.

When the prototype and its model are similar, similarity criteria is equal to the corresponding point and time, and their π formulas should also be the same, namely:

$$F\left(\pi_1, \pi_2, ..., \pi_{N-M}\right)_{\mathrm{p}} = 0 \tag{3}$$

$$F\left(\pi_1, \pi_2, ..., \pi_{N-M}\right)_{\mathrm{m}} = 0 \tag{4}$$

Where $\pi_{1_{\mathrm{m}}} = \pi_{1_{\mathrm{p}}}, \pi_{2_{\mathrm{m}}} = \pi_{2_{\mathrm{p}}}, ..., \pi_{(\mathrm{N\text{-}M})_{\mathrm{m}}} = \pi_{(\mathrm{N\text{-}M})_{\mathrm{p}}}$

ESTABLISHMENT OF SIMILARITY CRITERIA

Determination of Main Parameters and Their Dimensions

Pavement parameters: geometry size X, elastic modulus E, Poisson's ratio μ, cohesion C, internal friction angle φ; Loading parameters: uniform loading q; Pavement responses: stress σ, strain ε, displacement δ, strain rate $\dot{\varepsilon}$; Time parameters: time t. The dimensions of physical parameters are shown in Table 1.

Table 1. Physical Parameters and Their Dimensions

Parameter	X	E	μ	C	φ	t
Dimension	L	$L^{-1}MT^{-2}$	$L^0M^0T^0$	$L^{-1}MT^{-2}$	$L^0M^0T^0$	T
Parameter	q	σ	ε	δ	$\dot{\varepsilon}$	
Dimension	$L^{-1}MT^{-2}$	$L^{-1}MT^{-2}$	$L^0M^0T^0$	L	T^{-1}	

Determination of Similarity Criteria

For the above parameters, similarity criteria can be assumed as the following:

$$\pi = \mathrm{X}^a E^b \mu^c C^d \varphi^e t^f q^g \sigma^h \varepsilon^i \delta^j \dot{\varepsilon}^k \tag{5}$$

Where $a, b, c, d, e, f, g, h, i, j, k$ are needed to be determined. Adopting SI units, the relationships of dimensions are shown in Table 2.

Table 2. Dimensional Matrix

Parameters	X	E	μ	C	φ	t	q	σ	ε	δ	$\dot{\varepsilon}$
M	0	1	0	1	0	0	1	1	0	0	0
L	1	-1	0	-1	0	0	-1	-1	0	1	0
T	0	-2	0	-2	0	1	-2	-2	0	0	-1
Index	a	b	c	d	e	f	g	h	i	j	k

As the similarity criteria π is dimensionless, the following formula can be determined:

$$\begin{aligned} &b+d+g+h=0 \\ &a-b-d-g+j=0 \\ &-2b-2d+f-2g-2h-k=0 \end{aligned} \tag{6}$$

Assuming that a,b,f are unknown quantities, they can be calculated with the other quantities:

$$\begin{aligned} &a=-j \\ &b=-d-g-h \\ &f=k \end{aligned} \tag{7}$$

As there are three independent dimensions among the above parameters, the number of similarity criteria is eight.

The above calculation is equivalent to transpose the original dimensional matrix, and the resulted dimensional matrix is shown in Table 3:

Table 3. Dimensional Matrix

	i	j	c	d	e	k	g	h	a	b	f
	ε	δ	μ	C	φ	$\dot{\varepsilon}$	q	σ	X	E	t
π1	1	0	0	0	0	0	0	0	0	0	0
π2	0	1	0	0	0	0	0	0	-1	0	0
π3	0	0	1	0	0	0	0	0	0	0	0
π4	0	0	0	1	0	0	0	0	0	-1	0
π5	0	0	0	0	1	0	0	0	0	0	0
π6	0	0	0	0	0	1	0	0	0	0	1
π7	0	0	0	0	0	0	1	0	0	-1	0
π8	0	0	0	0	0	0	0	1	0	-1	0

Therefore, the eight similarity criteria are got as the following:

$$\pi_1=\varepsilon;\ \pi_2=\delta/X;\ \pi_3=\mu;\ \pi_4=C/E;\ \pi_5=\varphi;\ \pi_6=\dot{\varepsilon}t;\ \pi_7=q/E;\ \pi_8=\sigma/E$$

DETERMINATION OF SIMILARITY CONSTANTS

For the similar phenomena, they should have similarity criteria with the same value according to Similarity Theorem. Therefore, the similarity constants for asphalt pavement model can be determined as follows:

From the equation $\pi_1 = \varepsilon$, the equation $C_Z = 1$ can be determined. It is equivalent to the equation $\varepsilon_p = \varepsilon_m$, which shows strain is equal between the prototype and its model.

From the equation $\pi_2 = \delta / X$, the relationship $C_\delta = C_X$ can be derived.

From the equation $\pi_3 = \mu$, the relationship $\mu_p = \mu_m$ can be derived.

From the equation $\pi_4 = C / E$, the relationship $C_C = C_E$ can be got. In order to simplify the simulation to the prototype, the same material is proposed. So the equations $C_E = 1$ and $C_C = 1$ can be got.

From the equation $\pi_5 = \varphi$, the equation $C_\varphi = 1$ can be got.

From the equation $\pi_6 = \dot{\varepsilon} t$, the relationship $C_{\dot{\varepsilon}} = C_t$ can be derived.

From the equation $\pi_7 = q / E$, the equation $C_q = C_E = 1$ can be derived.

From the equation $\pi_8 = \sigma / E$, the relationship $C_\sigma = C_E$ can be got.

FINITE ELEMENT SIMULATION WITH ABAQUS

For the finite element model of rutting test in laboratory, the following parameters are used. Rutting test model is 0.3m long and 0.3m wide with a height of 0.05m, the amplitude of uniform loading is 0.7MPa, and the contact area of steel wheel is 0.048m by 0.018m. It was assumed that there is no vertical, transverse or horizontal movement at the bottom of the model, and horizontal movement perpendicular to the perimeters was also restrained whereas the remaining two directions were considered free. The meshes near the loading region are fine, and elastic modulus and Poisson's ratio of asphalt material are assumed to be 1200MPa and 0.35 respectively.

For the finite element model of asphalt pavement, the following parameters are used. The vehicle loading is simplified as two rectangular uniform loadings, each with a planar size of 0.2m by 0.18m (Xie Shuiyou, 2003), whose amplitude is 0.7MPa. As the actual pavement structure is infinite in the traveling direction, an influence region by vehicle loading is determined at first. Here, 3m×3m×0.9m, 3m×3m×0.8m, 3m×3m×0.7m are chose for the sizes of finite element model. The finite element model and meshes are shown in Figure 1. Three typical pavement structures are used, in which structure A is of three asphalt layers with one semi-rigid base layer, structure B is of three asphalt layers with one flexible base layer, and structure C is of two asphalt layers with one flexible base, whose detailed information can be found in the work by Cheng Xiaoliang.

According to Similarity Theory and similarity criteria, additional three models for rutting test corresponding to the above pavement structures can be obtained, which are also analyzed here. Taking the geometry constant C_X as ten, the sizes of rutting model were 0.3m×0.3m×0.09m, 0.3m×0.3m×0.08m and 0.3m×0.3m×0.07m, respectively.

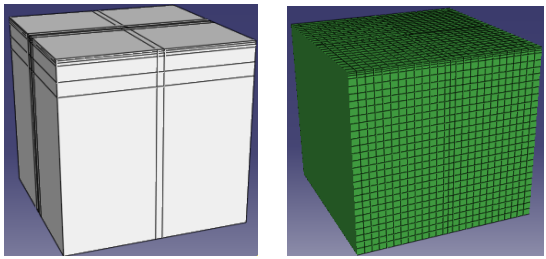

FIG. 1. Finite element model and meshes of asphalt pavement.

SIMILARITY ANALYSIS

Here we use standard rutting test model with dimensions of 0.3m×0.3m×0.05m and other three rutting test models to carry out the finite element analysis, and compare their similarities in maximum principal stress, maximum principal strain and shear stress, whose results are shown in Figure 2.

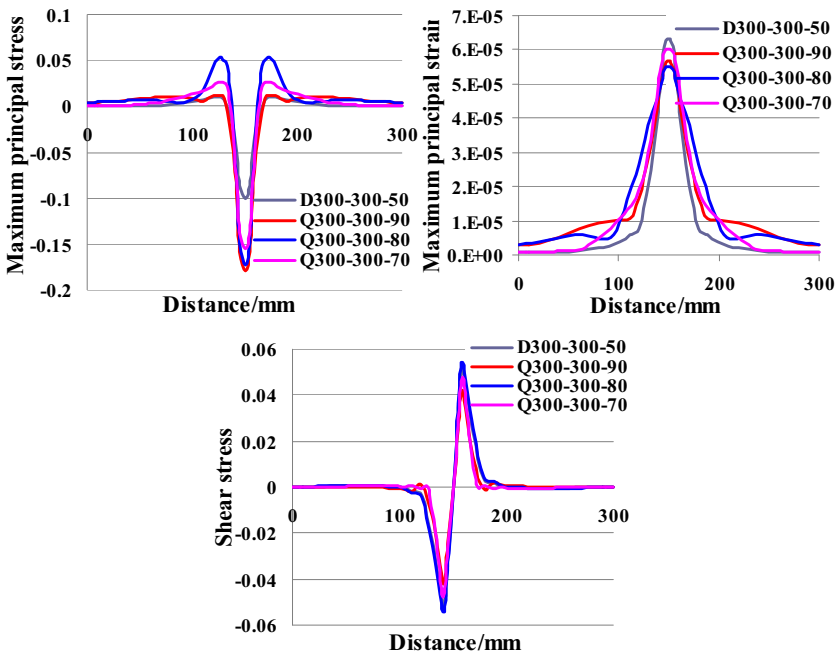

FIG. 2. Comparison between different rutting test models. a) Maximum pricipal stress (left top); b) Maximum principal strain (right top); c) Shear stress (bottom).

It can be seen from Figure 2 that the trends are approximately close to each other from the results of maximum principal strain and shear stress, while maximum principal stress near the wheel has a little difference between the four cases. It shows that standard rutting model can simulate the mechanical state of actual pavement structure generally, and the difference between them can be improved by adjusting the sizes of standard rutting test.

CONCLUSIONS

Based on Similarity Theory, this paper mainly analyzes the mechanical similarity between rutting test specimen and asphalt pavement structure. In order to simulate the actual pavement structure with rutting test in laboratory, the same material and loading conditions are proposed, strain and stress of corresponding points of the prototype and its model should be equal, and the displacement ratio between the prototype and its model should be equal to their geometry ratio.

The trends are similar for maximum principal strain and shear stress among different conditions, while maximum principal stress near the wheel shows a slight difference. It shows that standard rutting model can simulate the mechanical state of actual pavement structure generally, and the difference between them can be improved by adjusting the geometry of rutting test.

REFERENCES

Cheng, Xiao-liang (2007). "Research on rutting test based on Similarity Theory and finite element simulation." Master thesis, Harbin: Harbin Institute of Technology.

Cooley, L. A.; Kandhal, P. S.; Buchanan, M. S.; Fee, F.; and Epps, A. (2000). "Loaded wheel testers in the United States: State of the practice." *Transportation Research E-Circular E-C016*, Transportation Research Board.

Li, Qing-fu (2007). "The choice of finite element model of pavement structure." Henan: Henan Science Publishing House: 1-2.

Shen, Jin-an (2001). "The performance of asphalt and asphalt mixture." Beijing: People's Communications Publishing House.

Sun, Li-jun (2005). "Structural behavior theory of asphalt pavement." Beijing: People's Communications Publishing House.

Williams, S. G. (2003). "The effects of HMA mixture characteristics on rutting susceptivity." *Annual meeting of Transportation Research Board*, Washington D.C.

Xie, Shui-you (2003). "Study on effects of the tire contact pressure on asphalt pavement." Master thesis, Xi-an: Chang'an University: 65-66.

Three Integral Constant Determination Methods and Their Applications to Subgrade Settlement Grey Prediction Model

Zhao Jian-san[1], Tang Li-min[2], Zhang Deng-pan[3], Tang Ping-ying[4]

[1]Professor, School of Traffic and Transportation Engineering, ChangSha Univ. of Science and Technology, NO.45 Chiling Road, Tianxin District, Changsha, Hunan, 410076, P.R.China; E-mail: zjs.123@163.com
[2]Lecturer, School of Traffic and Transportation Engineering, ChangSha Univ. of Science and Technology, NO.45 Chiling Road, Tianxin District, Changsha, Hunan, 410076, P.R.China; E-mail: tlmttt@163.com
[3]Graduate, School of Traffic and Transportation Engineering, ChangSha Univ. of Science and Technology, NO.45 Chiling Road, Tianxin District, Changsha, Hunan, 410076, P.R.China; E-mail: Zhangdengpan@163.com
[4]Associate professor, School of Traffic and Transportation Engineering, ChangSha Univ. of Science and Technology, NO.45 Chiling Road, Tianxin District, Changsha, Hunan, 410076, P.R.China; E-mail: tpy157@yahoo.com.cn

ABSTRACT: In this paper, three integral constant determination methods are proposed. First, the first point of modeling data sequence is used. Second, the last point of modeling data sequence is used. Third, the minimum point of fitting error in modeling data sequence is used. According to the above methods, six-step forecasts are respectively made by using six-group subgrade settlement observation data of Shaohuai expressway. The method of selecting integral constant is proposed by comparing and analyzing the predication results. Meanwhile, smoothing test for part of data is made in predication. For the two-group data which are not satisfy smoothness condition, cumulative settlement is used to build subgrade settlement grey prediction model, and the prediction effect was significantly improved.

INTRODUCTION

There are two main kinds of methods for determining the relationship between subgrade settlement and time. One is the theoretical calculation method which includes conventional methods and numerical methods; the other is the forecast method which calculates the relation between settlement and time by using observation data. This method usually includes determination methods and indetermination methods. With the development of system theory and computing science since 1980s, the indeterminate method was developed. It has also gotten

broad application such as gray forecasting method and artificial neural network method etc.

Gray system theory creates the differential equation by transforming less or inexact raw data sequence which express system behavior characteristic. The raw data shows disorder because of the influence of circumstance on system, the disorder data sequence is called grey data sequence or grey process. The model that based on grey process is called the gray model (GM).The grey prediction takes the prediction data sequence as grey variable or gray process which changes with time. The raw data is first processed before the model is built. Then it gradually makes grey variable whitening through accumulation and correlation generating. And it shows regularity. a related development model, which corresponds to differential equation solution, is consequently created, and sub-grade settlement may be predicated.

Theorem 1：

$$x^{(0)}(t)+az^{(1)}(t)=b \tag{1}$$

Equation (1) is the gray differential equation.，which is represented by using GM (1, 1), where, $x^{(0)}(t)=\frac{dx^{(1)}}{dt}$， $z^{(1)}(t)=\frac{1}{2}\left[x^{(1)}(t)+x^{(1)}(t-1)\right]$.

Theorem 2：The column of least square estimate parameters of gray differential equation (1) satisfies the following equation:

$$\hat{a}=(a,b)^T=(B^TB)^{-1}B^TY \tag{2}$$

Solving equation (1), the discrete general solution is written as:

$$\hat{x}^{(1)}(k+1)=-\frac{C}{a}e^{-ak}+\frac{b}{a} \tag{3}$$

Where, C is an integral constant which can be determined through a definite solution condition. At present, in the actual predication models, the assumption is as follows:

$$\hat{x}^{(1)}(1)=x^{(1)}(1)=x^{(0)}(1) \tag{4}$$

From equations (3, 4), the constant C can be solved in the following formula:

$$C=-ax^{(0)}(1)+b \tag{5}$$

Thereby, the special solution of equation (3) under the condition of Equation (4) is:

$$\hat{x}^{(1)}(k+1)=(x^{(0)}(1)-\frac{b}{a})e^{-ak}+\frac{b}{a}\quad k=1,2....n \tag{6}$$

If the definite condition of equation (4) is adopted, the least square fitting of the curve passes the first point. However, the method lacks of theoretical basis. Under this condition, the oldest settlement data is the most important, it is not reasonable.

THREE INTEGRAL CONSTANT DETERMINATION METHODS OF SUBGRADE SETTLEMENT GRAY PREDICTION MODEL

Assuming that the fitting curve passes the m point of the time series，the definite condition is：

$$\hat{x}^{(1)}(m) = x^{(1)}(m) \quad ， \quad m = 1,2,\ldots,\text{n} \tag{7}$$

Then the forecast formula can be formulated as:

$$\hat{x}^{(1)}(k+1) = (x^{(0)}(m) - \frac{b}{a})e^{-a(k-m+1)} + \frac{b}{a} \quad ,\text{k=1,2, …,n} \tag{8}$$

As for the choice of m， in this paper, three methods are suggested.

①If the least square fitting of the curve passes the first point, then m=1. The condition of the fixed solution is the same as equation (4).

②If the least square fitting of the curve passes the last point, then $m = n$, namely $\hat{x}^{(1)}(n) = x^{(1)}(n)$；

③Assuming that the fitting curve passes each point, so the error of each point is solved. The point, whose error is mini, is selected as m .

Using the observation data of soft soil subgrade of Shaohuai expressway in Hunan province, three methods are compared according to the predications of six sets of data; preliminary decisions of three methods are made by using a gray-related decision theory. The steps are as follows:

1. For each set of data, a dynamic predication model of the same dimensions disheartened number is created. , namely, when GM (1, 1) model is used to forecast, a known progression is applied to create a GM (1, 1) model to forecast a solution instead of creating a model to forecast all the times. Then the solution is supplemented behind a known numerical sequence. Meanwhile, the oldest data is taken out, and the same dimensions of the numerical sequence are kept. Then another GM (1, 1) model is created and used to forecast the next solution, and the result is also supplemented behind the numerical sequence. The other oldest data is taken out. Just like the metabolism of the old and the new, forecasting one by one, filling vacancies in order of precedence, until the planed target is completed.

2. Different dimension $i\,(i \geq 4)$ is choused when a model is created. Meanwhile, sub-progression is selected from original progression according to different dimension i . If the following original progression is given:

$$X^{(0)} = (x^{(0)}(1), x^{(0)}(2), \cdots, x^{(0)}(n)) \tag{9}$$

Where n is the number of data. The last data $x^{(0)}(n)$ is called the origin, the progression, which included origin and is choused from $X^{(0)}$, is given as follows:

$$X_i^{(0)} = (x^{(0)}(n-i+1), x^{(0)}(n-i+2), \cdots, x^{(0)}(n)) \tag{10}$$

3. For the sub-progression, 1-AGO is conducted, and then $X_i^{(1)}$ can be solved.

Then disheartened differential equation is created, and the optimal solution is gotten. We build disheartened differential equation. Then we got its omnipotent solution. According to the above three methods of choosing m, three integral constants are respectively calculated, and then three corresponding special solutions of disheartened differential equation can be gotten. Different GM (1, 1) models are consequently gotten.

4. For each set of data, six data are respectively forecasted under different dimensions. Then the average of the predications is regarded as the final predication of the set of data.

5. Taking m as event a_1, the event assembles $A=\{a_1\}$. Regarding m as countermeasure b_1 when m equals to one. m take the fitting error minimum putting corresponding value, which is b_2. Noting m as countermeasure b_3, the event assembles $B=\{b_1,b_2,b_3\}$ Thus there is a situation assembles

$$S=\{s_{ij}=(a_i,b_j)\mid a_i\in A,b_j\in B\}=\{s_{11},s_{12},s_{13}\}.$$

Six sets of predications are regarded as the average of relative error of six targets In general, the predication effect is better when the average is smaller. Then we establish grey correlation decision matrix and find a better way of effect.

2 PREDICATION RESULTS OF THREE METHODS

Taking the last six data of each set as the forecast test value, the preceding data is provided building the mould array. Then we take every data group's predictive value as prediction results.

Table 1.K9+940(middle).Prediction results of cross section subgrade settlement observed data in three kind of method

Serial Number	Actual Value (mm)	Predictive Value (m takes 1)	Relative Error (%)	Predictive Value (m takes n)	Relative Error (%)	Predictive Value (m takes minimum errorpoint)	Relative Error (%)
1	15.9	15.5	2.5157	16.25	2.20126	15.5	2.5157
2	20.2	20.26	0.29703	20.53	1.63366	20.26	0.29703
3	25.85	26.47	2.39845	25.93	0.30948	26.47	2.39845
4	33.6	34.58	2.91667	32.76	2.5000	34.58	2.91667
5	42.5	45.18	6.30588	41.39	2.6118	45.18	6.30588
6	51.9	59.03	13.738	52.29	0.75145	59.03	13.738
Average Error(%)			4.6953		1.6679		4.6953

Table 2.K22+925(middle).Prediction results of cross section subgrade settlement observed data in three kind of method

Serial Number	Actual Value （mm）	Predictive Value (*m* takes 1)	Relative Error （%）	Predictive Value (*m* takes n)	Relative Error （%）	Predictive Value (*m* takes minimum errorpoint)	Relative Error （%）
1	125.8	121.89	3.1080	124.16	1.3037	121.89	3.1080
2	145.7	146.13	0.2951	144.39	0.8991	146.13	0.2951
3	168.6	175.2	3.9146	167.9	0.4152	175.2	3.9146
4	192.2	210.04	9.2820	195.25	1.5869	210.04	9.2820
5	227.6	251.82	10.6410	227.06	0.2373	251.82	10.6410
6	266.7	301.91	13.2020	264.04	0.9974	301.91	13.2020
Average Error（%）			6.7406		0.9066		6.7406

Table 3.K65+680（left）.Prediction results of cross section subgrade settlement observed data in three kind of method

Serial Number	Actual Value （mm）	Predictive Value (*m* takes 1)	Relative Error （%）	Predictive Value (*m* takes n)	Relative Error （%）	Predictive Value (*m* takes minimum errorpoint)	Relative Error （%）
1	52.7	52.6	0.1898	52.93	0.4364	52.68	0.0380
2	59.5	58.35	1.9328	58.57	1.5630	58.53	1.6303
3	64.54	64.73	0.2944	64.82	0.4338	65.02	0.7437
4	71.3	71.81	0.7153	71.73	0.6031	72.23	1.3044
5	79.6	79.67	0.0879	79.37	0.2889	80.24	0.8040
6	88.1	88.38	0.3178	87.83	0.3065	89.15	1.1918
Average Error（%）			0.5897		0.6053		0.9520

We take the forecasting result of the average error of every method as evaluation criterion for its data's prediction effect. The average is compared with the error. It is smaller, the prediction effect is better. Thus it makes up decision matrix as Table 4. It adopts a grey connect making policy, which is finding a way in Table 4. Finding a way in scheme matrix, it makes more effective for data prediction as much as possible.

Table 4.the average relative error of every data（%）

Subgrade section	K9+940 middle	K22+925 middle	K65+680 left	K95+100	K123+840	LK4+550
Method 1	4.6953	6.7406	0.5897	0.3555	0.6168	0.4280
Method 2	1.6679	0.9066	0.6053	0.3693	0.6731	0.4781
Method 3	4.6953	6.7406	0.9520	0.3555	0.6250	0.7374

Calculating the difference between the three methods and the ideal optimum vector, we can get the correlation coefficient and the ideal optimum vector from the difference sequence. Such as Table 5：

Table 5.The correlation coefficient of the three methods and the ideal optimum

Subgrade section	K9+940 middle	K22+925 middle	K65+680 left	K95+100	K123+840	LK4+550
Method 1	0.5000	0.4031	1.0000	1.0000	1.0000	1.0000
Method 2	1.0000	1.0000	0.9741	0.9555	0.9030	0.8998
Method 3	0.5000	0.4031	0.6187	1.0000	0.9847	0.5926

From Table 5, It can be conclude that the predictive effect of method 2 is better in the two group data (which is thickness). The more effect of method 1 has four groups (which is underlined). The more effect of method 3 has four groups (which is added frame). The last point is that the data is the newest and abundant information amount. It is also reflects the development of sedimentation tendency. The information of the first data reflects its development of sedimentation tendency. So the information is not enough for the current tendency. And the information is incorrect. The fitting error is smaller, the predictive effect is worse. The reason is that there is some interference data in sedimentation. We make use of least square method in GM (1,1) model. And the method makes the fitting error least, which leads to the model more sensitive and takes all interference data into consideration. Thus, the predictive effect is the poorest. According to the above analysis, we know that the method 3 is not advisable. If method 2 is adopted in all condition. Even through it would take better predictive effect, it is worse than method 1 in some situation.

3 TIME SERIES FORECAST METHOD OF NON-STANDARD GLOSSY SETTLING

We make a glossy inspection for the six data. Except subgrade section K9+940 and K22+925, the other four data can satisfy glossy condition. The smooth ratio of this two data is as following:

Subgrade section K9+940: {0.5194 0.4235 0.4624 0.3897 0.3563 0.3362 0.3270 0.3117 0.2902}

Subgrade section K22+925: {1.0810 0.6307 0.5682 0.3867 0.2927 0.3053 0.2709 0.2466 0.2255 0.2179 0.2097}

The two data above can satisfy $0 \le \varepsilon_k < 0.5$ expect subgrade section K22+925. They can not satisfy that the smooth ratio declines. Therefore, we can not take interval settlement as modeling data to build GM (1, 1) model. From Table 1、Table 2, we can make a provident. Actually, the predictive effect is non-ideal. Thus, we need to make a cumulative settlement for interval settlement. Its inspection makes it more smoothness. If it can satisfy its smoothness, we can take cumulative settlement as modeling data to build GM (1, 1) predictive model. Then we make an inverse accumulated generating for its predictive result. That is the predictive value of

cumulative settlement.

The smooth ratio of cumulative settlement is as following：

Subgrade section K9+940：{0.4736 0.4199 0.3864 0.3642 0.3486 0.3379 0.3300 0.3242 0.3198}

Subgrade section K22+925：{0.5045 0.4872 0.4455 0.3695 0.3235 0.2930 0.2717 0.2561 0.2445 0.2355 0.2285}

The above two sets of cumulative settlement's smooth ratio can satisfy smooth condition. Therefore, it would be taken cumulative settlement as modeling data. Then it would predict the posterior settlement and take interval settlement as modeling data. And its predictive result was making comparative analysis.

From the results, we can learn from its non--standard glossy settling time sequence forecast method. It adopts cumulative settlement to build grey modeling and reduce its randomness. Then it appears exponential increase law and proves its predictive results. Take cross section for example; the average error is 4.6953% when building cumulative settlement modeling. Meanwhile, the average error is 1.1450% when building interval settlement modeling. The predictive result would be made a progress. In cross section K22+925, the average error is 6.7406% when building interval settlement modeling. Meanwhile, the average error is 1.8200%when building cumulative settlement modeling. The predictive results are improved obviously. Thus, this passage suggests that we should adopt grey system theory when it needs to be tested. If the settlement time sequence can not satisfy its smooth condition, we should adopt cumulative for modeling. The prediction accuracy would be highly improved.

CONCLUSIONS

In this paper, three methods of determining integral constant are presented. For the six sets of observation data of Shaohuai expressway subgrade subsides, Six-step predications are respectively made. The selected method of modeling data curve is proposed by comparing and analyzing the predication results. Smoothing test of part of data is made in the predication. For the two-group data which does not satisfy the smoothing condition, cumulative settlement is used to create subgrade settlement gray system forecast model. The predictive result is remarkably improved. In addition, more attention should be paid to forecast result departure from regular value gravely because of ill condition for matrix in forecasting process.

ACKNOWLEDGMENTS

The authors appreciate the support of the Hunan Province S&T Plan Projects Foundation.

REFERENCES

Tang, Li-min, and Tang, Ping-ying (2008). "Analysis of subgrade settlement and study of prediction model's ill-conditioned problems." *Journal of china & foreign highway*, Vol. 28(2): 75-79.

Wang, Zhu-ming; and Zhang, Xiong-wu (2003). "Analysis and prediction of unequal step deformation monitoring for expressway." *The exploration of scientific technology*, Vol. (4): 26-28.

Zhang, Yi-ping; Yu, Ya-nan; Zhang, Shi-qiao; Gao, Wen-ming (2002). "The grey model theory and the method of asaoka in settlement prediction." *The theory and practice of systems engineering*, Vol. (9): 141-144.

Zheng, Zhao-ning, Wu, Yu-ying, et.al. (2001). "Ill-conditioned problems of GM model." *Management science in china*, Vol. 9 (5): 38-44.

Zhong, Cai-gen; Ding, Wen-qi; Wang, Mao-he (2005). "The apilication of nerual network model in expressway in settlement prediction of soft soil foundation." *China journal of highway*, Vol. 16 (4): 31-34.

Temperature Prediction Model for Flexible Pavements in Taiwan

Chi-Chou Liao[1], Bo-Ruei Chen[2], Shun-Hsing Chen[1], and Wei-Hsing Huang[3]

[1] PhD candidate, Department of Civil Engineering, National Central University, 300 Jungda road, Jungli, TAIWAN; 93342014@cc.ncu.edu.tw

[2] Master, Department of Civil Engineering, National Central University, 300 Jungda road, Jungli, TAIWAN; 953202038@cc.ncu.edu.tw

[3] Professor, Department of Civil Engineering, National Central University, 300 Jungda road, Jungli, TAIWAN; t321655@ncu.edu.tw

ABSTRACT: In this study, a large amount of temperature measurements were obtained from a test site incorporating 3 typical pavement sections to establish a pavement temperature prediction model for freeways in Taiwan. Using thermocouples embedded at 20-mm distance in depth, temperature profiles of 3 different pavement structures were determined for 24-hr periods covering seasonal variations. Predictions made by BELLS model revealed that, at pavement temperature higher than 40℃, the model tends to underestimate pavement temperatures. Considering the climatic characteristics in Taiwan, the air temperature at testing time is used in the model. Also, a single sine function on a 24-hr clock system is used to simplify the predicting equation. The proposed pavement temperature model shows a good correlation between measured and predicted temperatures and has a coefficient of determination greater than 0.93. The pavement temperature prediction model is judged to be easier to use than the BELLS model, due to the fact that temperature data for the previous day are no longer needed, and will be used for temperature adjustment of future falling weight deflectometer data in Taiwan.

INTRODUCTION

In the assessment of pavement capacity, the falling weight deflectometer (FWD) has been used extensively. Since the stiffness of asphalt concrete (AC) is greatly influenced by ambient and pavement temperatures, it is critical for the use of FWD to be able to determine an effective temperature of the asphalt layer. As the temperature of the asphalt concrete increases, its stiffness decreases that may lead to rut occurring on the asphalt pavement from wheel loads. A decrease in asphalt concrete stiffness results in lower structural capacity to support vehicle loads. In routine FWD data

collection, in addition to the deflections of pavement obtained by FWD, the in situ temperature of asphalt concrete needs to be determined non-invasively. In order to interpret FWD data appropriately, it is essential to estimate the pavement temperature accurately using information readily collectable at the time of testing.

The 1986 AASHTO Guide for Design of Pavement Structures (AASHTO, 1986) presented a temperature correction protocol for FWD deflections. This procedure requires the use of the average air temperature for the previous 5 days to predict pavement temperatures at selected depths. However, this procedure does not take into account temperature gradient effects due to diurnal heating and cooling cycles, which have a significant effect on the effective pavement temperature and its relationship with the AC modulus and the surface deflection (Lukanen et al., 2000). Therefore, there is an urgent need to develop new temperature models for predicting pavement temperatures in a convenient manner.

In the past, Park et al. (2001) developed a pavement temperature prediction model in Michigan. Unlike the 1986 AASHTO method, the model no longer requires temperatures for the previous 5 days but takes into account temperature gradients due to diurnal heating and cooling cycles. Lukanen et al. (2000) developed new temperature prediction and deflection correction procedures using data collected from the long-term pavement performance (LTPP) study. This temperature prediction model of LTPP is BELLS3 that can be used generally to predict effective temperature of AC pavement in the US. It provides a convenient temperature measurement procedure to obtain effective temperature for AC pavements. However, the BELLS3 model was developed based on daytime pavement temperature data, and it's applicability to nighttime remains unclear. Moreover, this model is valid only for AC thickness of 45 to 305 mm (1.8 to 12 in.), based on the LTPP program's database. Due to the very heavy traffic on freeways in Taiwan, there is a need to conduct routine FWD testing in the nighttime so as to minimize the impact of blocking traffic for testing. In addition, thickness of asphalt layers for freeways in Taiwan ranges from 320 to 415 mm, which is much thicker than typical pavements in other countries. Hence, the main objective of this study is to establish a pavement temperature prediction model applicable to the freeway pavements in Taiwan, such that FWD data can be used effectively for pavement structural evaluation.

EXPERIMENTAL PROGRAM

In this study, a test site incorporating 3 pavement sections representing typical freeway pavement structure in Taiwan was constructed. All pavement sections were instrumented with temperature sensors connected to portable data logger. The pavement cross-section information is summarized in Table 1. It is noted that freeway pavements in Taiwan are comprised of aggregate base, bituminous treated base (BTB), and asphalt concrete with a 15-mm open graded seal course on top.

Since the total thickness of asphalt layers ranges from 315 mm to 415 mm, it was decided to install thermocouples in the lower portion of asphalt layers and use temperature probe in the upper portion. In the lower portion, thermocouples were embedded at the interface of AC and BTB, and at 20, 30, 40 mm down to the BTB layer, and 10, 20 mm up from the bottom of AC. In the upper portion, to profile the

temperature gradient for AC, test holes were drilled approximately 0.5 cm in diameter and 20, 40, 60, 80, 100 mm in depth. A digital thermocouple probe was inserted in each hole for measurement. The air temperature and pavement surface temperature were obtained using an infrared temperature gun. Fig. 1 shows the schematic of temperature measurement layout. All temperature data were recorded at 10-minute intervals within a day. Temperature data collected in this study range from 12℃~37℃ for air temperature and 15℃~60℃ for pavement surface temperature, which cover the typical temperatures for the subtropical climate in Taiwan.

Table 1. Typical pavement cross-sections of freeways in Taiwan (mm)

Freeway number	Thickness			Total thickness
	AC	BTB	Aggregate base	of asphalt layer
Freeway 1	165	250	350	415
Freeway 3	115	200	250	315
Freeway 6	180	150	300	330

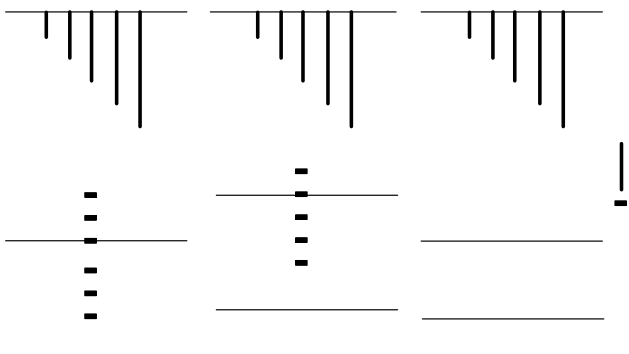

FIG. 1 Schematic of pavement cross-sections and temperature measurement set-up (mm).

BELLS3 TEMPERATURE PREDICTION MODEL

BELLS3 temperature prediction model was developed with data from the Long-Term Pavement Performance Project's Seasonal Monitoring Program. Named BELLS after the first letters of the author's last names. BELLS3 model predicted the

effective temperature of AC layer by using the infrared surface temperature reading, the average of previous day's high and low air temperatures, the time of day, and the AC layer thickness. BELLS3 model was established for routine FWD testing. The BELLS3 model for routine testing is as below:

$$T_d = 0.95 + 0.892IR + (\log d - 1.25)\left[1.83\sin(hr_{18} - 15.5) - 0.448IR + 0.621T_{avg}\right] + 0.042IR\sin(hr_{18} - 13.5) \quad (1)$$

where T_d is pavement temperature at layer mid-depth (℃), IR is infrared surface temperature (℃), T_{avg} is the average of previous day's high and low air temperatures on the day before testing (℃), and d is layer mid-depth (mm). $\sin(hr_{18} - 15.5)$ and $\sin(hr_{18} - 13.5)$ are sine function times with 18 hour period.

RESULTS OF AC TEMPERATURE MEASUREMENT

Pavement temperature data obtained from Freeway 3 on May 14, 2008, are shown in Fig. 2. It can be observed that, in the daytime, the highest pavement temperature occurred at the surface, while that in the nighttime (after 17:00) occurred in the BTB layer. Pavement temperature fluctuates more significantly in the daytime than in the night. The highest air temperature of 34℃ occurred at between 12:00 and 13:00, and the highest pavement surface temperature occurred at about the same but with a much higher value of 55℃. But as the depth increases, the time that the highest temperature occurs gets later. The variations in temperature at both pavement surface and mid-depth are found to be much higher than that of the BTB layer. Actually, the results indicate that the greatest temperature difference within a day at pavement surface, mid-depth, and BTB layer was found to be 25, 19, and 7℃, respectively. It was found that the maximum greatest temperature difference observed in July at the 3 locations were 30, 21, and 11℃, respectively. In summary, temperature variation in BTB layer is less notable, while AC is the principal layer to be considered for temperature effects in pavement structural analysis.

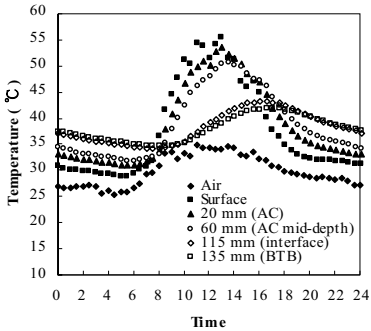

FIG. 2 Variations of temperature at different depth in a 24-hr period (Freeway 3 pavement section).

TAIWAN TEMPERATURE DATA WITH BELLS3 MODEL IN TEMPERATURE PREDICTION

Temperature data at the test site were collected continuously for a 12-month period, covering the full range of temperatures to be experienced in Taiwan. These data were fed to the BELLS3 model and evaluated for applicability of BELLS3 model to pavements in Taiwan. The relationships between the measured and predicted AC pavement temperatures are shown in Fig. 3. Regression analysis on the 8047 data points against the 45° straight line gives a coefficient of determination (R^2) of 0.88, which is considered acceptable. However, it is also noted in Fig. 3 that the predictions over the high temperature range (≧ 40℃) are relatively poor, and a tendency of under-prediction can be observed in this temperature range. It is judged that the BELLS3 model was developed using database obtained from north America, which is rarely exposed to a temperature regime of this high. Fitting the local temperature data of Taiwan to BELLS3 may generate under-predicted temperature of AC layer. Therefore, it was decided to develop a new pavement temperature prediction model that is suitable for local temperature situations in Taiwan.

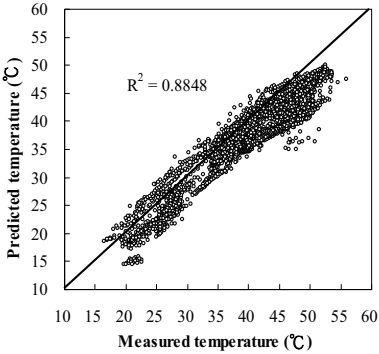

FIG. 3 Measured versus predicted pavement temperature using BELLS3 model.

PROPOSED TEMPERATURE PREDICTION MODEL

Published temperature models indicated that the input variables for a prediction model should be easily obtainable in the field during FWD testing and adequate to predict subsurface temperature. Hence, pavement depth, time of testing, air temperature, and pavement surface temperature were selected as input variables for proposed pavement temperature prediction model. Time variable is an important factor in describing temperature variation of pavements within day and night time. Fig. 4 shows the temperature variations with time in a 24-hour period. Eight 24-hour temperature variations obtained from different months in a year show closeness in their undulation, when they are transferred to sine function value between 1 and -1. This reveals that the behavior of temperature variations can be described by one representing sine curve. Fig. 5 shows the representing sine curve for pavement temperature variation with time. The equation for the sine curve is $f(t) = \sin(-6.3252t + 5.6989)$, where t is time when the AC surface temperature was measured, e.g., 1:30 p.m. = 13.5/24 = 0.5625. The time equation was used as a parameter in the development of Taiwan temperature prediction model.

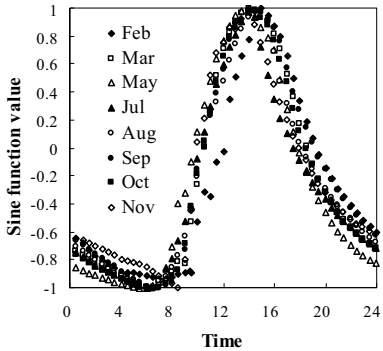

FIG. 4 Sine function curves at different months.

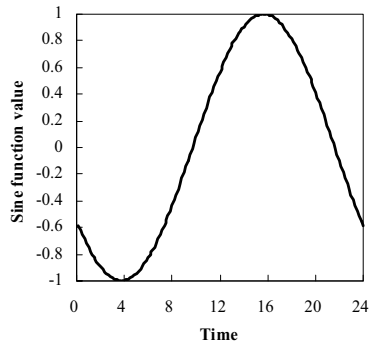

FIG. 5 The representative sine function curve of sin (-6.3252*t* + 5.6989).

Pearson correlation analyses showed that the correlation coefficient of the selected input variables and the mid-depth temperature were all higher than 0.8. Hence, all these variables are used in the proposed model. Using 8047 temperature observations from those sites summarized in Table 1, the following model is proposed to be used for prediction of pavement temperature in Taiwan.

$$T_d = f(t)\left[21.8450 + T_{air}(-1.5547 + 0.0223IR + 0.6433\log(d))\right] + \log(d)\left[IR(-0.8662 - 0.0109T_{air} - 0.4155f(t)) + (-18.5074 + 1.9254T_{air})\right] - 2.0030T_{air} + 2.4840IR + 10.2546 \quad (2)$$

where: T_d = pavement temperature at depth d in AC layer (℃),
T_{air} = air temperature when testing on t time (℃),
IR = infrared surface temperature (℃),
d = AC layer depth (mm), and
$f(t)$ = sine function time with 24 hours system.

Fig. 6 shows the relationships between the measured and predicted pavement temperature using the proposed model. When fitted to the 45° straight line, a coefficient of determination of 0.93 was found, which exhibits an improvement over that of the BELLS model. To validate the effectiveness of the proposed temperature prediction model, a total of 278 extra temperature observations were collected from other sections on Freeway 1 and 3. The measured vs. predicted mid-depth temperature relationships are shown in Fig. 7. The result shows these additional data have an R^2 value of 0.98, indicating a good fit.

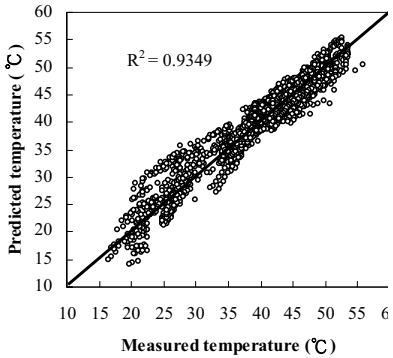

FIG. 6 Measured versus predicted temperature using the proposed model.

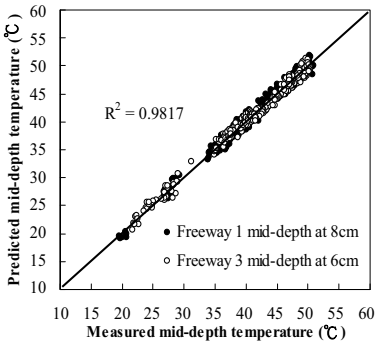

FIG. 7 Validation of the proposed model using field temperature data obtained from Freeway 1 and 3.

CONCLUSIONS

Based on a large amount of pavement temperature data obtained from a test site covering 3 typical freeway pavement sections, a pavement temperature prediction model is proposed for Taiwan's freeways. In this model, the air temperature at the time of testing, rather than the average air temperature in the day before testing, is used for predicting pavement temperature. In response to the necessity of conducting FWD tests in the nighttime, a single sine function time variable on a 24-hr clock system is adopted in the proposed temperature prediction model. With the climatic characteristics in Taiwan, the use of air temperature at the time of testing and a single sine function of time on a 24-hr clock system provide not only convenience during testing but also improved accuracy in predicting pavement temperatures for freeways in Taiwan.

REFERENCES

AASHTO Guide for Design of Pavement Structures. (1986). American Association of State Highway and Transportation Officials, Washington D.C.

Lukanen, E. O., Stubstad, R. N., and Briggs, R. (2000). "Temperature Predictions and Adjustment Factors for Asphalt Pavement." *Report FHWA-RD-98-085*. FHWA, U.S. Department of Transportation.

Park, D., Buch, N., and Chatti, K. (2001). "Effective layer temperature prediction model and temperature correction via falling weight deflectometer deflections." *Transportation Research Record 1764*, Transportation Research Board, Washington, D.C., 97–111.

Parallel Direct Solver for Linear Systems Resulting from Constitutive Modeling of Pavement

T.B. Jönsthövel[1], X. Liu[2], A. Scarpas[3], C. Vuik[4]

[1] PhD student at the groups of structural mechanics and numerical mathematics at Delft University of Technology, the Netherlands; t.b.jonsthovel@tudelft.nl
[2] Researcher at the group of structural mechanics at Delft University of Technology, the Netherlands; x.liu@tudelft.nl
[3] Associate Professor and coordinator at the group of structural mechanics at Delft University of Technology, the Netherlands; a.scarpas@tudelft.nl
[4] Director of the Delft Centre for Computational Science and Engineering Delft University of Technology, the Netherlands; c.vuik@tudelft.nl

ABSTRACT: Reliable and realistic computer simulations of pavement behavior are important for improving the design process of pavement materials. Most simulations involve 3D modeling and therefore large finite element meshes. Hence, the systems that result from discretization involve many degrees of freedom and are difficult to solve. Constitutive modeling is an expensive process when mesh sizes increase. The introduction of a parallel direct solver reduces both computation time and the number of iterations to solve the system and yielding more realistic simulations.

INTRODUCTION

Within the field of structural mechanics, pavement engineering plays an important role in understanding and modeling the effects on heavy duty materials like asphalt and concrete when exposed to different kind of forces. Not only the appliance of force but also weather conditions and aging have to be taken into account. It is of crucial importance that the industry is able to predict how materials react to various circumstances under different time spans. Understanding these effects may result in more careful engineering of these materials, which may replace the current trial and error design process. Moreover CAD methods will be more time and -cost efficient compared to laboratory tests.

COMPUTATIONAL FRAMEWORK

A framework for calculating material response, stresses and strains has been provided in (Scarpas 2004) and (Kringos 2007). In this framework both small and large strains are considered. The balance of forces and conservation of energy yields the virtual work

equation. Due to the non-linear material properties, the virtual work equation will have to be linearized in order to solve it.

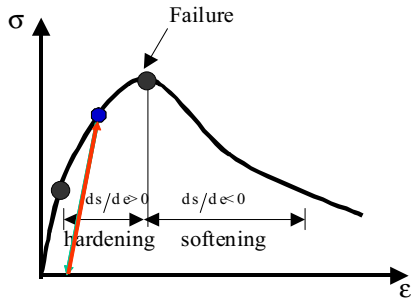

FIG. 1. Strain-stress curve of elasto-plastic material

The response of materials to distributed loads is captured in a stress-strain curve and is known as the constitutive relation. Different algorithms deliver different curves. A good fitting of the test data can justify the material response algorithms. The curve of figure 1 illustrates the loading of an elasto-plastic material. Three phases are considered. The first phase is a linear process and involves elastic response only. The other two phases are non-linear processes and involve the elastic-plastic response. When evaluating computer simulations, these phases require the most computing time because of their non-linear behavior.

The linearized virtual work equation is discretized by the finite element method. A mesh is created to represent the body of the material, the mesh elements are either tetrahedrals or cubes. The resulting grids will be unstructured in most real life applications. Sophisticated mesh generators like Cubit, TetGen or Amira produce meshes that are congruent with the structure of the material. For example, a material like asphalt contains three basic ingredients, stones, bitumen and air. To obtain realistic simulations of the material each ingredient should be represented as accurate as possible. The mesh should follow the borders between the ingredients.

The finite element discretization uses second order shape functions, the unknowns lie on the corners and in the centre of the vertices of the elements. The linearized virtual work equation has to be solved for the unknown displacement field. The displacement field has three dimensions, therefore the unknowns on the grid nodes have three components for the x, y and z direction respectively. The discretization of the linearized virtual work equation results into a short hand notation of the static, linear system that has to be solved,

$$K\Delta u = \Delta f \tag{1}$$

where K is the stiffness matrix, Δu the unknown incremental displacement field and Δf the difference between the internal and external stresses.

The stresses and strains within a body are determined with Algorithm 1. This algorithm has three main steps. The first step is the appliance of an external load to the body. This is either stress or strain regulated. The second step is the calculation of the

displacements as a response to the external load, which is equal to solving linear system (1). The third and last step is the appliance of the material properties, i.e. the calculation of the non-linear internal stresses and involves the constitutive models.

Algorithm 1. Balance of forces

for $t = 0...t_{end}$ **do**

Start with initial external load f_{ext}^{t}

for $i = 0$ until convergence **do**

Compute the stiffness matrix K^t

if $i = 0$ **then** $f_{\text{int}}^{0} = 0$ and $\Delta f^0 = f_{ext}^{t} - f_{\text{int}}^{0}$

Solve system $K^t \Delta u^i = \Delta f^i$

Update displacements $u^{i+1} = u^i + \Delta u^i$

Compute internal force, f_{int}^{i+1} and $\Delta f^{i+1} = f_{ext}^{i} - f_{\text{int}}^{i+1}$

Test $\dfrac{\Delta f^{i+1}}{\Delta f^0} < \varepsilon$

end do

end do

The stiffness matrix K is symmetric positive definite for all simulations. This is an important property as it is crucial for obtaining good convergence rates for many numerical solution methods. For small meshes the dimension of K allows for direct solution methods if the matrix is non-singular. However, with the refinement of the meshes the dimension and complexity of the linear system increases significantly and other numerical solution methods need to be found. Increasing the dimension of K induces great difficulties for direct solvers because computer memory and CPU power are limited. The condition number is defined as the quotient between the largest and smallest eigenvalues of a matrix. Large conditions numbers yield ill-conditioned systems, which are therefore difficult to solve. Not only grid refinement but also the non-linear material properties affect the solvability of system (1). When plasticity and viscosity builds up or hyper-elasticity applies, stiffness of the materials changes and stiffness matrix K will have to be reassembled. Large differences in stiffness between material ingredients, e.g. stone and bitumen, will result in large condition numbers and thus in slow converging solvers.

Most mechanic analysis algorithms use direct solvers for solving the linear system of the Newton-Raphson loop in Algorithm 1. These direct solvers are based on LU-decomposition of the stiffnessmatrix, i.e. compute $K = LU$ where L, U are lower and upper triangular matrices respectively. The decomposition process is both time and resource consuming. Open source implementations that can be found in LAPACK require large memory and powerful CPUs. Hence, in many cases the stiffness matrix is kept constant, e.g. $\forall t > 0 \; K^t = K^0$, to reduce the number of decompositions. This process is called initial stiffness. Obviously, when plasticity or viscosity builds up the stiffness of the body changes and the initial stiffness matrix does not represent the

stiffness of the body at an arbitrary load step *t*.

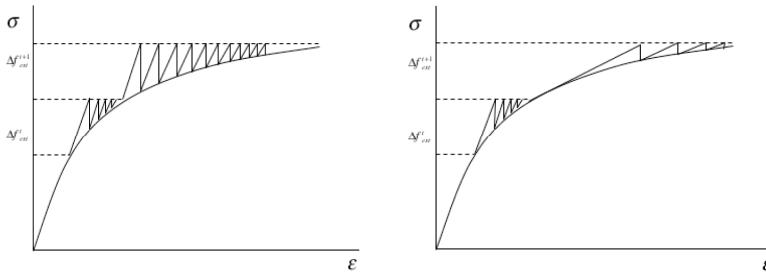

FIG. 2. Convergence pattern for Newton Raphson iteration process.

The approximation of the stiffness matrix affects the performance of the Newton-Raphson method and yields bad convergence rates and a large number of iterations. To reduce the number of iterations modification of the stiffness matrix is required, preferably every iteration of the Newton-Raphson loop, hence a fast (direct) solver is needed.

PARALLEL DIRECT SOLVER

Speed and scalability are two reasons for replacing the current direct solver with a more powerful linear solver. An obvious choice would be a parallel direct solver. Parallel direct solvers can handle large systems and divide the workload over a number of computing nodes. The requirements of speed and scale are easily satisfied. Moreover, adding more computing nodes will decrease computation times. Several open source implementations of parallel direct solvers are available. All implementations are based on LU decomposition of the linear system. This research will focus on MUMPS.

MUMPS is a public domain package and has been developed during the Esprit IV European project PARASOL (1996-1999) by CERFACS, ENSEEIHT-IRIT and RAL. The MUMPS package computes a LU decomposition of non-singular matrices. The MUMPS software is parallel and should therefore be executed on parallel machines only.

NUMERICAL EXAMPLE

The response of a pavement structure was simulated by means of CAPA-3D. The dynamic analysis option was utilized to subject the model to moving wheel-loading. The pavement profile w=1.5m wide and L=4.2m long was selected for the numerical simulations. Because of reasons of symmetry, only half of the pavement was simulated. The pavement profile was assumed to consist of three material layers, Fig. 1. The bottom layer represents a layer of soil with a thickness of h3=15 m. The middle layer represents a sub-base material with a thickness of h2=0.3 m. Both the subgrade and the sub-base layer are assumed to behave linear elastically. The top-layer represents the asphalt layer with thickness of h1=0.15. The finite element mesh consists of 20-nodded

brick elements. In order to reduce the dynamic wave reflection, layers of impendence elements were introduced to the boundaries of the mesh. The single moving wheel load (Type A, Eurocode 1-3, 220x320mm2, 0.8 MPa) with speed 60 km/h was applied on the top of the pavement. The running length of the moving wheel is about 2.0 m. Each full-length forward wheel movement is counted as a 'load repetition'. The parameters of the material constitutive model are obtained from mechanical data of base course asphalt mixes, which were given by report (Liu et al. 2007).

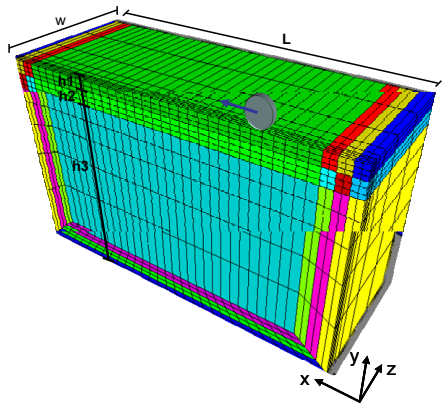

FIG. 3. Cubic element mesh for pavement loading simulation.

The following experiments have been done on a cluster with four workstations carrying one Intel Xeon E5450 3.0 GHz Quad-core Duo and 16Gb of 800 MHz DDR2 memory each, yielding 32 processors and 64Gb of memory in total. The workstations were connected by an 1-Gigabyte ethernet network.

Figure 4 shows the test results for parallel LU decomposition of three different matrices. Five different configurations are considered with 2, 4, 8, 16 and 32 processors respectively. Each workstation only hosts 8 processors, hence the gray dotted vertical line indicates the transition to a cluster of workstations. Two and four workstations when requesting 16 processors and 32 processors respectively. The bold lines represent the actual test results, the remaining black lines represent the theoretical linear speed up. An ideal parallel algorithm, with no communication overhead, should run twice as fast with twice as many processors involved. Apparently, this is not feasible when the communication between workstations, CPUs and memory is taken into account.

The results are promising. For every test case reasonable speed up is observed. When the dimension of the matrices increases, the performance of MUMPS improves because initial communication overhead becomes negligible compared to the computation process. Only when more workstations become involved the subsequent speed up disappears because of network delays and latency. An infiniband network connection could overcome these problems.

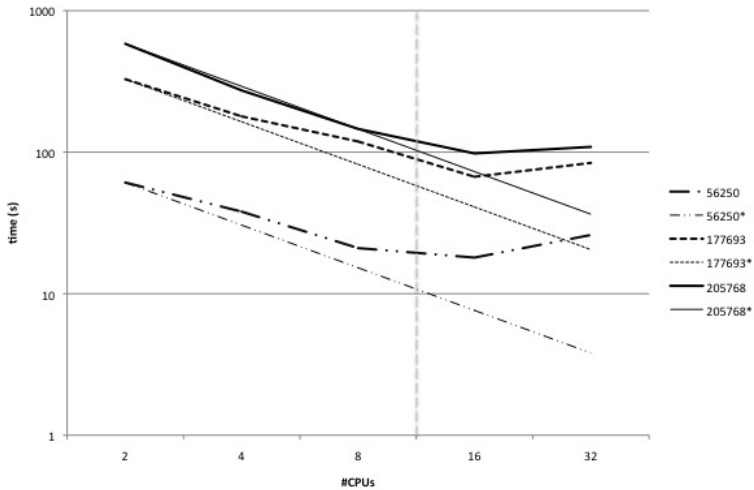

FIG. 4. Wall time of matrix decomposition for different cluster configurations.

CONCLUSIONS

The algorithm for evaluating the virtual work equation has two bottlenecks. The computation of the increment of the displacement field, which involves the direct solve of a massive linear system. And the slow converging Newton-Raphson iteration process, due to changing material stiffness and an inconsistent stiffness matrix. Both bottlenecks can be overcome by replacing the serial direct solver by a parallel direct solver. The parallel solver can handle much larger systems of equations and is much faster compared to the serial solver. Hence, lower decomposition times and modification of the stiffness matrix yield less iterations in the Newton-Raphson loop and therefore much lower overall computation time. Larger meshes and models are possible and more realistic 3D simulations can be done.

REFERENCES

CERFACS. *MUMPS.* (2008). http://graal.ens-lyon.fr/MUMPS.

Kringos, N. (2007). “Modeling of combined physical-mechanical moisture induced damage in asphaltic mixes.” Delft University of Technology, The Netherlands.

Liu, X. *et al.* (2007). “Advanced FEM modeling of polymer modified asphalt base course mixes by wheel tracking simulation.” *Report CM 2007-002*, Delft University of Technology, The Netherlands.

Scarpas, A. (2004). “a Mechanics based computational platform for pavement engineering.” Delft University of Technology, The Netherlands.

Dynamic Responses Model of Asphalt Pavement under Complex Vehicle Loads

QIAN Guoping[1], Ph.D, ZHENG Jianlong[2], Ph.D and ZHANG Honggang[3], M.D

[1]Associate Professor, Communication and transportation Engineering school of Changsha University of Science and Technology, Changsha P.R.China, 410076; guopingqian@sina.com

[2]Professor, Communication and transportation Engineering school of Changsha University of Science and Technology, Changsha P.R.China, 410076; ZJL@csust.edu.cn

[3]Instructor, Communication and transportation Engineering school of Changsha University of Science and Technology, Changsha P.R.China, 410076; liweizhanghonggang@126.com

ABSTRACT: The overweight vehicles create complex moving vehicle loads described as dynamic, three-dimension non-uniformly distributed contact stresses between tire and pavement surface. But existing calculation models and methods for structure mechanics of pavement cannot analyze the mechanical response of pavement under complex vehicle loads. Based on the theory of three-dimension elastic dynamics, the above problems were solved by using multidimensional Fourier Transformation technique after transforming moving coordinates, and general solution for multilayer elastic system under complex vehicular load was derived in this paper. Then, pivotal issues were analyzed for numerical methods implementation. Lastly, the calculation results were contrasted with results of spot test, which showed that the mechanical responses model and its numerical methods implementation are reasonable and correct.

INTRODUCTION

In recent years, with the economy development in China, road construction has rapidly developed, at the same time, road traffic situation has undergone tremendous changes, and the phenomenon of overweight vehicle has become widespread. “Heavy axle load” and "high tire pressure" are the most intuitive features of the overweight vehicles that create complex moving vehicle loads described as dynamic, three-dimension non-uniformly distributed contact stresses between tire and pavement surface (Qian et al. 2003.).

The existing design method for asphalt pavement is invalid under the condition of complex vehicle loads mentioned above, because existing calculation models and methods for structure mechanics of pavement cannot consider load modes beyond the simplest static load cases (Industry standards of P.R.China.2004.). With the trend of weight heavier and speed faster of vehicles, the difference between static load mode and the actual complex load of vehicles on the road become clearer, and the effect of complex vehicle load on pavement should not be ignored. So, research on the

dynamic responses model of asphalt pavement under complex vehicle loads becomes the urgent affairs.

In order to obtain the dynamic responses of asphalt pavement under complex vehicle loads, a reasonable model describing interaction between tire and pavement surface should be given, and a feasible dynamic responses model of asphalt pavement and its numerical methods implementation should be established.

TIRE-PAVEMENT SURFACE CONTACT STRESSES MODEL

The mechanical interaction between vehicle and road is implemented by the tire-pavement surface contact stresses, so reasonable description for the load and its distribution on tire-pavement interface is the foundation for exactly analyzing the mechanical responses of pavement structure.

The form of mechanic interaction between tire and pavement surface is three-dimensional contact stresses (vertical, longitudinal, transverse), shown as fig.1. Tire-pavement surface contact stresses are influenced by multi-factors, and the physical model is extremely complicated (DE BEER et al.1997.). Simultaneity, there are still many problems not to be solved so far. Based on the former research and reasonable assumptions, the mathematical expressions of three-dimensional contact stresses are derived as f_{zz}, f_{xz}, f_{yz}, which offer the mechanical boundary conditions for pavement mechanical responses model. The special research on the model for complex tire-road surface contact stresses under heavy traffic vehicles has been carried out (Qian et al. 2008.).

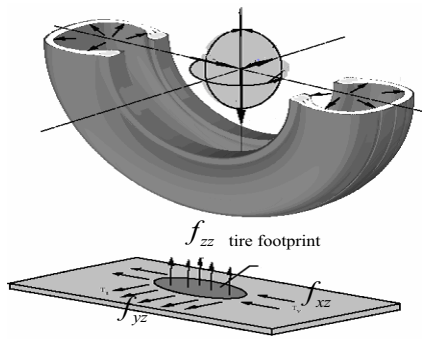

FIG.1. Tire-road Contact Surface and Contact Stress.

DYNAMIC RESPONSES MODEL OF ASPHALT PAVEMENT UNDER COMPLEX VEHICLE LOADS

The mechanical state of arbitrary point for elastic body in three-dimensional space coordinates $\{x, y, z\}$ under load is expressed as six stresses $\sigma_x, \sigma_y, \sigma_z, \tau_{xy}, \tau_{yz}, \tau_{zx}$, six strains $\varepsilon_x, \varepsilon_y, \varepsilon_z, \gamma_{xy}, \gamma_{yz}, \gamma_{zx}$ and three displacements u, v, w (Zhu et al. 1985.). If the elastic body suffers the external load moving at the constant speed along the x-axis, so moving coordinate axis η can be defined by,

$$\eta = x - \vec{v} \cdot t \tag{1}$$

Where, $\vec{v}$ is moving speed of the vehicle.

According to equation (1), mechanical problems under the original time-space coordinates $\{t,x,y,z\}$ can be transformed to those under the moving time-space coordinates $\{t,\eta,y,z\}$by displacing x withη. The mechanical boundary conditions $f_{zz}(t,x,y)$, $f_{xz}(t,x,y)$, $f_{yz}(t,x,y)$ become $f_{zz}(t,\eta,y)$, $f_{xz}(t,\eta,y)$, $f_{yz}(t,\eta,y)$, and the balance differential equations taking displacements as the basic unknown quantities under moving coordinates , can be replaced as equation(2).

$$\left.\begin{aligned}
&G(\frac{\partial^2 u}{\partial\eta^2}+\frac{\partial^2 u}{\partial y^2}+\frac{\partial^2 u}{\partial z^2})+(\lambda+G)(\frac{\partial^2 u}{\partial\eta^2}+\frac{\partial^2 v}{\partial\eta\cdot\partial y}+\frac{\partial^2 w}{\partial\eta\cdot\partial z})=\rho(\frac{\partial^2 u}{\partial t^2}-2\bar{v}\frac{\partial^2 u}{\partial\eta\cdot\partial t}+\bar{v}^2\frac{\partial^2 u}{\partial\eta^2})\\
&G(\frac{\partial^2 v}{\partial y^2}+\frac{\partial^2 v}{\partial z^2}+\frac{\partial^2 v}{\partial\eta^2})+(\lambda+G)(\frac{\partial^2 v}{\partial y^2}+\frac{\partial^2 w}{\partial y\cdot\partial z}+\frac{\partial^2 u}{\partial y\cdot\partial\eta})=\rho(\frac{\partial^2 v}{\partial t^2}-2\bar{v}\frac{\partial^2 v}{\partial\eta\cdot\partial t}+\bar{v}^2\frac{\partial^2 v}{\partial\eta^2})\\
&G(\frac{\partial^2 w}{\partial z^2}+\frac{\partial^2 w}{\partial\eta^2}+\frac{\partial^2 w}{\partial y^2})+(\lambda+G)(\frac{\partial^2 w}{\partial z^2}+\frac{\partial^2 u}{\partial z\cdot\partial\eta}+\frac{\partial^2 v}{\partial z\cdot\partial y})=\rho(\frac{\partial^2 w}{\partial t^2}-2\bar{v}\frac{\partial^2 w}{\partial\eta\cdot\partial t}+\bar{v}^2\frac{\partial^2 w}{\partial\eta^2})
\end{aligned}\right\}\quad(2)$$

Where, G is the shear module, and λ is the Lame elastic constant.

The space problem of three-dimensional elastic body suffered the dynamic moving load is solved by transforming differential equations (2) using the Fourier transformation of t (time coordinates), η (moving space coordinates) and y (fixed-space coordinates).

The Fourier transformations of function $u(t,\eta,y,z)$, $v(t,\eta,y,z)$, $w(t,\eta,y,z)$ are shown as (3).

$$\left.\begin{aligned}
u(t,\eta,y,z)&=\frac{1}{(2\pi)^3}\int_{-\infty}^{+\infty}\int_{-\infty}^{+\infty}\int_{-\infty}^{+\infty}U(\Omega,\xi,\Phi,z)\cdot e^{i\cdot\Omega\cdot t}\cdot e^{i\cdot\xi\cdot\eta}\cdot e^{i\cdot\Phi\cdot y}\cdot d\Omega\cdot d\xi\cdot d\Phi\\
v(t,\eta,y,z)&=\frac{1}{(2\pi)^3}\int_{-\infty}^{+\infty}\int_{-\infty}^{+\infty}\int_{-\infty}^{+\infty}V(\Omega,\xi,\Phi,z)\cdot e^{i\cdot\Omega\cdot t}\cdot e^{i\cdot\xi\cdot\eta}\cdot e^{i\cdot\Phi\cdot y}\cdot d\Omega\cdot d\xi\cdot d\Phi\\
w(t,\eta,y,z)&=\frac{1}{(2\pi)^3}\int_{-\infty}^{+\infty}\int_{-\infty}^{+\infty}\int_{-\infty}^{+\infty}W(\Omega,\xi,\Phi,z)\cdot e^{i\cdot\Omega\cdot t}\cdot e^{i\cdot\xi\cdot\eta}\cdot e^{i\cdot\Phi\cdot y}\cdot d\Omega\cdot d\xi\cdot d\Phi
\end{aligned}\right\}\quad(3)$$

Inserting equation (3) into (2) to get$U(\Omega,\xi,\Phi,z)$,$V(\Omega,\xi,\Phi,z)$,$W(\Omega,\xi,\Phi,z)$, and basic differential equations about variable z are derived as equations (4),

$$\left.\begin{aligned}
&\frac{\partial^2 U}{\partial z^2}-\left[\xi^2+\Phi^2-\frac{\rho}{G}(\Omega-\xi\cdot\bar{v})^2+\frac{1}{1-2\mu}\xi^2\right]\cdot U-\frac{\xi\cdot\Phi}{1-2\mu}\cdot V+i\cdot\frac{\xi}{1-2\mu}\cdot\frac{\partial W}{\partial z}=0\\
&\frac{\partial^2 V}{\partial z^2}-\left[\xi^2+\Phi^2-\frac{\rho}{G}(\Omega-\xi\cdot\bar{v})^2+\frac{1}{1-2\mu}\Phi^2\right]\cdot V-\frac{\xi\cdot\Phi}{1-2\mu}\cdot U+i\cdot\frac{\Phi}{1-2\mu}\cdot\frac{\partial W}{\partial z}=0\\
&(1+\frac{1}{1-2\mu})\frac{\partial^2 W}{\partial z^2}-\left[\xi^2+\Phi^2-\frac{\rho}{G}(\Omega-\xi\cdot\bar{v})^2\right]\cdot W+i\cdot\frac{\xi}{1-2\mu}\cdot\frac{\partial U}{\partial z}+i\cdot\frac{\Phi}{1-2\mu}\cdot\frac{\partial V}{\partial z}=0
\end{aligned}\right\}(4)$$

Where,$i=\sqrt{-1}$, ρ is quality density, μ is Poisson ratio.

Then, the differential equations (4) are solved by using linear differential operator, and the general displacement solution in wave-frequency domain under dynamic moving loads is derived as equations (5).

$$\left.\begin{aligned}
U(\Omega,\xi,\Phi,z)&=A\cdot n\cdot e^{-n\cdot z}+B\cdot n\cdot e^{n\cdot z}+C\cdot\xi\cdot e^{-m\cdot z}+D\cdot\xi\cdot e^{m\cdot z}\\
V(\Omega,\xi,\Phi,z)&=P\cdot n\cdot e^{-n\cdot z}+Q\cdot n\cdot e^{n\cdot z}+C\cdot\Phi\cdot e^{-m\cdot z}+D\cdot\Phi\cdot e^{m\cdot z}\\
W(\Omega,\xi,\Phi,z)&=i\cdot(A\xi+P\Phi)\cdot e^{-n\cdot z}-i\cdot(B\xi+Q\Phi)\cdot e^{n\cdot z}+i\cdot C\cdot m\cdot e^{-m\cdot z}-i\cdot D\cdot m\cdot e^{m\cdot z}
\end{aligned}\right\}(5)$$

Where, n and m are system parameters related with coordinates, defined by,

$$\left.\begin{aligned} n &= \sqrt{\xi^2 + \Phi^2 - \frac{(\Omega - \xi \cdot \bar{v})^2}{c_s^2}} \\ m &= \sqrt{\xi^2 + \Phi^2 - \frac{(\Omega - \xi \cdot \bar{v})^2}{c_d^2}} \end{aligned}\right\} \tag{6}$$

$$c_s^2 = \frac{G}{\rho}, \qquad c_d^2 = (1 + \frac{1}{1-2\mu}) \cdot \frac{G}{\rho} \tag{7}$$

$A(\Omega,\xi,\Phi)$, $B(\Omega,\xi,\Phi)$, $C(\Omega,\xi,\Phi)$, $D(\Omega,\xi,\Phi)$, $P(\Omega,\xi,\Phi)$, $Q(\Omega,\xi,\Phi)$ are the undetermined parameter functions of general solution of equations (4), which can be derived by constraint conditions of elastic body. Six undetermined parameter functions need six different constraint conditions. After the undetermined parameter functions and system parameters are solved, the solution in the time-space coordinates can be derived by equations (5) and (3).

The asphalt pavement can be treated as three-dimensional elastic multilayer system. Each layer has six undetermined parameter functions for the solution of multilayer elastic system.

Tire-pavement surface contact stresses can be used as the top surface stress boundary conditions (z=0), as follows,

$$\left.\begin{aligned} \sigma_z(t,\eta,y,z)\big|_{z=0} &= f_{zz}(t,\eta,y) \\ \tau_{\eta z}(t,\eta,y,z)\big|_{z=0} &= f_{\eta z}(t,\eta,y) \\ \tau_{yz}(t,\eta,y,z)\big|_{z=0} &= f_{yz}(t,\eta,y) \end{aligned}\right\} \tag{8}$$

There are six interlayer contact conditions in each interface between the k layer and the k+1 layer, which are shown as(taking example for interlayer continuous system),

$$\left.\begin{aligned} u(t,\eta,y,z)\Big|_{\substack{z=h_K \\ j=k}} - u(t,\eta,y,z)\Big|_{\substack{z=0 \\ j=k+1}} &= 0 \\ v(t,\eta,y,z)\Big|_{\substack{z=h_K \\ j=k}} - v(t,\eta,y,z)\Big|_{\substack{z=0 \\ j=k+1}} &= 0 \\ w(t,\eta,y,z)\Big|_{\substack{z=h_K \\ j=k}} - w(t,\eta,y,z)\Big|_{\substack{z=0 \\ j=k+1}} &= 0 \\ \sigma_z(t,\eta,y,z)\Big|_{\substack{z=h_K \\ j=1}} - \sigma_z(t,\eta,y,z)\Big|_{\substack{z=0 \\ j=k+1}} &= 0 \\ \tau_{\eta z}(t,\eta,y,z)\Big|_{\substack{z=h_K \\ j=1}} - \tau_{\eta z}(t,\eta,y,z)\Big|_{\substack{z=0 \\ j=k+1}} &= 0 \\ \tau_{yz}(t,\eta,y,z)\Big|_{\substack{z=h_K \\ j=1}} - \tau_{yz}(t,\eta,y,z)\Big|_{\substack{z=0 \\ j=k+1}} &= 0 \end{aligned}\right\} \tag{9}$$

Where, h_k is the thickness of *k*th layer.

Infinite depth ($z \to +\infty$) displacement boundary constraint conditions have the

form,

$$\left.\begin{aligned} u(t,\eta,y,z)\big|_{z\to\infty} &= 0 \\ v(t,\eta,y,z)\big|_{z\to\infty} &= 0 \\ w(t,\eta,y,z)\big|_{z\to\infty} &= 0 \end{aligned}\right\} \tag{10}$$

After solving the constraints equations (8), (9), (10), the parameter functions in wave-frequency domain $\{\Omega,\xi,\Phi,z\}$ are obtained, and the general solutions in wave-frequency domain $\{\Omega,\xi,\Phi,z\}$ of multilayer elastic system under dynamic moving non-uniformly distributed load are derived. Then, mechanical solutions of multi-layer in fixed time-space domain $\{t,x,y,z\}$ are obtained by multi-dimensional inverse Fourier Transforming and coordinate Transforming.

NUMERICAL METHODS IMPLEMENTATION

The pivotal issues are the numerical calculating for Fourier transformation in the course of model solving. The target is to figure out the original function(such as $w(t,\imath,y)$) using its obtained Fourier transformation $W(\Omega,\xi,\Phi)$.A general thought is given as following: Firstly, the continuous function $W(\Omega,\xi,\Phi)$ in the infinite interval wave frequency domain $\{\Omega,\xi,\Phi\}$ is separated into discrete dots of limited areas $\hat{W}(k_I,k_{II},k_{III})$ by sampling theorem. Then, the form of discrete dots $\hat{w}(n_I,n_{II},n_{III})$ of the original function $w(t,\imath,y)$ is obtained through a three-dimensional Inverse Discrete Fourier Transformation (referred to IDFT)for the discrete dots $\hat{W}(k_I,k_{II},k_{III})$; Finally, the original function $w(t,\imath,y)$ within the region is derived by the discrete dots $\hat{w}(n_I,n_{II},n_{III})$, implementing the function reconstruction. This process is shown in fig.2.

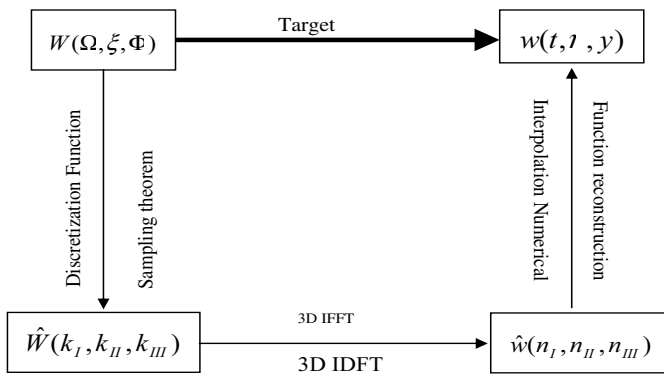

F IG.2. The process of transform.

TEST AND VERIFICATION

The pavement structure parameters for the FWD deflection tests in table1.With the comparison of FWD dynamic deflection test and calculated results shown in fig.3, we

can see that FWD dynamic deflection data calculated by the model in this paper is consistent with the test data, showing that the theory and its calculation method is reasonable and effective.

Table 1. The road structure parameters for the FWD deflection tests.

Layer structure	Poisson ratio	Thickness(cm)	Density(kg/m^3)	Modulus(MPa)
Surface course	0.35	15	2360	4950
Road base	0.20	20	2250	1250
Subbase	0.20	19	2230	1050
Subgrade	0.40	/	1850	355

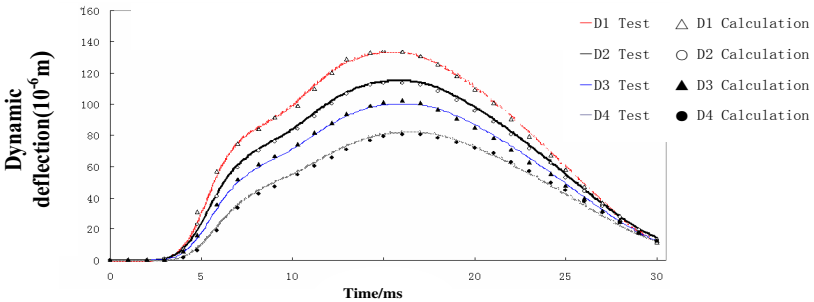

F IG.3. FWD dynamic deflection measured and calculated Comparison Chart.

The basic form and trend of the time-history curve (after filtering)for dynamic strain in the surface layers shown in fig.4 is similar with that of the related theoretical calculation results, which shows that the relevant theoretical model and its calculation method in this paper is reasonable and correct.

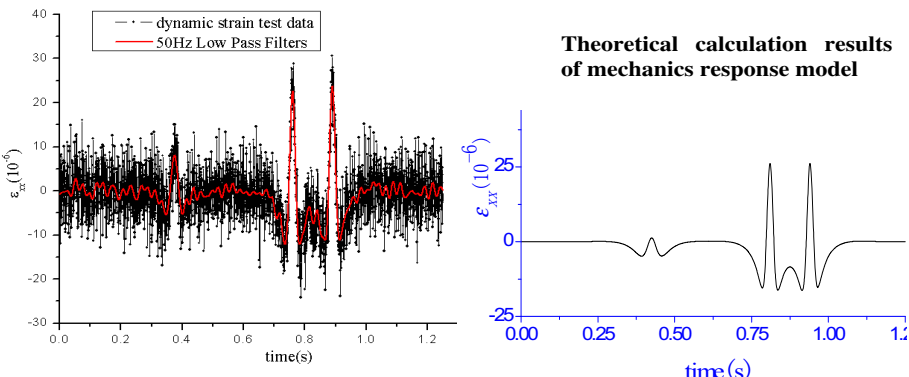

F IG.4. Horizontal-vertical dynamic stain test and calculation results in bottom of surface.

CONCLUSIONS

This paper put forward a dynamic responses calculating model of asphalt pavement under the complex moving vehicle loads described as dynamic, three-dimension non-uniformly distributed contact stresses between tire and pavement surface. But the actual mechanical responses are very complex, the further study is necessary. For example, the moving loads consider only constant speed, so it cannot be applied for mechanical calculation when the vehicle launches and brakes. And test verification work is relatively little or inadequate, the study should improve the corresponding test methods and verify a number of comprehensive mechanical responses.

ACKNOWLEDGEMENTS

The research was supported by Specialized Research Fund for the Doctoral Program of Higher Education (20050536001), Project supported by Hunan Provincial Natural Science Foundation of China (06JJ3025), the author would like to acknowledge with thanks the financial support.

REFERENCES

Qian, Guoping; Guo, Zhongyin; Ling, Jianming (2003). “Dynamic response analysis under the heavy traffic load of asphalt pavement structure.” Practical technology for high-grade roads Tongji University Press.

Industry standards of People's Republic of China (2004). “Specifications for design of highway Asphalt Pavement(JTGD50-2004).” China communications press.

DeBeer, M.; Fisher, C.; and Jooste, F. J. (1997). “Determination of pneumatic tire/pavement interface contact stresses under moving loads with some effects on pavements with thin asphalt surfacing layers.” Proceedings of the 8th International Conference on Asphalt Pavements, International Society for Asphalt Pavements, Seattle: 179-227.

Qian, Guoping (2008). “The study on the tire-road surface complex contact stress model under heavy traffic vehicles.” Journal of china and foreign highway, ol. 28 (4):211-215.

Zhu, Zhaohong; Wang, Binggang; Guo, Dazhi (1985). “Mechanical calculation of the pavement.” Beijing:China Communication Press.

Mix Design of Pervious Recycled Concrete

Jiusu Li [1]

[1]Associate professor, School of Communication and Transportation Engineering, Changsha University of Science and Technology, Chiling Road 45#, Changsha, Hunan, China, 410076; lijiusu@126.com

ABSTRACT: Rules and parameters of mix design for pervious recycled concrete were proposed. Making use of proportioning mix method for stone matrix asphalt (SMA) and open graded friction course (OGFC), volume indexes including volume of voids(VV), volume of cement paste (VP) as well as percent air voids in coarse aggregate(VCA) can be seen as key parameters guiding for mix design. Mix design procedures for pervious recycled concrete were then put forward. Both compressive strength and water seepage velocity were put forward as verification indexes. A practical mix design example was given and the compressive strength and VV test result show that the new mixing design method for no-fines pervious recycled concrete or conventional pervious concrete is practical and feasible.

INTRODUCTION

Pervious concrete, in its earliest form, can be traced to more than 150 years ago, although it was not until a little over 20 years ago that it was successfully employed in various applications in the United States and other countries. Recently, the research on pervious concrete has become an attractive issue due to its distinguished permeability, favorable durability and betterment of ecological environment(Palmer,2006; Bentz,2008). Pervious concrete is also becoming a viable option for owners and designers to consider. It has been successfully used in parking lots, driveways, service roads, walkways, sidewalks, curbs and gutters etc. The current research focused on molding process, factors affecting strength and permeability as well as porosity measuring method(Montes,2005). Recycled aggregate (RA) refers to particles obtained after operations such as crushing, sieving and grading of waste concrete. Although some literature is available on pervious concrete made with natural aggregate, few studies have reported on pervious concrete made with RA. As is known, the weakness of both high water absorption ratio and crushing value makes it difficult to produce higher strength recycled aggregate concrete (RAC), thus limited its wide application(Li,2008). For pervious concrete, strength is usually much lower than ordinary concrete. At this occasion, the strength of RA has much less effect on the strength of resulting pervious concrete. In addition, the rough surface with porous structure of RA can improve the bonding of the interfacial transition zone (ITZ) of

pervious RAC. These make it preferable to manufacture pervious concrete with RA. References associated with application of RA in pervious concrete, however, have been scarcely reported (Yan,2006). Furthermore, few studies focused on mixing design method of pervious concrete as well as pervious RAC. There are currently no standard mix proportioning methods for pervious concrete and pervious recycled concrete. Most of the existent mixing design methods are empirical and short of theoretical support. Enlightened by mixing design method of open graded friction course (OGFC) and stone matrix asphalt (SMA), this research aimed to propose a practical new mix proportioning method of no-fines pervious recycled aggregate concrete (NPRC).

MIX PROPORTIONING PARAMETERS

NPRC consists of three parts: RA, paste and voids (FIG.1a). Three parameters including volume of voids (VV), volume of paste (VP) and percent voids in coarse aggregate in NPRC mixtures (VCA_{NPRC}) are given to describe the structure of NPRC.

To ensure enough permeability, no sands were added into the mixture of NPRC. Pressure molding process is adopted owning to the poor workability of fresh NPRC mixture. After compaction, voids volume of NPRC is generally required to range from 18%-25%. For NPRC, its strength mainly depends on interlocking effect of RA. We regard, therefore, interlocking structure vital which is similar to OGFC and SMA. Percent voids in coarse aggregate in NPRC mixture, namely VCA_{NPRC}, should not exceed percent voids in coarse aggregate without the presence of cement and water (VCA_{RA}, FIG.1b). Otherwise, NPRC fails to form interlocking structure, hence weakens its strength. Not only that, nonclogged pores might also be clogged.

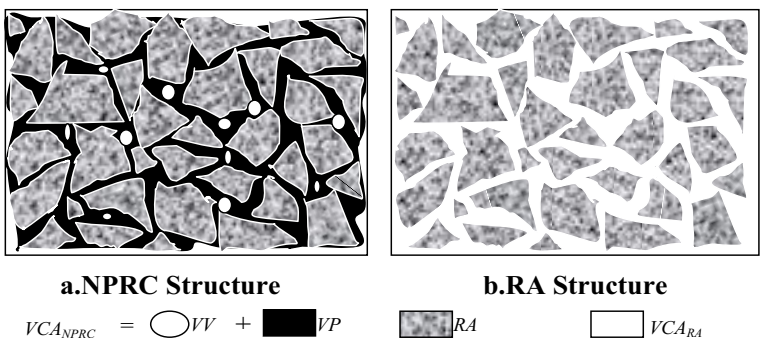

FIG.1. Structure of NPRC and RA

MIX PROPORTIONING METHOD

Standard and requirements of NPRC

It is essential to balance well between strength and voids space of pervious concrete. On the one hand, enough voids space enables NPRC permeable. On the other hand,

reasonable gradation of RA helps to form framework of RA, thus resulting NPRC with sufficient strength. This makes it favorable to use uniform gradation of RA because the corresponding accessible pores structure meets the requirements of the permeability although the strength might be reduced. Three types of uniform gradation as shown in Table 1 were used and compared in this study. The volumetric requirements of NPRC were specified for mix proportioning in Table 2.

Table 1 Grading Scope for Uniform Gradation

Gradation Type	Accumulative Percentage Retained（%）					
	2.36mm	4.75mm	9.50mm	16.0mm	19.0mm	26.5mm
4.75-9.5mm	95-100	80-100	0-15	0	—	—
9.5-16mm	—	95-100	80-100	0-15	0	—
9.5-19mm	—	95-100	85-100	40-60	0-15	0

Table 2 Volumetric Requirements of NPRC

Item	Unit	Requirements
VV	%	18-25
VCA_{NPRC}	%	$\leq VCA_{RA}$

Mix design procedure

(a) Measure relative bulk density of RA. Design initial gradation of RA according to grading scope specified in Table 1: variation of passing percentage of 4.75mm sieve provides three types of gradation curves. γ_{CA} can then be calculated by Eq.(1).

Where P1, P2, P3, P4, P5 is individual percentage of RA and $\gamma_1,\gamma_2,\gamma_3,\gamma_4,\gamma_5$ means their relative bulk density, respectively.

$$\gamma_{CA} = \frac{100}{\frac{P_1}{\gamma_1}+\frac{P_2}{\gamma_2}+\frac{P_3}{\gamma_3}+\frac{P_4}{\gamma_4}+\frac{P_5}{\gamma_5}} \quad (1)$$

(b)Measure packing density of RA in the conditions of pressure molding, and then calculate VCA_{RA} of each gradation according to Eq.(2).

$$VCA_{RA} = \left(1-\frac{\rho_s}{\gamma_{CA}\times\rho_W}\right)\times 100 \quad (2)$$

Where ρ_s is packing density under pressure molding state, ρ_w is density of water.

(c)Calculate surface area according to model in Reference (Mo,2008). The three parts of NPRC are RA, cement paste and voids. NPRC can be described by three major parameters provided that the RA is spherical: average RA diameter, distance between adjacent RA which reflects its compaction degree as well as slurry layer thickness.

$$\overline{d} = \frac{\sum_{i=1}^{n} w_i \overline{d_i}}{\sum_{i=1}^{n} w_i} \quad (3.a) \qquad \overline{d_i} = (d_i + d_{i-1})/2 \quad (3.b) \qquad V = N\times\frac{4}{3}\times\pi(\frac{\overline{d}}{2})^3 \quad (3.c)$$

$$A = N \times 4\pi(\frac{\overline{d}}{2})^2 \quad (3.d) \qquad m_p = h \times A \quad (3.e)$$

Where n is the sieve size number and N is the RA particle number; $\overline{d}$ is the representative diameter of RA; d_i is sieve size; w_i means the percentage individual retained; A stands for the total surface area , h is the thickness of slurry whereas m_p stands for the paste-RA ratio.

(d)Select an initial water-cement ratio. The initial w/c ratio can be 0.35 due to relatively higher water absorption of RA.

(e)Make specimens. For each gradation, more than 4 specimens should be prepared for testing relative bulk density (γ_{mb}) and theoretical density (γ_{mm}). γ_{mb} can be measured by wax-sealing method while γ_{mm} can be measured by vibrating vacuum method or by calculation according to Eq.(4).

$$\gamma_{mm} = \frac{100 + P_P}{\frac{P_1}{\gamma_1} + \frac{P_2}{\gamma_2} + \frac{P_3}{\gamma_3} + \frac{P_4}{\gamma_4} + \frac{P_5}{\gamma_5} + \frac{P_P}{\gamma_P}} \quad (4)$$

Where P_P stands for paste-RA ratio, γ_P is relative bulk density of cement slurry.

(f)Calculate VCA_{NPRC} and VV by Eq.(5) and Eq. (6).

$$VCA_{NPRC} = (1 - \frac{\gamma_{mb}}{\gamma_{CA}} \times P_{CA}) \times 100 \quad (5) \qquad VV = (1 - \frac{\gamma_{mb}}{\gamma_{mm}}) \times 100 \quad (6)$$

Where P_{CA} is the percentage of RA larger than 4.75 mm.

(g)Verify if VV is in the range of 18-25% and VCA_{RA} is greater than VCA_{NPRC} as specified in Table 2. Prepare specimens by changing paste-RA ratio approximately at a gap of 0.2%-0.4%.

(h)Test strength and permeability ratio. If strength cannot meet the need, adjustment of water-cement ratio can then be made and mix proportioning procedure should be returned to step (d). If permeability ratio cannot satisfy the requirements, adjustment of gradation might be needed. The procedure can go back to step (a).

(i)Determine optimum paste-RA ratio according to target VV (generally 20%). Content of various constituents can then be recalculated.

Mix proportioning example

The apparent density and bulk density of RA were tested as shown in Table 3. Density of cement is 3.1 g/cm^3 and target VV =20%. Try to design NPRC-10.

Table 3 Apparent Density and Bulk Density of RA

Sieve Size (mm)	Apparent Density (g/cm^3)	Bulk Density (g/cm^3)
9.5-13.2	2.640	2.322
4.75-9.5	2.638	2.346
2.36-4.75	2.661	2.456

Three gradation curves were designed as shown in Table 4. According to procedures described above, parameters were calculated or tested (Table 5).

Table 4 Gradation of NPRC

Sieve Size (mm)	Passing (%)		
	Grading No.1	Grading No.2	Grading No.3
16	100	100	100
9.5	95	95	95
4.75	5	10	15
2.36	0	0	0

Table 5 Calculation and Test of Parameters in Mix Proportioning of NPRC

Parameters	Grading No.1	Grading No.2	Grading No.3
A (m^2/kg)	0.341446	0.371813	0.365287
Initial m_p (h=600μm)	0.412	0.449	0.441
γ_{CA}	2.316	2.323	2.330
VCA_{RA}	41.48	40.71	41.06
$M_C : M_g : M_w$	1:2.427:0.35	1:2.227:0.35	1:2.268:0.35
γ_{mb}	1.570	1.674	1.617
VCA_{NPRC}	35.60	35.14	41.01
γ_{mm}	2.161	2.038	2.135
Theoretical VV (%)	17.09	9.79	13.13
Real VV (%)	18.89	11.36	14.28

Only grading No.1 was qualified in terms of VV. Grading No.1 was therefore employed and specimens were manufactured and cured. After 28d curing, the compressive strength was tested. It shows that the compressive strength can reach 8.72 MPa and permeability ratio can reach 8.2mm/s when w/c ratio is 0.31 and slurry thickness h is 600μm.

CONCLUSIONS

A new mix proportioning method not only for no fines pervious concrete made with ordinary aggregate, but also for no fines recycled pervious concrete is proposed in this paper. Enlightened by mix design method in SMA and OGFC, major parameters can be concluded and calculated. The real mix proportioning example indicates that this method both significant and practical.

ACKNOWLEDGMENTS

The study presented in this paper was a part of “A Project Supported by Scientific Research Fund of Hunan Provincial Education Department (06C113)”. The author

wishes to acknowledge Hunan Provincial Education Department for financial support.

REFERENCES

Bentz , D.R. (2008). "Virtual pervious concrete: Microstructure, percolation, and permeability." *ACI Materials Journal*. Vol.105(3): 297-301.

Li, J. S.; Xiao, H. N;.and Gong, J. Q. (2008)."Laboratory research on grading optimization of recycled aggregate concrete." *Journal of Building Materials (in Chinese)*, Vol.11(1): 105-110.

Mo, L. T.; Huurman, M.; and Wu, S. P., et al. (2008). "2D and 3D meso-scale finite element models for ravelling analysis of porous asphalt concrete." *Finite Elements in Analysis and Design*,Vol. 44(4): 186-196.

Montes, F.; Valavala, S.; and Haselbach, L. M. (2005). "A new test method for porosity measurements of portland cement pervious concrete."*Journal of ASTM International*, Vol. 2(1).

Palmer, J. W. (2006). "Focus on pervious concrete." *Concrete Construction - World of Concrete*. Vol. 51(8): 47-49.

Yan, H. D., and Huang G. H. (2006). "Study on pervious road brick prepared by recycled aggregate concrete." *Key Engineering Materials*, Vol.302-303: 321-327.

Influence of Water Saturated State on Moisture Susceptibility of Asphalt Mixture

Liang Zhou[1], Feicheng Chen[2], Yuan Jiang[3] and Qi Xie[4]

[1]PhD Candidate, Key Laboratory of Road and Traffic Engineering of Ministry of Education, Tongji University, Shanghai P.R.China, 201804. Email:tinyzhou2014@sina.com

[2]PhD Candidate, Key Laboratory of Road and Traffic Engineering of Ministry of Education, Tongji University, Shanghai P.R.China, 201804. Email:chenfeicheng@126.com

[3]Research Engineer, Liao Ning Provincial Communications Road Transport Administration Bureau, Shenyang P.R. China, 110003. Email:yangjiang79@yahoo.com.cn

[4]Research Engineer, Xinjiang Oilfield Company, Karamay P.R. China, 834000. Email: pengmin8325@yahoo.com.cn

ABSTRACT: Various test procedures and index exist to identify the susceptibility of asphalt mixtures to moisture damage. This paper concerns on Marshall in Saturation State test that can be used to quantify the moisture damage of asphalt mixture. The procedure consists of Marshall test prior to different water bath for an extended period of time. The Retained Marshall Stability Ratio in Immersion Saturated State (RRISS) after the absorption test is used as an indication of sensitivity of the compacted mixture to moisture damage. The results show that RRISS is able to discern different asphalt mixture combinations in terms of their moisture susceptibility.

KEY WORDS: water saturated state; moisture susceptibility; asphalt mixture

INTRODUCTION

Moisture has for a long time been recognized as a serious contributor to premature damage of asphalt pavements. Stripping occurs when the bond between the asphalt and the aggregate is broken by water. The water may be sent on or in the aggregate because of incomplete drying or it may come from some other source after construction, such as penetration of rainwater, rise of underground water, and/or absorption of water vapor.

Numerous test procedures have been developed to evaluate hot mix asphalt (HMA) stripping potential in the laboratory. The most commonly used procedures are static immersion Marshall, vacuum saturation Marshall, tensile strength ratio (TSR), Freeze-thaw tests. Static soaking is often used when pressure and vacuum techniques are not necessary or hard to get in the pavement section laboratory. In such a case, water enters asphalt mixture samples while it is submerged and saturation may not occur in a short soaking period.

The primary objective of this paper is to investigate the influence of saturated state on the lab-measured moisture susceptibility of HMA mixture. A rational method was suggested for the HMA mixture. A new index, which is Retained Marshall Stability Ratio in Immersion Saturated State (RRISS), can be used for this purpose to determine the moisture susceptibility.

MATERIAL AND TEST METHODS

Raw Material

Andesite aggregate was used with the SBS modified asphalt. Standard tests were performed to evaluate the characteristics of each material. AH-70 penetration SBS modified asphalt cement was obtained from Haiwei (Hengshui) Ltd. Co., in Hebei province, China, with penetration of 65dmm at 25^{o}C, ductility of 137cm at 15^{o}C, and softening point of 73^{o}C. All aggregate properties met the requirements in Technical Specification for Construction of Highway Asphalt Pavement (JTG F40-2004). Hydrated lime was added at 25% by mass of limestone filler.

Sample preparation

The combined gradation aggregate used in the study was given in Table1. Volumetric design procedures in SUPERPAVE were employed to design the asphalt mixture. Cylindrical samples, 100 mm in diameter, were compacted by the Superpave Gyratory Compactor (SGC).

Table 1 Design gradation of aggregate

Sieve size/mm	16	13.2	9.5	4.75	2.36	1. 18	0.6	0.3	0.15	0.075
Passing/%	100	93	68	47	27	16	13	9	7	5

Air void levels for gyratory-compacted specimens were targeted to fall between 4 percent, considered to be a lower limit for laboratory fabricated specimen, and 8 percent, considered to be an upper limit for constructed pavements. The actual air voids of SGC specimens ranged from 3.9 to 8.2 percent.

Compaction to a specified height and targeted air void level was accomplished by varying the number of gyrations based on the relation between air content and

number of gyrations. The two ends of specimen were trimmed to get a specimen in specific height. The cutting was performed with a water-cooled masonry saw equipped with a diamond-tipped blade. After the wet saw cutting, the samples were thoroughly washed to remove any loose fine material resulting from the cutting process. The samples were measured and weighed. The specific gravities required to compute the air void content of individual test samples were determined. The corresponding maximum theoretical densities of the mixtures were also determined.

Moisture absorption test

This test was performed on the cylindrical samples by immersing the specimens into the water bath at 35 °C, 50 °C and 60 °C. The specimens are placed in water bath and allowed to equilibrate to the specific testing temperature ±1 °C. The amount of soaking time in which specimen achieving saturated state was recorded.

The moisture absorption was determined using the following equation (1):

$$A = (W_{wet} - W_{dry}) / W_{dry} \quad (1)$$

Where: A, moisture absorption ratio of specimen,%; W_{wet}, weight of saturated surface-dry conditioned specimen in air, g; W_{dry}, weight of dry specimen in air, g.

Marshall test

Once the moisture absorption measurements were performed, within each type of air void contents, half of the specimens were treated as control samples to test Marshall Retained Stability, and others were subjected to measure The Retained Marshall Stability Ratio in Immersion Saturated State (RRISS). Comparisons were given on Marshall Retained Stability and RRISS. The RRISS can be calculated using the following equation (2):

$$S_0 = S_1 / S_2 \times 100\% \quad (2)$$

Where: S_0 is Retained Marshall Stability Ratio in Immersion Saturated State, %; S_1 is Average Marshall Stability in Saturated State, kN; S_2 is Average Marshall Stability, kN.

RESULTS AND DISCUSSION

Factors affecting specimen in water saturated state

Figure 1 presents the moisture absorption level. The air void of specimen were 4%,6% and 8%,respectively and water bath temperature were 35,50 and 60 °C. Note that all the data in Figure 1 illustrated the similar trend. As the air void of specimen was identical, a decrease of soaking time was observed for all specimens with the increase of water bath temperature. An increase of soaking time occurred with the

rise of air void when the water temperature remained invariable.

It can be seen from Figure 1, not all specimens get an absolute saturated state according to the Standard Test Method of Asphalt and Asphalt Mixture for Highway Engineering (JTJ 052-2000),under the specification at 60 °C for 48 hours (2 days).

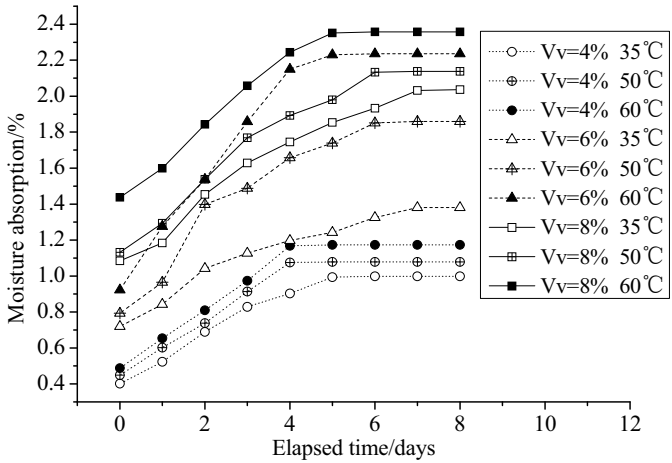

Fig.1. Chart of moisture absorption in different water bath

It is known that void pathways in specimens are not relatively straight and vertical, but convoluted and most tend towards the perimeter of a compacted specimen. Therefore, air void can be divided into two categories: opening void and closed void. Once a specimen was placed in the water bath, water started to diffuse into the opening void of the mix. Some air was trapped in the inner of the void. Water was hard to continue to access the pathway. As the soaking period increasing, more than 4 days, relative high humidity in the voids could lead to a percolation phenomena. Some water accessed more into the pathway. Some others were held on the pathway as a result of the surface tension of water. Therefore, air was trapped in the void completely, forming “quasi-closed void”. It is thought that the specimens were in saturated state. Thus, specifying only an invariable time (48 hours) as a limiting criteria may not be proper. It is therefore suggested that time be variable in order to reach absolutely saturation level.

It should be noted that the relative arrangement of aggregate (and thus void interconnectivity) of pavement section is not similar to specimen obtained using the gyratory compactor, even though total void space (volume percentage) might be similar. Therefore, the adjustment above as compared to the specification requirement should be based on the pavement section results.

Influence of water saturated state on results

Figure 2 presents the comparison of Retained Stability Ratio (legend B, D and F) and RRISS value (legend A, C and E) for the mixture studied. Moisture susceptibility of asphalt mixture is evaluated by comparing the ratio value. The lower the value of the ratio, the more prone the mixture will be to moisture damage; the higher the ratio value means the less moisture susceptibility. The mean values were compared to evaluate the results of the controlled specimens to those of the conditioned from each type. It can be seen from Figure 2 that the results from Marshall Retained Stability did not seem to be sensitive to air void content. The average Retained Stability values, in this case, were not significantly different for all air void contents. All the results were above 0.9. However, for RRISS value, the gap between the respective test results of all samples appears to widen with the increased air void content. In other words, Marshall Retained Stability is not as effective as RRISS when assessing the moisture susceptibility of the same mixture.

The effect of air void in specimen was found to affect the moisture damage performance in the laboratory. Larger range of air void (6%~8%) resulted in distinction, however, RRISS could not distinct moisture susceptibility when the air void was small, i.e., 4%.

According to specification in China, a ratio value of 0.8 can be used as the threshold value to distinguish between ‘ good ’ and ‘ poor ’asphalt mixture laboratory moisture susceptibility. That is, mixtures with RRISS more than 0.8 are relatively resistant to moisture damage. Line was the requirement of relevant standard about moisture susceptibility (See Figure 2). Minimum acceptable RRISS (0.8) is achieved when the air void is 5.2% in the study. Other mixtures with air void larger than 5.2% failed the requirement.

CONCLUSIONS

The main factors affecting the moisture susceptibility include air void, amount of soaking time and water bath temperature. The period of soaking time should not be conformed to a fixed value. The choice of any field application should be made on the basis of field trials. The results of Retained Stability did not seem to be sensitive to the air void content. A new index of RRISS can be used to measure the moisture susceptibility of the mixture being tested. The ratio of 0.8 in specification is the criterion to identify a moisture susceptibility of a mixture. The critical air void can be backcalculated to evaluate the mixture in the study.

Further research was suggested for other aggregate and asphalt binders and to correlate the laboratory tests with field performance.

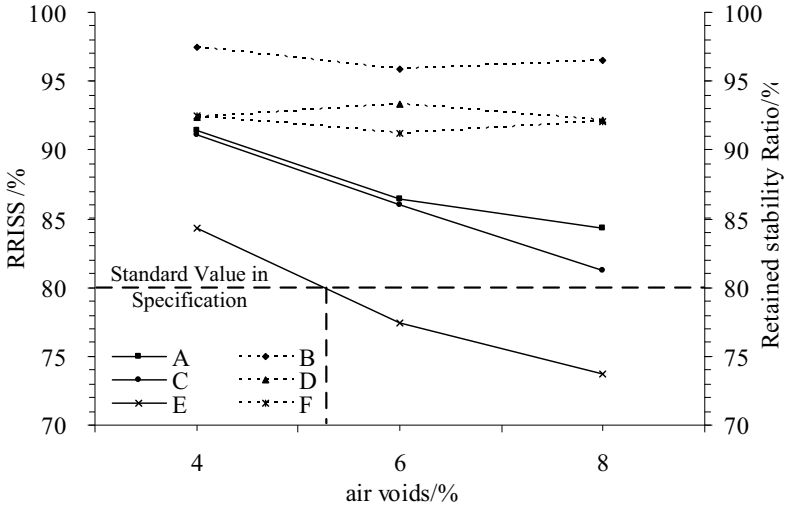

Fig.2. Comparison chart of RRISS Ratio and Retained Stability Ratio

REFERENCES

A. Atakan, et.al. (2005). "Effects of various additives on the moisture damage sensitivity of asphalt mixtures" *J Construction and Building Materials.* Vol. 19: 11-18.

B. Choubane, et.al. (2000). "Effects of different water saturation levels on the resistance of compacted HMA samples to moisture induced damage", Transportation Research Board. Washington, D.C.

Chen X., Huang B. (2008). "Evaluation of moisture damage in hot mix asphalt using simple performance and Superpave indirect tensile tests". J Construction and Building Materials. Vol. 22: 1950-1962

Edith A.; Eyad, M. et.al. (2007). "Influence of Air Void Distribution on the Moisture Susceptibility of Asphalt Mixes". J Journal of Materials in Civil Engineering

G. D. Airey, et.al. (2008). "The influence of aggregate, filler and bitumen on asphalt mixture moisture damage". J Construction and Building Materials. Vol. 22: 2015-2024

D. Hall, Kevin (2001) "Development of a Void Pathway Test for Investigating Void Interconnectivity in Compacted Hot-Mix Asphalt Concrete". Transportation Research Board. Washington, D.C.

Development and verification of creep constitutive model for asphalt mixture based on continuum damage theory

Jiupeng Zhang [1], Yuhui Pi [2] and Xiaoming Huang[3]

[1]PhD, Key Laboratory for Special Area Highway Engineering of Ministry of Education, Chang'an University, Southern Middle Section of Xi'an city Second Circular Road, Xi'an, 710064; jiupeng.zhang@hotmail.com

[2]Graduate Research Assistant, School of Transportation, Southeast University, 2# Sipailou, Nanjing, 210096; piyuhui@163.com

[3]Phd, Professor, School of Transportation, Southeast University, 2# Sipailou, Nanjing, 210096; huangxm@seu.edu.cn

ABSTRACT: The three-stage creep behavior of asphalt mixture could be considered as the results of a competition between damage and hardening. Therefore, the damage and hardening variables were both introduced into *Burgers* model for modification. The series-wound dashpot in *Burgers* model was modified with a hardening variable and the undamaged mechanistic model was derived from rheological. Then, Kachanov's equation of damage evolution was adopted and a new creep constitutive model coupled with damage was established by Lemaitre's effective stress principle. Subsequently, static creep tests of two asphalt mixtures were conducted to validate the modified model, and an algorithm was established to determine the model parameters from typical laboratory data. The proposed model and algorithm were demonstrated through laboratory test results, and the analysis results matched the test perfectly. It is indicated that the proposed model can describe the three-stage behavior well.

INTRODUCTION

With the expansion of road engineering, more and more attentions are paid to the rheology characteristic and engineering application of asphalt mixture. Researchers have investigated rheology characteristic of asphalt mixture from different aspects, and many rheological models have been established (Shen, 2001). But asphalt mixture is a typical viscoelastic material with certain micro-holes and micro-cracks called initial damage, and the damage increases under loading and environmental factors (Guan, 2005). We believe that the three-stage creep behavior could be considered as the results of a competition between damage and hardening. The hardening of viscosity is the main cause of the decelerating stage, the accelerating stage is mainly due to the damage effect and the damage mechanism and the hardening one keep their balance in the stationary stage (Zhang, 2008b).

In this paper, based on the study on creep behavior of asphalt mixture under different temperature and stress, this paper attempts to introduce the damage and hardening variables into Burgers model for modification, and establish a damage-creep constitutive model for asphalt mixture from rheological and continuum damage theory. Then the proposed model is demonstrated through laboratory test results.

DEVELOPMENT OF DAMAGE-CREEP MODEL FOR ASPHALT MIXTURE

Modification of Burgers Model and Undamaged Constitutive Model

Firstly, *Burgers* model is selected for modification because of its good applicability and accurateness for the decelerating and stationary stages (Zhang, 2008a). The model is considered as the combination of modified dashpot and *Van Der Poel* model in tandem, as shown in FIG.1.

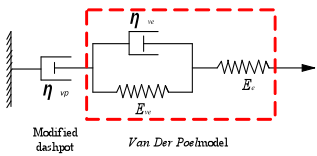

FIG.1 Modification of Burgers model

By introducing the hardening parameter, viscosity of modified dashpot cdould be considered as the function of strain (Uzan, J., 1985), and the viscous strain rate could be repesented as

$$\dot{\varepsilon}_{vp} = \frac{g(\sigma)}{\eta_{vp}} = \frac{B\sigma^m}{A\varepsilon_{vp}^n} \tag{1}$$

Where, ε_{vp} and $\dot{\varepsilon}_{vp}$ are the viscous strain and viscous strain rate; η_{vp} is the viscosity of modified dashpot, $\eta_{vp} = A\varepsilon_{vp}^n$; $g(\sigma)$ is theloading function, $g(\sigma)=B\sigma^m$; σ is theloading stress; and *A, B, n, p* are material parameters.

So the undamaged mechanistic model is expressed as

$$\varepsilon = \frac{\sigma_0}{E_e} + \frac{\sigma_0}{E_{ve}}\left(1-e^{-E_{ve}t/\eta_{ve}}\right) + \left[\frac{B}{A}(n+1)\right]^{\frac{1}{n+1}} \sigma_0^{\frac{m}{n+1}} t^{\frac{1}{n+1}} \tag{2}$$

Damage Variables and Damage-Creep constitutive model

Affective area of material bearing the load decreases with the damage process, and the effective stress of material is express as (Sun, 1999)

$$\tilde{\sigma} = \frac{\sigma}{1-D} \tag{3}$$

Where, D is the damage variable, $0 \le D \le 1$; $\tilde{\sigma}$ is the effective stress; σ is *Cauchy* stress, namely nominal stress.

A reasonable damage variable D should be chosen for asphalt mixture when continuum damage theory is applied to research the damage-creep behavior. For uniaxial compressive condition, *Kachanov* damage-creep law is widely used, and it is expressed as (Yu, 1997)

$$\dot{D} = C\sigma^v (1-D)^{-v} \tag{4}$$

Where, C and v are the material parameters dependent on the temperature.

By integral of equation (9), critical failure time (t_R) of damage-creep behavior could be obtained as

$$t_R = \left[C(v+1)\sigma^v\right]^{-1} \tag{5}$$

So the evolution equation of damage variable could be obtained as

$$D = 1-\left(1-t/t_R\right)^{1/(v+1)} \tag{6}$$

Deformation of damage material could be express as a function of effective stress, and the strain expressed by effective stress for undamaged material is equal to the one expressed by *Cauchy* stress for damaged material. It is to say constitutive model of damaged material is the same as that of undamaged material in form, and constitutive model of damaged material could be obtained at once the *Cauchy* stress is instead of the effective stress. Submitting equation (6) into equation (2) and (3), the damage-creep constitutive model of asphalt mixture could be obtained as

$$\varepsilon = \frac{\sigma_0}{\left(1-t/t_R\right)^{1/(v+1)}E_e} + \frac{\sigma_0}{\left(1-t/t_R\right)^{1/(v+1)}E_{ve}}\left(1-e^{-E_{ve}t/\eta_{ve}}\right) + \left[\frac{B}{A}(n+1)\right]^{\frac{1}{n+1}}\left[\left(1-t/t_R\right)^{-1/(v+1)}\right]^{\frac{m}{n+1}}\sigma_0^{\frac{m}{n+1}}t^{\frac{1}{n+1}} \tag{7}$$

The equitation (7) can be simply rewritten as

$$\varepsilon = \frac{P_1\sigma_0}{\left(1-t/P_7\right)^{P_8}} + \frac{P_2\sigma_0}{\left(1-t/P_7\right)^{P_8}}\left(1-e^{-P_3 t}\right) + P_4\frac{\sigma_0^{P_5}t^{P_6}}{\left(1-t/P_7\right)^{P_8\times P_5}} \tag{8}$$

Where, $P_1=\frac{1}{E_e}$ $P_2=\frac{1}{E_{ve}}$ $P_3=\frac{E_{ve}}{\eta_{ve}}$ $P_4=\left[\frac{B}{A}(n+1)\right]^{\frac{1}{n+1}}$, $P_5=\frac{m}{n+1}$, $P_6=\frac{1}{p+1}$, $P_7=t_R$, $P_8=\frac{1}{(v+1)}$

VERIFICATION OF DAMAGE-CREEP MODEL

Preparation of Asphalt mixture Specimens

Two asphalt mixture of dense gradation (named as AC13 and AC20, which are types of grading specified by Chinese asphalt construction specification) are selected, and 70# asphalt is used for mixture design. Mixtures design results are given in Table1.

Table 1 Design of the four asphalt mixture

Asphalt Mixes	Passing percent of the below sieves (sized in mm) /%												Asphalt content/%
	26.5	19	16	13.2	9.5	4.75	2.36	1.18	0.6	0.3	0.15	0.075	
AC20	100	95	85	75	64	43	29	18	12	10	7	5	4.0
AC13	100	100	100	94	83	63	47	30	20	10	7	6	4.5

Firstly, prepare 165 mm high Gyratory specimens to the 4% air void content, and then core the nominal 100 mm diameter test specimens from the center of the gyratory specimens. Prepare the ends of the specimen by sawing with a double-bladed saw to obtain the cylindrical specimens, 100 mm in diameter and 150 mm in height. The ends of all test specimens shall be smooth and perpendicular to the axis of the specimen. A two-double rubber membrane is used and between the rubber membranes, there is a

lube layer.

Laboratory Test Results and Verification of the Damage-Creep model

UTM is selected to conducted uniaxial repeated load permanent deformation test of the three mixtures under different temperature and compressive stress, and test temperature and stress is shown in Table 2.

Table 2 Test temperature and compressive stress

Test terms	Values		
Test temperature/°C	40	50	60
Peak value of compressive stress/MPa	0.7	0.8	1.0
Preload/kPa	15		

Creep strain curves of the two asphalt mixtures under different temperature and stress are shown in FIG.2 and FIG.3. Based on the test results, Origin7.0 software is selected for nonlinear regression of the tests results, and the fitting curves are also shown in FIG.2 and FIG.3. Fitting parameters are shown in Table 3 and Table 4.

Table 3 Fitting parameters of the damage-creep model for AC13

Temp. (°C)	Stress (MPa)	Fitting parameters								R^2 (%)	Standard Deviation
		P1	P2	P3	P4	P5	P6	P7	P8		
40	0.7	0.1805	0.0812	0.2834	0.720	1.425	0.3	592	0.5027	93.5	1.727E-04
	0.8	0.1961	0.0812	0.2812	0.703	1.423	0.3	418	0.5036	91.7	1.500E-04
	1.0	0.2083	0.0816	0.2887	0.694	1.422	0.285	276	0.4996	90.4	1.985E-04
50	0.7	0.2273	0.0951	0.2984	0.998	1.425	0.3	195	0.4862	89.4	1.688E-04
	0.8	0.2381	0.0952	0.2945	1.057	1.428	0.31	150	0.4898	93.1	2.484E-04
	1.0	0.2500	0.0956	0.2963	0.958	1.429	0.3	100	0.4882	89.3	1.495E-04
60	0.7	0.2632	0.1072	0.3234	1.480	1.422	0.3	75	0.4882	94.2	2.392E-04
	0.8	0.2778	0.1075	0.3231	1.431	1.423	0.3	50	0.4968	92.4	1.759E-04
	1.0	0.2899	0.1071	0.3241	1.411	1.426	0.3	35	0.5054	93.0	1.814E-04

Table 4 Fitting parameters of the damage-creep model for AC20

Temp. (°C)	Stress (MPa)	Fitting parameters								R^2 (%)	Standard Deviation
		P1	P2	P3	P4	P5	P6	P7	P8		
40	0.7	0.1667	0.0600	0.2836	0.522	1.422	0.3	1671	0.4900	88.4	2.423E-04
	0.8	0.1739	0.0600	0.2850	0.492	1.423	0.3	1006	0.4974	92.0	1.909E-04
	1.0	0.1825	0.0595	0.2883	0.505	1.424	0.3	839	0.5003	94.4	2.225E-04
50	0.7	0.1887	0.0705	0.3071	0.718	1.427	0.305	487	0.5052	88.9	1.541E-04
	0.8	0.1980	0.0692	0.3066	0.691	1.428	0.3	281	0.4900	94.2	2.190E-04
	1.0	0.2079	0.0715	0.3090	0.687	1.428	0.3	118	0.4919	89.4	1.807E-04
60	0.7	0.2347	0.0796	0.3215	0.952	1.426	0.3	126	0.5006	91.9	1.479E-04
	0.8	0.2525	0.0795	0.3263	1.019	1.428	0.3	96	0.4976	94.3	1.648E-04
	1.0	0.2688	0.0799	0.3223	1.006	1.424	0.3	56	0.4974	93.5	2.367E-04

We can gain the derivative of equation (8), and then the creep strain could be obtained by submitting the fitting parameters. The creep strain curves of two asphalt mixtures are shown in FIG.4 and FIG.5.

It could be concluded that at lower test temperature and stress, asphalt mixture exhibits only the decelerating and stationary stages (or it needs very long time to present the accelerating stage). But at higher test temperature and stress, asphalt mixture easily exhibits whole three stage, and the duration of the stationary stage is

very short.

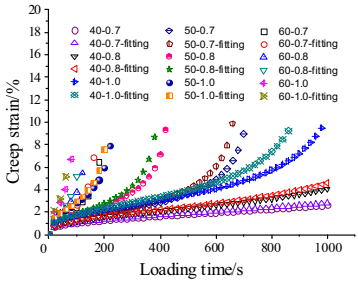

FIG.2 Creep strain curves of AC20

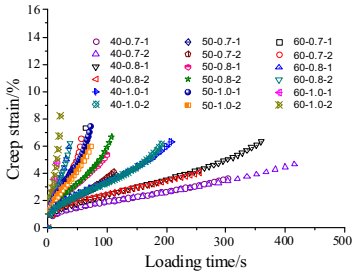

FIG.3 Creep strain curves of AC13

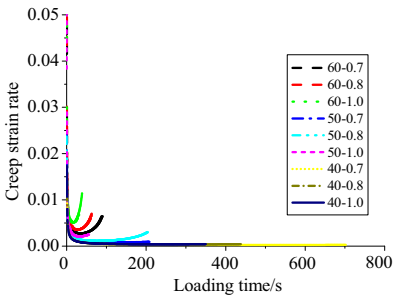

FIG.4 Creep strain rate curves ofAC20

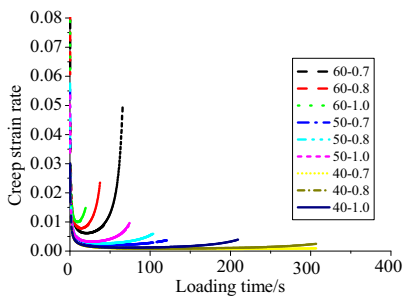

FIG. 5 Creep strain rate curves of AC13

Analysis of the flow time

Flow time, F_t, is the significant characteristic of the three-phase creep behavior. The loading time at which accelerating stage starts is referred to as the "flow time", that is to say the flow time is the loading time at which creep strain rate is the minimum. Fortunately, we can gain the quadric derivative of equation (8), and let $\ddot{\varepsilon} = 0$. After submitting the relevant parameters, the flow time could be calculated by some algebraic manipulations. The calculated and the actual flow time captured from UTM are shown in Table 5.

Table 5 Calculated and actual F_t of each mixture

Asphalt mixture	Temp. (°C)	Stress (MPa)					
		0.7		0.8		1.0	
		Actual value	Calculated value	Actual value	Calculated value	Actual value	Calculated value
AC-13	40	184	158.5	135	111.8	87	73.8
	50	65	52.2	38	40.2	25	26.8
	60	22	20.1	16	13.5	10	9.4
AC-20	40	562	447.3	285	269.3	171	174.2
	50	150	130.5	100	75.3	37	31.5
	60	57	63.8	36	25.8	16	15.1

It has been discovered that calculated value is close to experimental value. It could be concluded that the damage-creep constitutive model describe the three stage' creep behavior of asphalt mixture well. The Flow time can be used as an index to research the damage-creep characteristic of asphalt mixture, and the bigger value denotes the longer time which is needed to enter into the tertiary phase for asphalt mixture. Parameters of the proposed model may have a close relation to temperature and stress, and it is worth further studying.

CONCLUSIONS

Most of the existing component-combined model can not describe the three-stage creep behavior of asphalt mixture yet. The three-stage creep behavior could be considered as the results of a competition between damage and hardening. The hardening of viscosity is the main cause of the decelerating stage, the accelerating stage is mainly due to the damage effect and the damage mechanism and the hardening one keep their balance in the stationary stage. By applying rheological and continuums damage theory comprehensively, and coupling the nonlinear component-combined model with damage factor, a damage-creep constitutive model is established for asphalt mixture. Validated by the laboratory test of two asphalt mixtures under different temperature and stress, the proposed model describes the three-stage creep behavior well. And the flow time could be used as an index to research the damage-creep characteristic of asphalt mixture, and the bigger value denotes the longer time which is needed to enter into the tertiary phase for asphalt mixture.

We noticed that the proposed model describe the static creep behavior well, but the applicability for triaxial and repeated load needs to be further studied and validated. Parameters of the proposed model may have a close relation to temperature and stress, and it is also worth further studying.

REFERENCES

Guan, H. (2005). *A research on viscoelastic fatigue damage model of asphalt mixture*. Central South University, Changsha.

Shen, J. (2001). *Road Performance of Asphalt and Asphalt Mixture*. China Communication Press, Beijing

Sun, J. (1999). *Rheology of geomaterials and its engineering application*. China Architecture and Building Press, Beijing.

Uzan, J.; A. Sides; and M. Perl. (1985). "Viscoelastoplastic model for predicting performance of asphalt mixtures". *Transportation Research Record 1043*, Transportation Research Board, Washington, D.C., 78-79.

Zhang, J.; Huang, X.; and Li, H. (2008a). "Research on permanent deformation of asphalt mixture under repeated load". *Journal of Southeast University*, 38(3), 511-515.

Zhang, J.; Huang, X.; and Li, H. (2008b). “Study on damage-creep characteristics and model of asphalt mixture”. *Chinese Journal of Geotechnical Engineering*, 38(12), 1867-1871.

Yu, S., and Feng, X. (1997). *Damage mechanics*. Tsinghua University Press, Beijing.

On Dynamic Pore Pressure in Moisture Damage of Asphalt Pavement

CUI Xin-zhuang[1], CAO Wei-dong[2], LIU Shu-tang[3] and DONG Lin-lin[4]

Department of Transportation Engineering, School of Civil Engineering, Shandong University, 250061, Jinan, China; PH (086) 531-88399613; FAX (086) 531-88399613; e-mail: [1]cuixz@sdu.edu.cn; [2]cwd2001@sdu.edu.cn; [3]gtreesl@sdu.edu.cn; [4]luishui927@163.com.

ABSTRACT: For studying the accelerating role of dynamic pressure in moisture damage of asphalt pavement, based on fast Lagrangian finite difference method and Biot dynamic consolidation theory, fluid-solid coupling analysis was done considering asphalt mixtures as porous medium. Results revealed that development and dissipation of the dynamic pore pressure are coinstantaneous and this makes the positive and negative dynamic pore pressure and seepage force both alternate. The pumping phenomenon of saturated asphalt pavement under moving vehicle load was proved. The dynamic pore pressure increases with vehicle velocity. Effective stress and deflection of pavement all decrease due to the dynamic pore pressure. The maximum dynamic pore pressure occurs at the bottom of the surface course. So it's suggested that a drain course should be set up to change the drained condition from single-sided drain to both-sided drain, and thus the moisture damage can be limited effectively.

INTRODUCTION

Many investigations indicated that plenty of asphalt pavement damages such as stripping, raveling, potholes, pumping and map cracking occurred only one or two years after open to traffic, and consequently the inner structure was seriously damaged (Kandhal 1994). All above damages are called as moisture damages.

Dynamic water pressure plays an important accelerating role during moisture damage. However, the data of in situ dynamic water pressure is scarce. Although Liu (2002) attempted to measure it, the peak value of dynamic water pressure and its total process of developing and dissipating were not obtained because too low sampling frequency was used. Kettil (2005) succeeded in simulating two-dimensional coupled hydro-mechanical wave propagation in road structures; however, the three-dimensional calculation for dynamic pore pressure wasn't stable.

In this paper, employing Biot dynamic consolidation theory and 3D finite difference method, the dynamic fluid-solid coupling numerical analysis of saturated asphalt pavement was done. Dynamic deflection, dynamic pore water pressure and seepage force under single vehicle load were calculated and the mechanism of accelerating moisture damage of dynamic pore pressure was analyzed.

DYNAMIC FLUID-SOLID COUPLING THEORY

In general, when the voidage of asphalt mixture ranges from 8% to 15%, moisture damage is most serious because water is easy to flow into the pavement surface course and difficult to be drained out. In this case, asphalt mixture can be considered as porous medium. According to Biot consolidation theory, the dynamic equilibrium equation of three-dimensional saturated elastic porous medium is:

$$G\nabla^2 \boldsymbol{u} + \frac{G}{1-2v}\nabla \mathrm{div}\boldsymbol{u} = \nabla p + (1-n)\rho_s \frac{\partial \boldsymbol{v}_s}{\partial t} + n\rho_f \frac{\partial \boldsymbol{v}_f}{\partial t}$$

Where $\boldsymbol{u}$ and $\boldsymbol{v}_s$ are displacement and velocity vector of solid medium, respectively; $\boldsymbol{v}_f$ is velocity vector of fluid; G, v, n and ρ_s are shear modulus, Poisson ratio, voidage and density of solid medium, respectively; ρ_f is density of fluid; p is pore pressure.

The continuous seepage differential equation is:

$$\frac{k}{\gamma_f}\nabla^2 p = n\beta_f \frac{\partial p}{\partial t} + \frac{\partial(\mathrm{div}\boldsymbol{u})}{\partial t}$$

Where k is coefficient of permeability; β_f is compression coefficient of fluid; γ_f is bulk density of fluid.

The flow of fluid causes scouring force on solid skeleton that is called as seepage force in continuous porous medium mechanics. Seepage force is a kind of bulk force and on stream line can be expressed as: $j = \gamma_f i$, Where i is hydraulic gradient.

MATERIAL MODELS AND MECHANICS PARAMETERS

A typical semi-rigid pavement was analyzed with fast Lagrangian finite difference method. The pavement structure was shown in Table 1. We used elastic constitutive model for surface course and base course and Mohr-Coulomb elastic-plasticity model for embankment soil. The voidage of asphalt mixture is 8%. Surface courses are saturated and penetrable by water, but base course is assumed to be not penetrable. In analysis, material damp was considered with Rayleigh linear combination method.

WHEEL LOAD MODEL AND BOUNDARY CONDITIONS

Wheel loads were simplified as uniform pressure on two circles. The equivalent

circle radius δ is 10.65cm, as shown in Figure 1. The time history curve of single wheel load f is shown in Figure 2 and it is expressed as (Huang 2003):

$$\begin{cases} f = f_{\max} \sin^2(\frac{\pi}{T}t) & 0 \le t \le T \\ f = 0 & t > T \end{cases}$$

Where f_{max} is the peak value of load, f_{max} = 0.7; T is the duration of single wheel load which have inverse relation with vehicle speed.

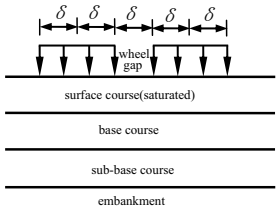

Figure 1. Wheel load model.

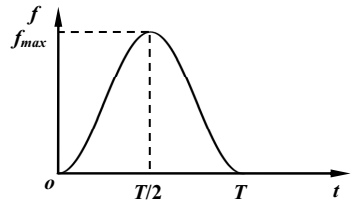

Figure 2. Time history curve of wheel load.

Table 1. Pavement structure.

Course	Material	Thickness /cm	Permeability coefficient /(×10^{-8}m/s)
Upper surface course(USC)	AK-16A asphalt concrete	4	213
Middle surface course(MSC)	AC-25Ⅰasphalt concrete	6	107
Lower surface course(LSC)		8	
Base course(BC)	Cement-stabilized macadam	32	—
Sub-base course(SBC)	Flyash-lime-soil	18	—
Road bed(RB)		80	—
Upper embankment (UE)	Silty clay	70	—
Lower embankment (LE)		100	—

The viscous boundary method introduced by Lysmer and Kuhlemeyer (1969) was employed on infinite boundaries to absorb energy of stress wave and prevent stress wave from reflecting. The interface between surface course and base course is impervious, so herein the hydraulic gradient along the vertical direction is zero, i.e. $\partial u/\partial z = 0$, where u is dynamic water pressure. On road face, u is zero.

RESULTS AND DISCUSSION

Dynamic deflection. Defining that the upward deflection of the pavement is positive, time history curves of the deflection under wheel gap were shown in Figure 3. Due to inertia, it isn't T/2 when the negative peak value appears, but between T/2 and T. The positive peak appears when t=2T approximately.

In order to compare drained condition with the undrained, permeability coefficient of asphalt concrete is set very small to simulate the undrained condition. Figure 4 shows the influence of drained condition on pavement deflection. The absolute peak value of deflection decreases on undrained condition. The reason is that undraining makes the dynamic water pressure increase and consequently the effective stress decreases according to Terzaghi effective stress principle.

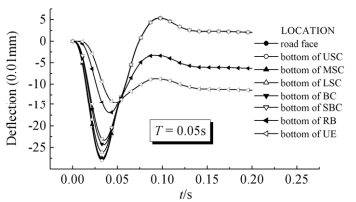

Figure 3. Deflection-time curves.

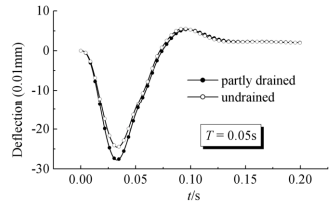

Figure 4. Effect of drained condition.

Dynamic pore pressure. Figure 5 shows the development and dissipation curves of dynamic pore water pressure under wheel gap. We can see that dynamic water pressure first increases to the positive peak value, then decreases gradually to the negative peak value and at last is turned into hydrostatic pressure. The negative water pressure is also called as suction. This calculation result proves the process that water is pumped out and sucked into pavement surface course repetitively under traffic loads.

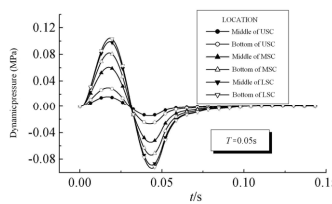

Figure 5. Time history curves of dynamic pore pressure.

Attenuation curves of water pressure peak values under wheel gap versus depth are shown in Figure 6 when T = 0.03s，0.04s，0.05s，0.06s，0.07s, respectively. It can be seen that the smaller T is, the larger the absolute value of dynamic water pressure is. This is because the higher the vehicle speed is, the more the development speed of dynamic pore pressure is than the dissipation speed. Dynamic pore pressure increases with depth and the maximum absolute value appears at the bottom of surface course. So if a draining course is set at the bottom of surface course to make single-sided drained condition turn to double-sided draining, the moisture damage can be limited.

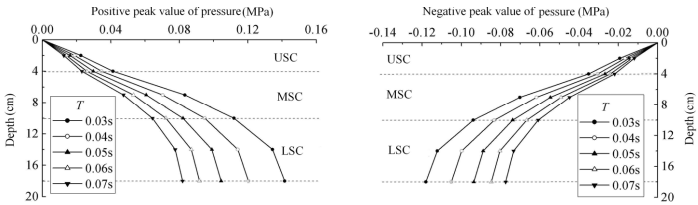

(a) Positive peak value **(b) Negative peak value**

Figure 6. Vertical attenuation of peak value of dynamic pore pressure.

The dissipation of dynamic pore pressure is simultaneous with its development. In order to prove this process, partly drained and totally undrained cases were analyzed numerically, respectively, as shown in Figure 7. For totally undrained condition, the shape of time history curve of dynamic pore pressure is similar to that of wheel load shown in Fig.2 and there isn't suction. Moreover, the maximum pore pressure is larger than that from partly drained condition. This implies that developing and dissipating process are simultaneous. Otherwise it can't be obtained that positive and negative pore pressures appear alternately. The simultaneity makes the positive peak value not appear when t=T/2, but appears before this time.

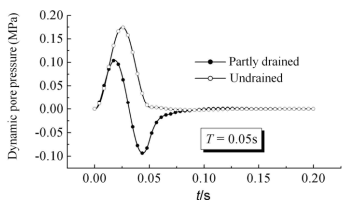

Figure 7. Effect of drained condition on pore pressure.

Curves of vertical total stress, effective stress and dynamic pressure versus time are shown in Figure 8. In the initial period of loading, it's difficult for water to flow out. This makes the total stress is mostly borne by water and consequently effective stress is approximately zero. Compared with total stress, peak value of effective

stress decreases and lags due to positive dynamic pressure, and its period is protracted due to negative dynamic pressure.

Seepage force. Time history curves of seepage force on asphalt mixture are shown in Figure 9. Note that upward seepage force is positive. Positive and negative seepage forces are also alternant and the maximum absolute value of seepage force appears in the middle surface course.

Due to emulsification and displacement of water, the cohesion between asphalt film and aggregate gets weak. This is the chemical mechanism of moisture damage. Then under seepage force, asphalt film is damaged further and scoured out of pavement surface gradually and at last the aggregates without cohesion each other are taken away by high speed wheels. This is the accepted dynamic mechanism of moisture damage.

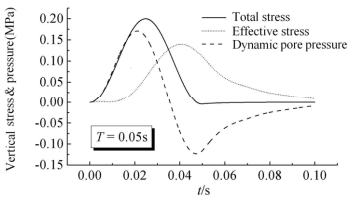

Figure 8. Stress-time curves.

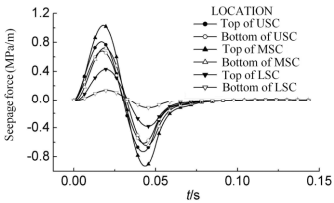

Figure 9. Seepage force-time curves.

CONCLUSION

Based on FDM and Biot dynamic consolidation theory, the dynamic response of saturated asphalt pavement was analyzed. Some points were revealed: (1) the dissipation of dynamic pore pressure is simultaneous with its development and this is the reason of pumping phenomenon; (2) the damaged asphalt films are scoured out of pavement surface by repetitive seepage force. This is the dynamics mechanism of moisture damage; (3) the maximum of dynamic pressure and the maximum of seepage force appear at the bottom and the middle of surface course, respectively.

ACKNOWLEDGEMENTS

This work was supported by Chinese Natural Science Foundation (No.50708056), Shandong Province Reward Fund for Excellent Young and Middle-aged Scientists (No.2008BS09015), Shandong Province Natural Science Foundation (No. Q2006F02) and Key Technologies R&D Program of Shandong Province (No.2008GG10006009).

REFERENCES

Huang, Y H. (1993). *Pavement Analysis and Design*. Pearson Education, Delhi.

Kandhal P S. (1994). "Field and laboratory investigation of Stripping in asphalt pavements: state of the art report." *Transportation Research Record*, 1454, 36-47.

Kettil P, Engström G, Wiberg, N E. (2005). "Coupled hydro-mechanical wave propagation in road structures." *Computers and structures*, 83, 1719-1729.

Liu P, Ling H W, Han J. (2002). "Measurement of pore water pressure in asphalt pavement." *Shanghai Highway*, 4, 20-22.

Lysmer J, Kuhlemeyer R L. (1969). "Finite Dynamic Model for Infinite Media." *Journal of* Engineering *Mechanics*, 95, 859-877.

Influence of ATB on Pavement Performance

WEI Jian-guo[1] and ZHENG Jian-long[2]

[1] Associate professor, School of Transportation Engineering, Changsha University of Science and Technology, Changsha, China, 410076; jianguowei9969@126.com
[2] Professor, School of Transportation Engineering, Changsha University of Science and Technology, Changsha, China, 410076; zjl@csust.edu.cn

ABSTRACT: In order to study the influence of asphalt treated base (ATB) on pavement performance, a multi-layer elastic theory program is utilized to calculate the stress and strain in different pavement structures. Based on an instant heat conducting hypothesis, a finite element model is established to calculate the temperature stress and the strain of pavement structure when temperature reduces. Then the stress and strain of all the structural layers are calculated considering the corporate effect of loading and temperature. It is found that the stress caused by quickly-lowered temperate is far more lager than that caused by load. Thus it is revealed that the cracking in pavement is mainly caused by the temperature. Through contrast it is proved that the stress and strain caused by load and temperature of pavement with ATB30 are less than those of semi-rigid pavement. So ATB is proved to be an efficient way to decrease crack in asphalt pavement based on above calculation and theory analysis.

INTRODUCTION

Crack is one of main distresses in asphalt pavement allover the world. It exists in whether cold or other area, and just the extent is different. A great deal researches have been taken on in asphalt pavement with semi-rigid base for meeting the demand of traffic volume increase, and plentiful achievements have been obtained. Yang shuangyang et al.(2006) thought the graded gravel could reduce the reflective cracks. And Cho yoonho et al. (2006) developed a cement-treated base with 25% fly ash and 10% expansive additive, which had lower shrinkage and thereby could prevent cracks.

Because semi-rigid base will arises cracks unavoidably, the application scope of the base is restricted. However, some researches prove that ATB can improve the pavement performance and reduce the cracks. Haider et al. (2007) found that an ATB effectively meaned a thicker HMA layer. Ying ronghua et al. (2007) found that the crack resistance of asphalt concrete containing large stone aggregate was larger than that containing little stone aggregate.

So this article will study the influence of ATB on pavement performance

through numerical simulation with ANSYS, and compare with common pavement structure with semi-rigid base.

CALCULATION MODEL AND PARAMETERS

Two pavement types (structure 1 and structure 2) are taken in research with ANSYS. And detailed composing of pavements is listed in table 1. These pavement types are commonly used in China, which usually is composed by asphalt concrete(AC)、asphalt treated base(ATB)、cement stabilized macadam(CSM) and cement stabilized gravel(CSG).

Table 1. Structure of Two Pavements

Structure 1		Structure 2	
Layer Type	**Layer Thickness(cm)**	**Layer Type**	**Layer Thickness(cm)**
AC13	4	AC13	4
AC20	6	AC20	6
ATB30	11	AC25	7
CSM-1	17	CSM-1	19
CSM-2	16	CSM-2	18
CSG	20	CSG	20

Elastic multi-layer theory is used to calculate the layer's maximum stress and strain of two pavement structures under BZZ-100 standard axle load in different temperatures.

In temperature stress calculation, pavement structure is thought as elastic layer system. Plane stress model is chosen. According to axial symmetry, side length of model is 4 m, and subgrade thickness is 3m. Displacement of X and Y direction is restricted for model's right and underside, and X direction of left side is only restricted according to symmetry. Air convection coefficient is 400J/s•m^2•℃. Temperature changes above 1m of soil subgrade, and the temperature of area after 1m deep is 15℃ constant. The other parameters can be seen in Table 2.

Table 2. Model Parameters

Structure Layer	Compress Modulus (MPa)				Poisson Ratio	Thermal Conductivity (c/m•h•℃)	Swelling & Shrinkage Coefficient (10^{-5}/℃)
	15 ℃	5℃	-5 ℃	-15 ℃			
AC13	2000	3500	6200	10000	0.2	1	2.5
AC20	1800	3000	5300	8500	0.2	1	2.5
ATB30(AC25)	1400	2400	4200	6500	0.2	1	2.5
CSM-1	1500				0.3	1.1	1.5
CSM-2	1300				0.3	1.1	1.5
CSG	1100				0.3	1.1	1.5
Soil Subgrade	38				0.35	1.2	15

STRESS AND STRAIN CALCULATION CAUSED BY LOAD

The maximum stress and strain of layer bottom in different structures are calculated in different temperatures, and the results are listed in table 3 and table 4.

Table 3. Maximum Stress and Strain of Structure 1

Structure Layer	15℃		5℃		-5℃		-15℃	
	Tensile Stress (MPa)	Strain (με)	Tensile Stress (MPa)	Strain (με)	Tensile Stress MPa	Strain (με)	Tensile Stress (MPa)	Strain (με)
AC13	-0.055	25.6	-0.054	22.1	-0.051	17.5	-0.048	13.9
AC20	-0.044	46.6	-0.052	23.1	-0.049	12.8	-0.033	9.5
ATB30	-0.015	30.3	0.051	38.8	0.150	38.5	0.182	36.0
CSM-1	0.028	29.7	0.034	30.4	0.037	29.7	0.037	28.0
CSM-2	0.049	34.9	0.048	33.5	0.046	31.7	0.044	29.8

Table 4. Maximum Stress and Strain of Structure 2

Structure Layer	15℃		5℃		-5℃		-15℃	
	Tensile Stress (MPa)	Strain (με)	Tensile Stress (MPa)	Strain (με)	Tensile Stress (MPa)	Strain (με)	Tensile Stress (MPa)	Strain (με)
AC13	-0.054	26.6	-0.053	23.1	-0.050	18.2	-0.048	14.5
AC20	-0.047	45.4	-0.042	26.7	-0.017	17.1	0.026	14.0
AC25	-0.026	30.7	0.051	43.7	0.170	45.4	0.289	42.9
CSM-1	0.025	31.4	0.032	32.5	0.036	32.2	0.037	30.9
CSM-2	0.050	36.4	0.050	35.1	0.049	33.6	0.047	32.1

From Table 3 and Table 4, it is found that the maximum tensile stress and strain of layer bottom in structure 1 are smaller than those in structure 2.

STRESS AND STRAIN CALCULATION CAUSED BY COOLING

The temperature of every site in model is 15℃, and the original environment temperature is 15℃. Air temperature reduces 2℃ one hour, and the temperature field of model can be found at 5℃、-5℃、-15℃ though transient heat transfer analysis. Then stress and strain caused by temperature can be calculated, and the results are listed in table 5 and 6, in which "-" means compressive stress.

It is can be seen that, when temperature decreases to -5℃ and -15℃, the tensile stress of surface、layer bottom of AC13 and AC20 is big, and which is larger than ultimate flexural tensile strength of HMA (table 7).

The tensile stress and strain of the surface and the bottom of AC13、AC20、ATB30 layer in structure 1 are smaller than those in structure 2. And the compressive stress and strain of the bottom of cement stabilized macadam(CSM) and cement stabilized gravel(CSG) in structure 1 are larger than or equal to those in structure 2. Because the compressive resistance ability of CSM and CSG is stronger than the tensile resistance ability, so this has little influence on pavement mechanical behavior.

Table 5. Stress and Strain of Structure 1 with Temperature Dropping

Structure Layer	15℃～5℃		15℃～-5℃		15℃～-15℃	
	Stress (MPa)	**Strain** (με)	**Stress** (MPa)	**Strain** (με)	**Stress** (MPa)	**Strain** (με)
surface	0.85	244	2.4	388	4.8	482
AC13	0.66	205	1.75	311	3.3	368
AC20	0.399	151	0.91	204	1.435	206
ATB30	0.095	52	0.02	14	-0.321	77
CSM-1	-0.128	-90	-0.364	-256	-0.659	-464
CSM-2	-0.279	-230	-0.635	-523	-1.03	-847

Table 6. Stress and Strain of Structure 2 with Temperature Dropping

Structure Layer	15℃～5℃		15℃～-5℃		15℃～-15℃	
	Stress (MPa)	**Strain** (με)	**Stress** (MPa)	**Strain** (με)	**Stress** (MPa)	**Strain** (με)
surface	0.88	252	2.477	402	4.805	484
AC13	0.684	213	1.829	325	3.348	373
AC20	0.404	154	0.947	212	1.439	207
ATB30	0.171	91	0.228	91	0.0754	31
CSM-1	-0.0998	-70	-0.306	-215	-0.578	-406
CSM-2	-0.2755	-227	-0.625	-515	-1.017	-836

Table 7. Tensile Strength of Mixture (MPa)

Temperature	-15℃	-5℃	5℃	15℃
AC13	2.1	1.9	1.6	1.0
AC20	1.5	1.3	1.2	0.7

SUPERPOSITION STRESS AND STRAIN CAUSED BY TEMPERATURE AND LOAD

Stress and strain of pavement caused by temperature or load are analyzed, but we also know that pavement endures both load and temperature effect at the same time actually. So it is necessary to analyze the superposition stress and strain caused by temperature and load. For calculation vehicle load is used with BZZ-100, and wheel load simplifies as uniform distributed load of 100KN with circular and double ring. The analysis results can be seen in Table 8.

It is could be seen from Table 8 that, the temperature stress caused by rapid cooling is much larger than stress caused by vehicle load, so the temperature stress is the main influence factor of pavement cracking. The stress and strain caused by temperature and superposition of temperature and load of the surface layer's (AC13、AC20、ATB30) in Structure 1 are all smaller than those in Structure 2. Especially for ATB30 layer, its tensile stress of temperature and superposition at 5℃ are 55.5% and 65.8% of those of AC25 layer in Structure 2, and the strain are only 56.9% and 67.2% of those in Structure 2. At -5℃, the tensile stress of temperature and superposition in Structure 1 are 8.8% and 42.7% of those of AC25 layer in Structure 2, and the strain are only 15.4% and 38.5% of those in Structure 2.

Table 8. Stress and Strain Calculation Results

Structure Type		Structure	Load Effect		Temperature Effect		Coupling Analysis	
			Stress (MPa)	Strain (με)	Stress (MPa)	Strain (με)	Stress (MPa)	Strain (με)
5℃	1#	AC13	-0.054	-22.1	0.660	205.0	0.606	182.9
		AC20	-0.052	-23.1	0.399	151.0	0.347	127.9
		ATB30	0.051	38.8	0.095	52.0	0.146	90.8
		CSM-1	0.034	30.4	-0.128	-90.0	-0.094	-59.6
		CSM-2	0.048	33.5	-0.279	-230.0	-0.231	-196.5
	2#	AC13	-0.053	-23.1	0.684	212.7	0.631	189.6
		AC20	-0.042	-26.7	0.404	153.9	0.362	127.2
		AC25	0.051	43.7	0.171	91.4	0.222	135.1
		CSM-1	0.032	32.5	-0.100	-70.0	-0.068	-37.5
		CSM-2	0.050	35.1	-0.276	-227.3	-0.226	-192.2
-5℃	1#	AC13	-0.051	-17.5	1.750	311.0	1.699	293.5
		AC20	-0.049	-12.8	0.910	204.0	0.861	191.2
		ATB30	0.150	38.5	0.020	14.0	0.170	52.5
		CSM-1	0.037	29.7	-0.364	-256.0	-0.327	-226.3
		CSM-2	0.046	31.7	-0.635	-523.0	-0.589	-491.3
	2#	AC13	-0.050	-18.2	1.829	325.0	1.779	306.8
		AC20	-0.017	-17.1	0.947	212.0	0.930	194.9
		AC25	0.170	45.4	0.228	91.0	0.398	136.4
		CSM-1	0.036	32.2	-0.306	-215.0	-0.27	-182.8
		CSM-2	0.049	33.6	-0.625	-515.0	-0.576	-481.4

It can be found that, when ATB30 layer is set above CSM, the layer's stress and strain are smaller than those of common HMA layer under temperature and load effect. Then ATB30 layer can dissipate and adsorb the stress or strain transferred form CSM layer, and delay or prevent the extension of crack, so the force environment of asphalt pavement can be improved. At the same time, ATB can improve the temperature condition of surface and CSM layer, and reduce the influence of cooling and temperature gradient on CSM, so the warping degree and crack opening extend of CSM layer can be reduced. From the compose character, there have much coarse aggregate and few asphalt content, so ATB mixture has small shrinkage factor. Then it can block the extension path of crack tip effectively, and adsorb the load stress and temperature stress. Finally, the stress-focus phenomenon is reduced.

So, using ATB is an effective method for reducing the asphalt pavement crack.

CONCLUSIONS

Stress and strain caused by load and temperature of different pavement

structures are calculated, and coupling effect also is researched. It is found that temperature stress caused by quickly cooling is much larger than load stress, so the temperature stress is the main influence factor of pavement crack.

The stress and strain of temperature and superposition in structure 1 are smaller than those in common pavement of semi-rigid base asphalt.

Because ATB can dissipate and adsorb the stress of CSM, then it can delay or prevent the upward extension of reflective crack. Also it can improve the temperature environment of surface and CSM layer, and improve the force condition. So using ATB is an effective method for reducing asphalt pavement crack.

ACKNOWLEDGMENTS

The authors appreciate the support of Natural Science Foundation of Hunan Province (07JJ6091, Science and Technology Plan Projects of Hunan Province（2008GK3001）, Key Laboratory of Road Structure and Material of Communications（Changsha）Fund、Key Laboratory of Road Engineering of Education Ministry Fund.

REFERENCES

Cho, Yoon-Ho; Lee, Kang-Won; and Ryu, Sung-Woo. (2006). “Development of cement-treated base material for reducing shrinkage cracks”. *Transportation Research Record*, Vol.1952:134-143.

Haider, Syed Waqar; Chatti, Karim; Buch, Neeraj; Lyles, Richard W.; Pulipaka, Aswani S.; Gilliland, Dennis. (2007). “Effect of design and site factors on the long-term performance of flexible pavements”. *Journal of Performance of Constructed Facilities*, Vol. 21(4): 283-292.

Yang, Shang-Yang; Zhang, Xu-and Zhang, Long-Yun. (2006). “Effects of temperature change on cracking of semi-rigid asphalt concrete pavement”. *Rock and Soil Mechanics*, Vol.27: 627-630.

Ying, Rong-Hua; Zheng, Jian-Long; Chen, Xiao; and Feng, Hao. (2007). “Effect of coarse aggregate on cracking resistance of asphalt concrete”. *Engineering Mechanics*, Vol.24(5): 176-179.

Characteristics and Prediction of Permanent Deformation in HMA

Ying Gao[1], Xiaoming Huang[2], Zhaohui Qi[3], Jiupeng Zhang[3]

[1] Associate Professor, Transportation School, Southeast University, 2 Sipailou, Nanjing, Jiangsu, P.R.China, 210096, gy@seu.edu.cn)

[2] Professor, Transportation School, Southeast University, 2 Sipailou, Nanjing, Jiangsu, P.R.China, 210096, Huangxm@seu.edu.cn)

[3] Ph.D. Transportation School, Southeast University, 2 Sipailou, Nanjing, Jiangsu, P.R.China, 210096)

ABSTRACT：Permanent deformation (rutting) in the asphalt pavement is one of the main reasons cause the pavement damage. The focus of this paper is to study the factors affecting the permanent deformation by tri-axial creep test and the permanent deformation predicting of asphalt pavement. Four popular asphalt mixtures, AC13F, AC13C, AC16 and AC20 were chosen to do the repeated load tri-axial creep test under different voids, asphalt contents, different temperature and load levels. Based on the test result, it was concluded the Flow Number (Fn) of repeated load tri-axial creep test can distinguish the rutting resistance ability of different Hot Mixed Asphalt (HMA) mixtures. Temperature and Load levels have great influence on Fn of HMA as they do for asphalt pavement. The formula used for prediction of pavement permanent deformation was gotten based on the curve between the permanent deformation and loading number under different load and temperature levels. The formula was then calibrated by ALF test data.

KEYWORDS: Hot Mixed Asphalt Mixture；Permanent Deformation；Repeated Load Tri-axial Creep Test；Flow Number；Prediction

INTRODUCTION

Permanent deformation (rutting) in the asphalt pavement is one of the main reasons cause the pavement damage. The structure strength of pavement may decrease because of rutting. Water gather in the lower area formed by permanent deformation and cause permeability damage. The surface of pavement becomes

rougher with rutting and driving become uncomfortable. Rutting is one of control factors in many countries' pavement design guide.

The usual used pavement structure in China is asphalt surface layers lay on semi-rigid base layers. The permanent deformation in this kind of pavement mainly occurs in asphalt layers. The focus of this paper is to study the factors affecting the permanent deformation of HMA by tri-axial creep test and to predict the permanent deformation in asphalt pavement.

TEST METHOD

The test method for HMA rutting in this study is repeated load tri-axial creep test as described in NCHRP report 465 and 513. From the reports, the flow number (Fn) from the tri-axial repeated load creep test was selected as the simple performance test (SPT) candidates for evaluating an HMA mixture's resistance to rutting.

The specimens are 100 mm in diameter and 150 mm in height cored from the center of the laboratory prepared gyratory specimens. The load cycle consisting of a 0.1-s haversine pulse load and a 0.9-s rest time is applied for the test duration. The designed stress level covers the range between 700 to 1000 kPa with a confined stress of 138 kPa. The temperature covers the range from 40 to 60°C. The ends of each specimen were sawed with double-bladed saw. Two latex sheets separated with silicone grease were used to reduce the friction between the specimen ends and the loading platens.

MIXTURE DESIGN PROPERTIES

The HMA gradations are shown in table 1. The gradations are chosen based on the rutting investigation at expressway from Liangyungang to Xuzhou. Deeper rutting appears on the sections with AC13F and AC20 HMA mixture while lower permanent deformation occurs on the sections with AC13C HMA mixture.

Table 1. Gradations used in the test

Gradations	% Passing by Weight at each Sieve Size											
	26.5 mm	19 mm	16 mm	13.2 mm	9.5 mm	4.75 mm	2.36 mm	1.18 mm	0.6 mm	0.3 mm	0.15 mm	0.075 mm
AC13F	100	100	99.5	94.3	83.3	63.4	47.4	30.1	20.0	10.0	7.3	5.8
AC13C	100	100	99.3	92.7	77.4	46.6	32.1	21.0	14.6	8.2	6.4	5.4
AC16	100	100	98.6	85.2	66.8	47.2	31.3	19.5	14.0	9.2	7.5	5.9
AC20	100	95.0	85.0	75.0	64.0	43.0	29.0	18.0	12.0	10.0	6.5	5.0

(Note: AC13F means the fine gradation HMA mixture with 13mm nominal maximum aggregate size(NMAS); AC13C means the coarse gradation HMA mixture with 13mm NMAS; AC16 means the HMA mixture with 16mm NMAS; AC20 means the HMA mixture with 20mm NMAS)

The optimal asphalt content (OAC) for each HMA was obtained according to Superpave mixture design method. The Air voids of specimen were controlled at 4±0.5% or 7±0.5%.

TEST RESULT

Repeated load tri-axial creep test were done on HMA specimens with four kinds of gradation types and two kinds of asphalt binders. The cumulative permanent deformations along with the number of load cycles were recorded. The mixture response parameters form the test are flow number (Fn), which defined as the number of load repetitions at which shear deformation starts, plastic strain (εp) per load cycle, and strain ratio between plastic strain and recoverable axial strain (εp/εr), intercept (a) and slope (b) from a regression analysis of the linear portion of the permanent strain versus number of cycles in log space.

HMA Mixtures

Different HMA mixtures have different permanent deformation characteristics. The rutting investigation on Lianyungang-xuzhou expressway shows the AC13F and AC20 mixtures have poor high temperature stability. Table 2 shows the repeated tri-axial creep test result of different HMA mixtures under 40℃temperature and 700KPa stress.

Table 2. Test result for HMA mixtures with different gradations

Gradation Type	Fn	ε p	b	a	εp/εr
AC13F	2049	1.886	0.232	0.250	5.864
AC13C	4895	0.913	0.417	0.049	5.876
AC16	3280	2.124	0.330	0.201	7.053
AC20	2400	2.316	0.354	0.160	8.232

Table 2 shows that AC13F and AC20 mixtures have lower Fn value than that of AC16 and AC13C mixtures. The test result was coincident with the actual facts. The Flow Number (Fn) of repeated load tri-axial creep test can distinguish the rutting resistance ability of different Hot Mixed Asphalt (HMA) mixtures.

Temperature

The characteristics of asphalt binder change with the change of test temperature. So do the HMA mixture. Table 3 shows the Fn values from the repeated tri-axial creep tests for different HMA mixtures under different temperature levels at 700 kPa stress.

Table 3. Fn Values Under Different Test Temperatures

Gradation Types	40℃	50℃	60℃
AC13F	2049	503	298
AC13C	4895	1137	381
AC16	3280	879	245
AC20	2400	573	190

No matter what kind of asphalt binder was used, the permanent deformation characteristics of all HMA mixtures were greatly affected by test temperature. The Fn value decrease rapidly with the increase of test temperature. The Fn value under 60℃ is only around 10% of that under 40℃.

Stress

The effect of stress on HMA high temperature stability was studied. The standard stress for pavement design in China is 700kPa. But overload is quite common on expressway. Table 4 shows the Fn values from the repeated tri-axial creep tests for different HMA mixtures under different stress levels at temperature 40℃.

Table 4. Fn Values Under Different Stress Levels

Gradation Types	700KPa	800KPa	1000KPa
AC13F	2049	1712	771
AC13C	4895	3235	2338
AC16	3280	1789	1357
AC20	2400	1580	965

Table 4 shows the Fn value of HMA decrease with the increase of stress. The Fn under 1000 kPa is around 50% of that under 700kPa. Stress has great effect on the permanent deformation characteristics of HMA.

Air Voids

The designed air voids for the HMA is 4%. The requirement for pavement compaction on site is no less than 98% density of designed mixture. The specimen with 4% and 7% of air voids were tested under temperature 40℃.

Table 5. Fn Values Under Different Air Voids

Gradation Type \ Stress		700KPa	800KPa	1000KPa
AC13C	Air Voids 4%	4895	3235	2338
	Air Voids 7%	1700	1300	965
AC16	Air Voids 4%	3280	1789	1357
	Air Voids 7%	1457	1150	800
AC20	Air Voids 4%	2400	1580	965
	Air Voids 7%	1253	935	640

Table 5 shows air voids have great effect on the permanent deformation characteristics of HMA. The Fn value decrease 40~60% while the air voids of mixture increase from 4% to 7%. So compaction is quite important to high temperature stability of HMA pavement.

Though the designed air voids is 4%, the air voids in specimen may not be exactly 4%. Tests were done on AC16 and AC13F under all stress levels and different air voids levels. It was found that the variability of Fn value was less than 10% when the air voids vary ±0.5% from the designed air voids. It's commended the air voids of specimen should be designed air void±0.5%.

PAVEMENT PERMANENT DEFORMATION PREDICTION EQUATION

A group of mixture response parameters include flow number Fn, plastic strain ε p, recoverable axial strain εr, load cycles N, Temperature T and stress P, were gotten every six seconds during the test. More than 1200 groups of parameters can be gotten for each specimen. Each gradation type HMA has more than 32400 groups of parameter with three test temperatures, three test stress levels and three specimens. A power-law model, mathematically expressed by equation 1, was gotten based on the curve between the permanent deformation and loading number under different load and temperature levels.

$$\varepsilon_p = 10^{-7.5281} N^{0.575024} P^{0.67597} T^{2.509417} \qquad R^2=71.3\% \qquad (1)$$

An ALF test section was constructed in Beijing with the same material used in the lab. The pavement structures are 8 cm asphalt surfaces (AC-13C、AC-16 and AC-20) on 30 cm cement stabilized macadam base. The formula 2 was the calibrated one with ALF test data.

$$\varepsilon_p = 10^{-13.74004505} N^{0.467510996} P^{3.167141881} T^{2.236125325} \quad (2)$$

CONCLUSIONS

1) Flow Number Fn of repeated load tri-axial creep test can distinguish the rutting resistance ability of different Hot Mixed Asphalt (HMA) mixtures.
2) Temperature and Load levels have great influence on Fn of HMA. The air voids of specimen should be within the designed air void±0.5%.
3) A Pavement Permanent Deformation Prediction Equation was gotten from the test and calibrated by ALF test data which is

$$\varepsilon_p = 10^{-13.74004505} N^{0.467510996} P^{3.167141881} T^{2.236125325}.$$

ACKNOWLEDGMENTS

Great appreciation should be given to West Regions Transportation Project Office and Road Planning and Design Department of Transportation Ministry for their support of the study. The authors also acknowledge Yuqing Zhang, Wang and Rongji Cao for their contribution to the test.

REFERENCES

ARA, Inc., ERES Division, Guide for Mechanistic-Empirical Design of New and Rehabilitation Pavement Structures[R]. Appendix GG-1, National Research Council, Washington, D.C., 2005.

Bonaquist, R. F.; D.W. Christensen; and William Stump, III. Simple Performance Tester for Superpave Mix Design: First-Article Development and Evaluation[R]. Transportation Research Board NCHRP Report 513. National Research Council, Washington, D.C., 2003.

Chenjie. The Causes and Curing of Rutting on Expressway [J]. Northern Transportation, 2007.6.

Huang, Xiaoming; Zhang, Xiaobin; Deng, Xuejun. Asphalt Pavement Rutting Prediction of High-Grade Highway [J]. Journal of Southeast University, 2000.9, Vol 30, No.5.

Kamil, Elias Kaliush. Simple Performance Test For Permanent Deformation Of Asphalt Mixtures[D]. Arizona State University, Arizona State. 2001.

Sousa, Jorge B.; Joseph Craus; Carl L. Monismith. Summary Report on Permanent Deformation in Asphalt Concrete[R]. SHRP-A/IR-91-104. National Research Council, Washington, D.C., 1991.

Witczak, M.W., and Kaloush, K. Simple Performance Test For Superpave Mix Design[R]. Transportation Research Board NCHRP Report 465. National Research Council, Washington, D.C., 2001.

Witczak, M.W., and K. Kaloush. Repeated Normal Permanent Deformation Tests, NCHRP Project 9-19, Task C. Team Report SPT-WST-2(H) (WesTrack Experiment), Arizona State University, 2000.

Ying, Gao; and Xiaoming Huang. Research on Pavement design guide, section 11[R], School of Transportation, Southeast University, Nanjing, China, 2007.11.

Zhang, Yuqing. Research on Deformation Characters and Experiment Method of Asphalt Mixtures in High Temperature [D]. School of Transportation, Southeast University, Nanjing, China, 2006.11.

Zhao, Yanqing. Permanent Deformation Characterization of Asphalt Concrete Using a Viscoelastoplastic Model [D]. Department of Civil Engineering, North Carolina, 2002.

Evaluation of Low-Temperature Properties of Long-Term-Aged Asphalt Mixtures

LI Ningli[1], LI Tiehu[2], CHEN Huaxin[3], ZHANG Zhengqi[4]

[1]Scholar, College of civil engineering, Hebei University of Technology, 8 Guangrong road, Tianjin 300132; College of Materials Science and Engineering, Northwestern Polytechnical University, 127 west Youyi road, Xian 710072; lnl808@163.com

[2]Professor, College of Materials Science and Engineering, Northwestern Polytechnical University, 127 west Youyi road, Xian 710072; litiehu@nwpu.edu.cn

[3]Associate Professor, Highway College, Chang'an University, Middle section, South erhuan road, Xian 710064; chx@gl.chd.edu.cn

[4]Professor, Highway College, Chang'an University, Middle section, South erhuan road, Xian 710064; z_zhangqi@126.com

ABSTRACT: Asphalt aging is an important factor to cause pavement cracking. Currently, researchers primarily conduct ageing tests on asphalt binder to study the ageing effect on asphalt pavements. However, the ageing effect is also dependent on the air void and aggregate properties. Therefore, this paper conducted ageing tests on asphalt mixtures to account for the influences of ageing effect on in-situ pavements. The LTAC properties of both plain asphalt mixtures and polymer-modified asphalt mixtures were investigated. Laboratory flexural and flexural creep tests were conducted on the beam specimens of asphalt mixtures, including those subjected to the short-term oven ageing and others subjected to the long-term oven ageing. Results indicate that polymer-modified asphalt mixtures have superior LTAC performance than that of plain asphalt mixtures. The long-term ageing has more significant effect on the LTAC properties than short-term ageing. The long-term oven ageing test is recommended to evaluate LTAC properties of the aged in-situ asphalt pavement. A performance index for the evaluation of the LTAC properties of the aged asphalt pavements was proposed.

INTRODUCTION

The low-temperature properties of asphalt pavement have been studied for many years to determine the roles of material, environmental and structural factors that affects the cracking propagation. Among the material factors, the ageing of asphalt

mixtures has been recognized as a key factor in the low-temperature cracking of asphalt pavement. During the processes for mixing and compacting loose asphalt mixtures, short-term ageing occurs. During the service life of the pavement, long-term ageing occurs. This long-term ageing process is slow, but continuous. Oxygen and ultraviolet radiation cause hardening of the asphalt, which decreases its flexibility, and, consequently, deterioration takes place. Thus, ageing should be considered in evaluating the low-temperature, anti-cracking (LTAC) properties of asphalt mixtures. To the present time, however, ageing has not been considered in appraising the LTAC properties of asphalt mixtures in China.

MATERIALS AND MIXTURE DESIGN

Materials

Both plain asphalt and polymer-modified asphalt from the Luxiang Petroleum Asphalt Factory are used in this research. The basic physical properties of plain asphalt and polymer-modified asphalt are shown in Table 1. The coarse aggregate and the fine aggregate are manufactured from limestone.

Table 1. Basic Physical Properties of Plain Asphalt and Polymer-Modified Asphalt

	Penetration (25 ,0.1mm)	Softening point ( )	Ductility (5cm/min,cm)
Plain asphalt	91	45.5	>150
Polymer-modified asphalt	75	65.6	42.53

Note: the test temperature of ductility of plain asphalt is 15 ,that of polymer-modified asphalt is 5 .

Mixture Design

The experiment was conducted for four different mixtures. A Marshall compactor was used to compact the specimens. The optimum asphalt content, air void, and density for AC-13I plain asphalt mixture were 4.8%, 4.5%, and 2398 kg/m^3, respectively, and those values for the AC-13I polymer-modified asphalt mixture were 5.0%, 4.2%, and 2431kg/m^3, respectively. Analogously, the optimum asphalt content, air void, and density for the Superpave-12.5 plain asphalt mixture were 4.6%, 4.5%, and 2371 kg/m^3, respectively, and those values for the Superpave-12.5 polymer-modified asphalt mixture were 4.9%, 4.3%, and 2382kg/m^3, respectively.

EXPERIMENTAL PROGRAM

Specimen Preparation

In this research, two methods are described that simulate field ageing of asphalt mixtures: the short-term oven ageing (STOA) test and the long-term oven ageing (LTOA) test. In the STOA test, the asphalt mixture was spread evenly in a flat pan, placed in a force-ventilated drying oven to age for 2 h ± 5 min at 135 ^{o}C±1 ^{o}C, and mixed once every hour with a shovel. After two hours' ageing, the asphalt mixture was taken out of the oven, placed in the mixing pot, and mixed for 120 seconds in order to assure uniformity of the mixture. Then, the treated asphalt mixture was formed into board rut specimens with dimensions of 300 mm (length), 300 mm (width), and 50mm (height). The board rut specimen was cut into beam specimens with dimensions of 250 mm (length), 30mm (width), and 35mm (height).

The LTOA test beam specimen was formed into board rut specimens with dimensions of 300 mm (length), 300mm (width), and 50mm (height), using the asphalt mixture that have experienced short-term ageing, and placed into the oven at a temperature of 85 ^{o}C ±3 ^{o}C for 120 h ± 0.5 h and cut into beam specimens with dimensions of 250 mm (length), 30 mm (width), and 35 mm (height).

The original beam specimen was used to form the asphalt mixture into the board rut specimen with dimensions of 300 mm (length), 300 mm (width), and 50 mm (height) dimension, and that board rut specimen was cut into a beam specimen with dimensions of 250 mm (length), 30mm (width), and 35mm (height).

Test Methods

The flexural test and the flexural creep test are adopted in this research. The MTS 810 (material test system) is used to perform the flexural test and the flexural creep test for evaluating the LTAC properties of asphalt mixtures.

EXPERIMENTAL RESULTS AND ANALYSIS

Results of the Flexural Test

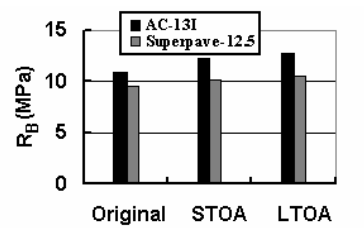

FIG.1. Comparison of R_B of polymer-modified asphalt mixtures at -10 after different ageing

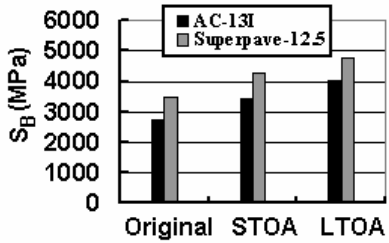

FIG.2. Comparison of S_B of polymer-modified asphalt mixtures at -10 after different ageing

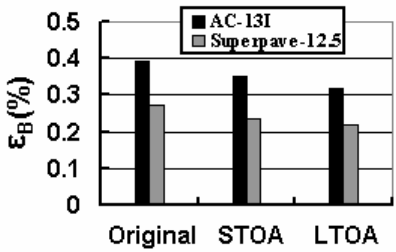

FIG.3. Comparison of ε_B of polymer-modified asphalt mixtures at -10 after different ageing

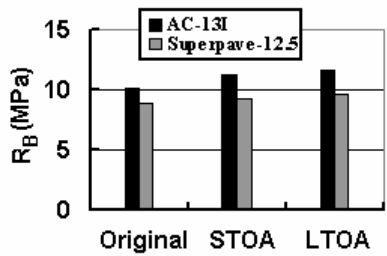

FIG.4. Comparison of R_B of plain asphalt mixtures at -10 after different ageing

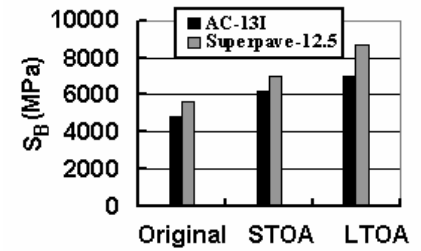

FIG.5. Comparison of S_B of plain asphalt mixtures at -10 after different ageing

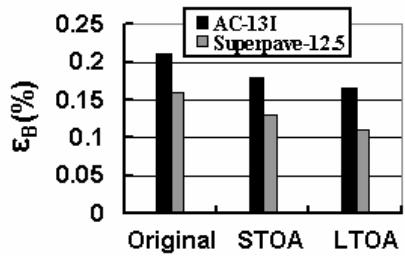

FIG.6. Comparison of ε_B of plain asphalt mixtures at -10 after different ageing

As shown in Fig. 1 through Fig. 4, the flexural strengths of both the plain asphalt mixture and the polymer-modified asphalt mixture increase with ageing time. During the specimen failure, the asphalt binder stiffens and the interface strength increases with increasing ageing time. The longer the asphalt mixture is aged, the greater the flexural strength becomes.

When the length of ageing increases for both the plain asphalt mixture and the polymer-modified asphalt mixture, the maximum tensile strains of the mixtures are reduced. The sequence is LTOA < STOA < Original, as shown in Fig. 3 and Fig. 6.

As shown in Fig. 2 and Fig. 5, as the ageing time increases, the flexural strength increases and the maximum tensile strain decreases. Thus, the creep stiffness of the mixture will be increased. Since asphalt binder stiffens with ageing time, it becomes brittle and its capability to dissipate stress through viscous flow decreases. The low temperature flexibility of asphalt binder decreases, and as a result, the LTAC property of the mixture also deceases.

Results of the Flexural Creep Test

The results of the flexural creep test of the mixture are showed in Fig. 7 and Fig. 8, from which it is noted that creep rate of the mixture is reduced as ageing time increases. The sequence is LTOA < STOA <Original. The creep rate of the STOA

polymer-modified asphalt mixture is reduced to approximately 60% of that of the original polymer-modified asphalt mixture, and the creep rate of the LTOA polymer-modified asphalt mixture is decreased to approximately 20% of that of the original polymer-modified asphalt mixture. The creep rate of the STOA plain asphalt mixture is reduced to approximately 40% of that of the original plain asphalt mixture, and the creep rate of the LTOA plain asphalt mixture is reduced to approximately 15% of that of the original plain asphalt mixture. This information indicates that LTOA has a significant effect on the LTAC properties of mixtures.

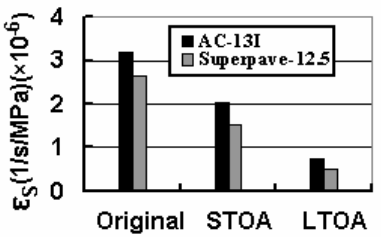

FIG.7. Comparison of ε_s of polymer-modified asphalt mixtures at 0 after different ageing

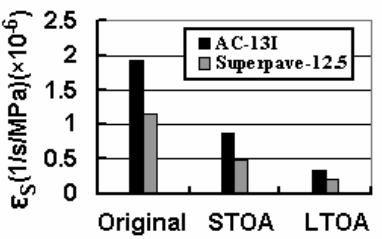

FIG.8. Comparison of ε_s of plain asphalt mixtures at 0 after different ageing

Evaluation of Low-Temperature Properties of Long-Term-Aged Asphalt Mixtures

In order to accurately evaluate the LTAC properties of asphalt mixtures, a performance index is proposed. If η stands for the attenuation degree of creep rate between the original asphalt mixture and the LTOA asphalt mixture, the following equation can be proposed:

$$\eta = \frac{\varepsilon_o - \varepsilon_a}{\varepsilon_o} \tag{1}$$

Where: η is attenuation index; ε_o is creep rate of the original specimen; and ε_a is creep rate of the LTOA specimen.

Table 2. Attenuation Index of Polymer-Modified Asphalt Mixtures and Plain Asphalt Mixtures

	Polymer-modified asphalt mixtures		Plain asphalt mixtures	
	AC-13I	Superpave-12.5	AC-13I	Superpave-12.5
Attenuation index	0.771	0.811	0.821	0.827

As shown in Table 2, AC mixtures have superior LTAC performance to that of Superpave mixtures. Polymer-modified asphalt mixtures have superior LTAC performance to that of plain asphalt mixtures. This is generally a uniform finding in practical engineering applications. It indicates that the attenuation index can effectively characterize the LTAC properties of in-situ aged pavements.

CONCLUSIONS

1. The ageing of asphalt mixtures is recognized as one of the primary factors that affect the LTAC properties of asphalt pavement. However, ageing has not been considered in evaluating the LTAC properties of asphalt mixtures in China.
2. Experimental results indicate that long-term ageing has a more significant effect on the LTAC properties than short-term ageing. The long-term, oven-ageing test is recommended to evaluate the LTAC properties of aged in-situ asphalt pavement.
3. A performance index for the evaluation of the LTAC properties of aged asphalt pavements was proposed, and results have shown that it can effectively characterize the LTAC properties of in-situ aged pavements.

ACKNOWLEDGEMENTS

The authors acknowledge the financially support provided by the Ministry of Communication, China.(Fund No.2001-318-000-38) and Shaanxi Programs for Science and Technology Development (Fund No. 2005k06-G5).

REFERENCES

JTJ 052-2000. (2000). “Standard Test Method of Asphalt and Asphalt Mixtures for Highway Engineering.” The People’s Communications Press, Beijing.

Kliewer, J. E., Zeng, H., and Vinson, T. S. (1996). “Aging and Low-Temperature Cracking of Asphalt Concrete Mixture.” *Journal of Cold Regions Engineering*.,

Vol.10(3):134-148.

Shen, J.A. (2001). "Performance of Asphalt and Asphalt Mixtures." The People's Communications Press, Beijing.

Zeng, H. (1995). "On the low temperature cracking of asphalt pavements." *PhD thesis*, *Division of highway Engineering*, Royal Institute of Technology,TRITA-IP FR 95-7, Stockholm.

Zhang, D.L. (1998). "Asphalt Pavements." The People's Communications Press, Beijing.

Zhang, Y. (2004). "Asphalt Mixture's Crack Resistance at Low Temperature and Asphalt Mixture Design Method in Perennially Frozen Soil Zone." *Master Degree Thesis*, Chang'an University, Xian.

Mechanical Study of Steel Bridge Pavement with Composite Asphalt Materials

C. Y. Wu and Y. Li

Highway Research Department, Jiangsu Transportation Institute, Nanjing, China

ABSTRACT: The mechanical analysis is applied for the steel box girder bridge with orthotropic plate and pavement by means of Finite Element Method. The interaction between steel bridge and pavement is evaluated by the three stages in calculation. The analysis is focused on the mechanical features and the influential factors of the large components (cross diaphragm) and the local components (U-shaped ribs). Considering the mechanical effects by the heavy-duty vehicle load and heavy-load with braking, the interfacial shear failure is studied as one of the main reasons of damages. Moreover, in view of this major form of damage, this paper provides the corresponding mechanical analysis of the indicators.

INTRODUCTION

As we known, forces in steel bridge deck pavement are more complex than those in asphalt pavement. Two types of forces exist in deck pavement, one is bending tensile stress and another is shear stress. It is more complicated in the forces of the bridge deck, that include the stresses caused by the bridge contracting deformation, the stresses caused by bridge plate deformation, the bending stresses caused by local deformation, and temperature stress caused by the change of temperature. Usually, deck pavement has a general thickness with 3-10 cm, which has the much lower stiffness than the steel plate, so usually a larger shear stress often occurs in the interface between bridge deck and asphalt pavement. When the horizontal forces of vehicle load are transferred to pavement, it will result in sliding damages between the interfaces and layers. Because the bridge deck pavement is suffered by the greater bending stress and shear stress, some diseases such as cracking, sliding, rutting are often observed in bridge deck pavement.

The use of finite element software is used for constructing a new computing model, such as Sheikh (2000) and est. However, previous models rarely considered the steel

box girder mechanics and gave many simplifications to steel structure when analyzing the deck pavement. And previous studies did not consider that the overall structure of the bridge would influence the force situation of pavement. We think that the types and spans of bridges, cable-stayed bridge, suspension bridge and the continuous bridge, can not be ignored.

FEM MODEL OF STEEL DECK

The structure of steel box-girder bridge is composed of the bridge panel, the diaphragm, the vertical stiffening rib and so on. In steel box-girder bridge, the bridge deck, diaphragm and vertical stiffening rib work together to bear the overall loads. In order to facilitate the analysis, three stages analytical method in the course of the mechanical calculation are proposed through the main type of damage and mechanics research of bridge deck pavement,.

Shear interfacial failure is the main damage style of bridge deck pavement. This paper chooses the maximal interfacial shear stress and the maximal stress as control indicators.

Stage I: Integral bridge model

In Stage I, the bridge deck pavement analysis needs to consider the overall structure of the bridge. The whole deformation of the bridges would cause vertical negative moment, the overall displacement of the bridge deck, bridge vibration and so on. The establishment of the bridge model is very difficult to pavement design but is relatively normal to the structural design of the bridge deck. To improve the bridge deck pavement mechanical calculation, structure design can help bridge deck to analyze force and negative situation of the bridge structure suffered by the vehicle load. However, in most bridges, the first stage can not influence the local deck pavement stresses. Therefore, this article will focus on Stage II and Stage III.

Stage II: Local steel box-girder model

Stage II simulates of the local steel box Girder Bridge and the pavement subjected to the vehicles. This phase model describes the local steel box of Girder Bridge and decking pavement.. The vehicle load in the surface is uniform-speed traveling in this phase. The two control target indicates are calculated such as the largest layer strain and the largest layer shear stress. The model would do some sensitivity analysis by changing the modulus and thicknesses of pavement and by considering the overloading of vehicles.

Stage III: the maximal interfacial shear stress under the horizontal load

Stage III calculates the effects of the vertical and horizontal slope, the braking effect and the maximal shear stress of pavement and steel bridge. Synthesizing the maximal shear stress of Stage I, Stage II and Stage III, the final stress indicators of the bridge deck pavement design and the test verification are determined (FIG 1).

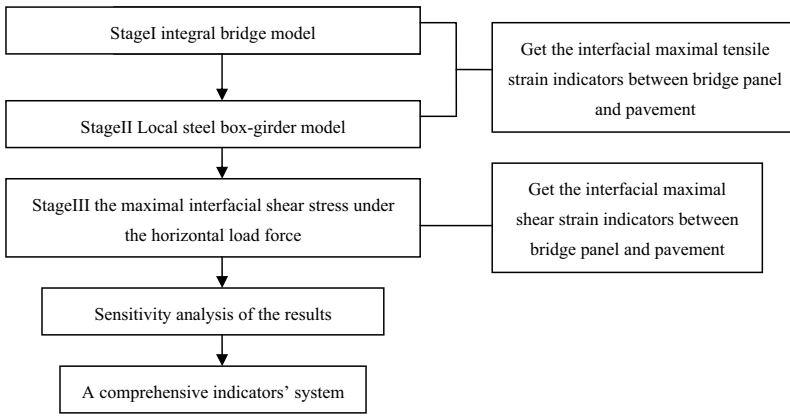

FIG.1. Three-phase diagram calculation

THE CALCULATION ANALYSIS OF STAGE II

Longitudinal stiffening rib, longitudinal and cross diaphragm and bridge decking is simulated by FEM's shell unit, asphalt concrete pavement using three-dimensional entity unit to simulate.

Steel box girder finite element model

Steel box Girder Bridge is a box-type structure which is composited by upper bridge decking, longitudinal diaphragm, cross diaphragm and bridge decking at bottom. The steel box girder become more complex by means of increasing the number of the longitudinal and cross diaphragm and using a certain rib of the U-shaped to strengthen the longitudinal stiffness（FIG.2）. The standard example of pavement is for 25mm RA (a type of resin asphalt) and 55mm SMA.

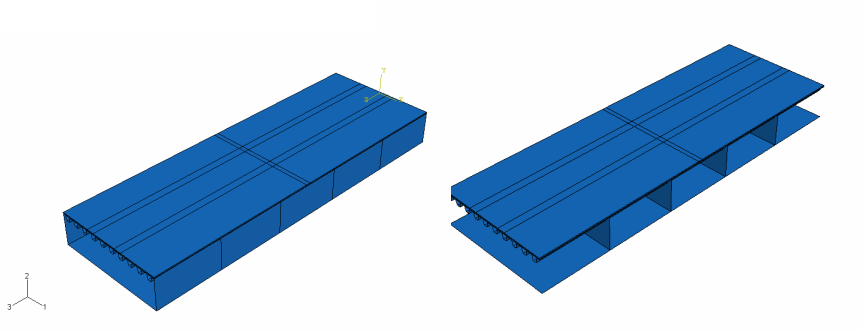

FIG.2 A simplified model of steel box girder

Steel box girder components are simulated by shell units, while asphalt concrete pavement is simulated by three-dimensional entity unit. Layer connection is simulated as continuous situation. Shown as the internal structural figure below, the span is 15 m with 5 cross diaphragm spans, whose distance between cross diaphragm is 3.0 m. And the distance between longitudinal diaphragms is 8 m, one of longitudinal spans in the overall box girder's width is selected. The thickness of steel diaphragm and bridge is 14 mm.

Three kinds of vertical load locations of steel box girder model are placed at the top centre of the cross diaphragm (A-1), between two adjacent cross diaphragm in the middle span (A-2), and at the top centre of the cross diaphragm near the support (A-3) (FIG.3).

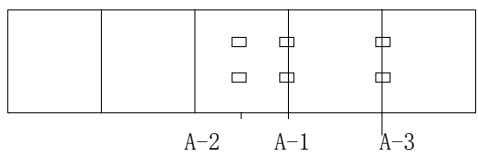

FIG.3 Disadvantage location of load in longitude direction

Three kind of transversal load locations of steel box girder model are placed on the two sides of one end of U-shaped rib (B-1), the top centre between two U-shaped rib (B-2) and top centre of U-shaped rib (B-3) (FIG.4).

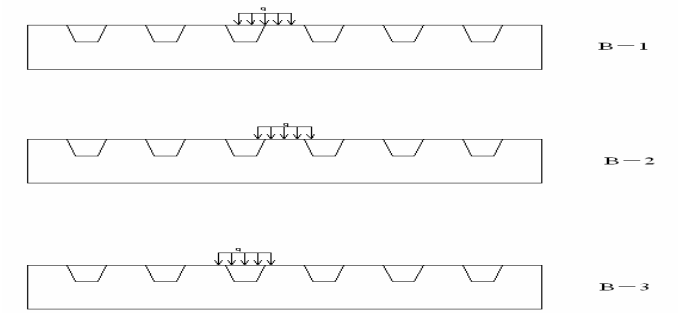

FIG.4 Disadvantage location of load in transversal direction

Table.1 Longitudinal stress and strain of different load location

Load location	Shear stress MPa	Tensile stress MPa	Tensile strain με
A－1	0.105	0.675	95.7
A－2	0.529	1.17	158
A－3	0.110	0.77	140

Note: The above shearing stress is the largest shear stress on bridge decking and pavement interface；the above tensile stress is the largest tensile stress on bridge decking and pavement interface；the tensile strain is the largest tensile strain on bridge decking and pavement interface.

Table.1 shows that load location A-2 is much greater than A-1 and A-3 in a variety of indicators of stress and strain. Therefore, the disadvantage load location of steel box girder has to choose A-2, which is loaded at the centre of the two cross diaphragm and in the middle of the span.

Table.2 Transversal stress and strain of different load location

Load location	Shearing stress MPa	Tensile stress MPa	Tensile strain με
B－1	0.399	0.93	118.3
B－2	0.46	0.87	82.8
B－3	0.12	0.23	59.7

Table 2 shows clearly that the tensile stress and tensile strain of load location B-1 is much greater than B-2 and B-3. Although the indicators of shearing stress and shear strain are a little smaller, but can't be showed on numerical clearly. Therefore, the weakest transversal load location has to choose B-1, which is one side of U-shaped crossed by tire.

Standard example calculation of the weakest load location

The standard example of pavement is for 25mm RA (a type of resin asphalt) and 55mm SMA. RA is a upper layer, and SMA is bottom layer. The result below is the standard example calculated in the weakest load location (Table.3):

Table.3 The calculation result of the largest stress and strain of the phase II of the standard example

Largest stress and strain	Longitudinal (The direction of the length of the box beam ）	Transversal (The direction of the width of the box beam）
Shearing stress between steel plate and RA layer MPa	0.529	0.399
Shearing stress between RA layer and SMA layer MPa	0.322	0.09
Tensile stress of RA layer MPa	1.17	0.93
Tensile stress of SMA upper layer MPa	0.31	0.09
Tensile strain of RA layer με	151.9	118.3
Tensile strain of SMA upper layer με	158	56.3

THE CALCULATION ANALYSIS OF STAGE III

When the vehicle brakes, the bridge pavement will hold the horizontal force caused by vehicles. In particular, this phenomenon often occurs in the region with large volume of traffic, resulting in the shear failure of decking pavement. The load factor selected in the model is 0.5, the standard vertical load is 0.707MPa, and horizontal load is half of the vertical load, which is 0.354MPa (Table.4). In the table, the SMA modulus are becoming from 500MPa to 2000MPa.

Table.4 the maximal stress and strain result by horizontal load

type	longitudinal		transversal	
	Shear stress MPa	Tensile strain με	Shear stress MPa	Tensile strain με
2000MPa	0.615	189.5	0.351	130.5
1500MPa	0.522	147.2	0.361	100.9
1000MPa	0.482	107.2	0.286	71.3
500MPa	0.419	71.5	0.237	43.4

CONCLUSIONS

In steel bridge pavement FEM model, longitudinal stiffening rib, longitudinal and cross diaphragm and bridge decking are simulated by shell unit, and asphalt concrete pavement is simulated by three-dimensional entity unit. The calculation stage I is the integral bridge model, the stage II is the local steel box-girder model, and the stage III is the maximal interfacial shear stress indicators under the horizontal load force. The standard example of pavement is for 25mm RA (a type of resin asphalt) and 55mm SMA. Through mechanical analysis, it shows that the most disadvantage load occurs in the centre of the two cross diaphragm of the longitude direction and one side of U-shaped crossed by tire in the transversal direction. The results showed that RA's largest shear stress occurred in the steel bridge layer between the RA and SMA, SMA's largest shear stress occurred in the RA and SMA layer between the layers. When increasing the horizontal load, the longitude shear stress increases about 0.1 MPa in average.

REFERENCES

A H. Sheikh, M. Mukhopadhyay. (2000) "Geometric nonlinear analysis of stiffened plates by the spline finite strip method" *Computers and Structures,* No.76.

N. E. Shanmugam. (1987) "Strength of Axially Loaded Orthotropic Plates *Journal of Structure Engineering*, Vol. 113 No. 2.

G. H. Gunther, S. Bild, G. Sedlacek. (1987) "Durability of Asphaltic Pavements on Orthotropic Decks of Steel Bridges". *J. Construct. Steel Research.*

S. Bild. (1987) "Design Criteria for Bituminous Pavements on Orthotropic *Steel Bridge Decks*". *Can. J. Civ. Eng.*

A Cyclic Cohesive Crack Model Based on Bounding Surface Concept

Rongzong Wu[1], M. ASCE and John T. Harvey[2], M. ASCE

[1]Project scientist, University of California Pavement Research Center, 1353 S. 46th St, Bldg. 452 Richmond, CA 94804; rzwu@ucdavis.edu
[2]Director and Associate Professor, University of California Pavement Research Center, 1 Shields Avenue, 3153 Engineering III, Davis, CA 95616; jtharvey@ucdavis.edu

ABSTRACT: Cohesive crack model (CCM) is essentially a type of non-linear fracture mechanics that can deal with large fracture process zones in inhomogeneous materials such as asphalt concrete (AC). CCM has been successfully used to model cracking under monotonic loading conditions. Its application to fatigue cracking is however limited due to the lack of well-developed mechanisms to account for progressive cracking damage caused cyclic loading. This paper incorporates the bounding surface concept into cohesive crack model and provides a systematic way for introducing hysteresis loop during loading and unloading into CCM. Model behaviors of the resulting cyclic CCM are then examined for reasonableness and flexibility.

INTRODUCTION

As stated by Bazant and Plans (1998), cohesive crack model (CCM) is essentially a non-linear fracture mechanics that can deal with large fracture process zone in inhomogeneous materials such as asphalt concrete (AC). CCM is also called fictitious crack model (Hillerborg et al., 1976). It has been mostly used for cases with monotonic loading conditions (Planas et al., 2003) while applications to fatigue problems with cyclic loading is very rare. Dealing with fatigue behavior implies that hysteresis loops must be taken into account, which has not been well established for CCM. For example, the work by Toumi and Bascoul (2002) assumes an ad hoc hysteresis loop and the model works only for cases when failure occurs in several load repetitions, which strictly speaking is not fatigue failure.

The main objective of this paper is to present a systematic way of introducing hysteresis loop into CCM so that it can be used to model fatigue failure in composite materials like AC. Specifically, bounding surface concept in plasticity theory is borrowed and incorporated into CCM to achieve the objective. The resulting model is then evaluated for reasonableness.

MODEL CONSIDERATIONS

To start with something simple, assume that the normal of any fatigue crack is the same as the principle direction corresponding to the first principle tensile stress. This implies that there is no shear stress on the crack face and all the crack opening displacement is normal to the crack face. Denote the first principle tensile stress as ξ, the softening function for monotonic cohesive crack model can be expressed as:

$$f(\xi, w) := \xi - f_t \exp\left(-w\frac{f_t}{G_f}\right) = 0 \tag{1}$$

where f_t is the tensile strength, G_f is the specific energy for crack propagation under monotonic loading, and w is the crack opening displacement. According to the monotonic softening function, there will be no crack opening unless the tensile strength f_t will be exceeded otherwise. This means no crack will be induced under fatigue loading due to the low stress amplitudes. This implication is not realistic and needs to be addressed by introducing a mechanism to allow crack opening displacement even if the tensile strength is not exceeded. A similar mechanism has been well established in bounding surface plasticity theory, which allows plastic flow under cyclic loading even if the stress amplitude is less than the monotonic yielding stress. For more details about bounding surface plasticity, please refer to the works by (Dafalias and Popov, 1975; Holland, 1997; and Wu and Harvey, 2008)

The following section presents the development of a cyclic cohesive crack model by incorporating bounding surface concept with monotonic cohesive cracking model.

CYCLIC COHESIVE CRACK MODEL

The counterpart to the yielding function of plasticity theory is the softening function in CCM. In bounding surface plasticity, the classical yielding function is typically taken as the bounding surface. Similarly, the monotonic softening function is taken as the bounding surface here for cyclic CCM. To avoid confusion, quantities on the bounding surface are denoted with a bar at the top. The bounding surface is then recast into:

$$f := \bar{\xi} - K(\bar{w}) = 0 \tag{2}$$

in which $\bar{\xi}$ is the image stress of the real maximum principle tensile stress ξ and $K(\bar{w})$ is the current tensile strength that decreases with increasing $\bar{w}$:

$$K(\bar{w}) = f_t \exp\left(-\bar{w}\frac{f_t}{G_f}\right) \tag{3}$$

and $\bar{w}$ is the internal variable that controls softening of tensile strength and it is in proportion to the accumulated crack opening displacement:

$$\dot{\bar{w}} = a \cdot < \dot{w} >_+ \tag{4}$$

where a is a material constant. This means w will increase whenever $\dot{w} > 0$ and remain constant otherwise. The value for a should be no more than one for fatigue loading since a=1 corresponds to monotonic loading.

The distance between real maximum principle tensile stress and its image is defined as:

$$b = \frac{\xi}{\bar{\xi}} \tag{5}$$

where b is a scalar whose value varies between $+\infty$ when $\xi = 0$ to 1 when current stress point is on the bounding surface.

Loading/unloading criteria is very critical in plasticity theory. Here a very simple criteria is assumed: it is loading whenever $\dot{\xi} > 0$, unloading whenever $\dot{\xi} < 0$ and neutral loading whenever ξ remains constant. It is assumed that during unloading, the $\xi \sim w$ locus is a straight line running through the origin (0, 0).

For bounding surface plasticity, the plastic flow is determined at the image stress state rather than at the actual stress state. Similarly, the increase in crack opening displacement w during loading is determined as:

$$\dot{w} = \dot{\lambda}\frac{\partial f}{\partial \bar{\xi}} = \dot{\lambda} \tag{6}$$

where λ is called cracking parameter, borrowed from the name of its counterpart in plasticity. Note that $\dot{\lambda} > 0$ since it is positive during loading and zero during unloading. This implies:

$$\dot{\bar{w}} = a \cdot \dot{\lambda} \tag{7}$$

In order to solve for the additional unknown b, an additional equation is required. Following the formulation outlined in (Kaliakin) and later used by (Holland) and (Wu and Harvey), the additional equation is provided by first introducing the hardening (or really should be softening for cracking) modulus defined at the image stress state:

$$\bar{K}_p \equiv -\frac{\partial f}{\partial \lambda} = -\frac{\partial f}{\partial \bar{w}}\frac{d\bar{w}}{d\lambda} = a \cdot K'(\bar{w}) \tag{8}$$

Similar to plasticity theory, the following relation can be derived by differentiating the bounding surface, i.e., equation (2):

$$\dot{\lambda} = \frac{1}{\bar{K}_p}\dot{\bar{\xi}} \tag{9}$$

The additional equation is then provided by introducing the following equality between hardening modulus at the actual stress state (K_p) and at the image stress state (i.e., $\bar{K}_p$):

$$\dot{\lambda} = \frac{1}{\bar{K}_p}\dot{\bar{\xi}} = \frac{1}{K_p}\dot{\xi} \tag{10}$$

and define K_p in terms of distance b and $\bar{K}_p$ based on material behavior. A power law between them is assumed for now:

$$K_p = -K_p \cdot c \cdot b^{\kappa} \tag{11}$$

where c and κ are material constants that controls the rate of crack opening displacement inside the bounding surface. The negative sign is necessary considering that fact that $\dot{\bar{\xi}}$<0 while $\dot{\xi} > 0$ during cyclic loading. As κ increases, cracking modulus K_p increases, this in turn leads to decrease in crack opening displacement rate.

With the above equations, the cyclic CCM based on bounding surface concept is now complete. Crack opens whenever ξ is increasing, or in other words when current stress is moving towards the bounding surface and the distance b is decreasing. During crack opening, the incremental cracking parameter $\Lambda\lambda = \dot{\lambda}\Lambda t$ is solved by satisfying both equations (2) and (10).

SIMPLIFIED SOLUTION SCHEME

The cyclic cohesive crack model is given in differential form and needs to be integrated during solution. The integration procedure is referred to as solution scheme here. Before developing the solution scheme, the model is further simplified here. As shown below, this simplification allows one to avoid using *b* explicitly in the solution scheme. This removes the need to deal with the $+\infty$ value for distance *b* and is very helpful in terms of numerical implementation. To start, combine equations (10) and (11) into:

$$\dot{\xi} = \dot{\lambda} K_p = -\dot{\lambda} \bar{K}_p \cdot c \cdot b^{\kappa} \tag{12}$$

using equation (9) and differentiating the bounding surface, the above equation can be recast into:

$$\dot{\xi} = -\dot{K}(\bar{w}) \cdot c \cdot b^{\kappa} \tag{13}$$

after substituting $b = \bar{\xi}/\xi = K(\bar{w})/\xi$ into the equation, it can be integrated to yield:

$$-c \cdot \Delta \left[K(\bar{w})^{\kappa+1} \right] = \Delta \xi^{\kappa+1} \tag{14}$$

which is essentially the consistency condition for the proposed cyclic cohesive crack model. To facilitate the derivation, define a new function *g* as:

$$g(\xi, \bar{w}) := \xi^{\kappa+1} + c \cdot [K(\bar{w})]^{\kappa+1} \tag{15}$$

Then the consistency condition becomes:

$$\phi(\xi, \bar{w}) := g(\xi, \bar{w}) - g(\xi, \bar{w})|_{t=t_n} = 0 \tag{16}$$

where ϕ is the final form of the consistency condition.

For any given stress history in terms of $\xi = \xi(t)$, the solution scheme based on known quantities for $t = t_n$ can be summarized as follows:

1. determine current $\bar{w}$ using equation (16)
2. determine current crack displacement w using equation (7) and (6), in fact $\Delta w = \Delta \bar{w}/a$

MODEL BEHAVIORS

In this section, the model behaviors under fatigue loading will be investigated. The loading is assumed to be uniaxial tension with haversine waveform. It is of interest to evaluate the stress vs. crack opening curve, variation of the resulting fatigue with stress amplitude, and the energy dissipation.

Loading

It is assumed that a material point is subjected to cyclic uniaxial tension with a haversine waveform. For such a loading the applied stress is also the first principle tensile stress:

$$\xi = \sigma = \frac{1}{2}\sigma_0[1 + \sin(\omega t - \frac{\pi}{2})] \tag{17}$$

where σ_0 is the maximum tensile stress for each cycle, ω is the radian frequency and t is the time. The stress increases from 0 to σ_0 and then goes back to zero for each load repetition.

Stress vs. Crack Opening Displacement Curve

An example of stress vs. crack opening displacement curve is shown in **Figure 1**, which indicates that maximum crack opening increases with increasing number of load repetitions when the maximum stress is maintained at a constant (1.5 MPa in this case). The incremental decrease in w for each cycle also increases with the number of load repetitions. The accelerated deterioration is expected due to the softening effect of crack opening displacement.

Figure 1 also indicates that the solution for the loading branch of the 8th load repetition can not be finished. This is because the material has been softened too much and can not sustain the applied stress level of 1.5 MPa anymore. This point is taken as the failure point and a macro crack is assumed to have formed as the result of the failure.

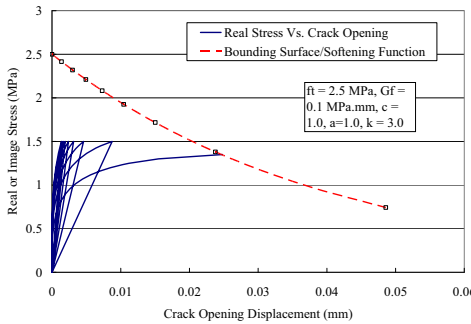

Figure 1. Stress vs. crack opening displacement curve, and the progressive softening

Variation of Fatigue Life with Stress Amplitude

The number of load repetitions required to reach the failure point defined in the previous section can be calculated using equations (14) and (16). Essentially, if failure occurs in the N+1th load repetitions, then the following conditions holds:

$$\Delta\xi^{\kappa+1} > c \cdot [K(\bar{w}_N)]^{\kappa+1} \tag{18}$$

where $\bar{w}_N$ denotes the value of $\bar{w}$ at the end of load repetition N. Accordingly, N can be calculated as:

$$N = \lfloor c \cdot f_t^{\kappa+1} / \sigma_0^{\kappa+1} \rfloor \tag{19}$$

where the $\lfloor \cdot \rfloor$ operator calculates the largest integer that is less than the operand. If we take this as the definition for fatigue life, then it is a power function of stress amplitude with a negative exponent. This trend is consistent with typical fatigue life estimates.

Total Dissipated Energy

The area enclosed by the $\xi \sim w$ curve for each cycle is the specific energy dissipated in the cycle. The dissipated specific energy during load cycle *N*+1, denoted as D_{N+1}, can be calculated as:

$$D_{N+1} = \int_{t=N\cdot T}^{t=(N+1)T} \xi dw - \frac{1}{2}\sigma_0 \cdot w_{\max,N+1} \tag{20}$$

where ξ satisfies the following equations:

$$\xi^{\kappa+1} = c \cdot \left[K(\bar{w}_N)^{\kappa+1} - K(\bar{w}_N - a \cdot w)^{\kappa+1}\right] \tag{21}$$

Values for D_{N+1} can be calculated using numerical integration. One can prove that $D_{N+1} \propto \frac{c}{a}$. By adjusting the values for *a* and *c*, one can control the total amount of energy required to be dissipated to reach fatigue failure.

SUMMARY AND CONCLUSIONS

This paper presents an extension to cohesive crack model to account for progressive fatigue cracking failure. The extension is achieved by incorporating the bounding surface concept typically used for plasticity theory. The resulting cyclic cohesive crack model is found to yield reasonable stress vs. crack opening curves for stress-controlled fatigue tests. It is also found to lead to a reasonable power law for fatigue life as a function of stress amplitude. The total dissipated energy can also be adjusted to match laboratory test data if necessary.

The proposed cyclic cohesive crack model is only one example of incorporating bounding surface concept with cohesive crack model. Readers are encouraged to explore other alternatives to better match observed behaviors of interested material.

The proposed cyclic cohesive crack model also needs to be combined with the bulk material behavior to form a complete constitutive model. Also note that the behavior after fatigue failure is not defined here. These will however be left for future studies.

ACKNOWLEDGEMENTS

The authors are grateful for the support provided by California Department of Transportation through University of California Pavement Research Center.

REFERENCES

Bazant, Z. P., and Planas, J. (1998). Fracture and Size Effect in Concrete and Other Quasibrittle Materials, CRC Press.

Dafalias, Y. F., and Popov, E. P. (1975). "A model of nonlinearly hardening materials for complex loading." *Acta Mechanica*, 21(3), 173-192.

Hillerborg, A., Modeer, R. M., and Petersson, P.-E. (1976). "Analysis of crack formation and crack growth in concrete by means of fracture mechanics and Finite Elements." *Cemenet and Concrete Research* (6), 773-782.

Holland, T. J. (1997). "Numerical Methods for Implementing the Bounding Surface Plasticity Model for Clays," Ph.D. Dissertation, University of California, Davis.

Kaliakin, V. N. (1985). "Bounding Surface Elastoplasticity-Viscoplasticity for Clays," Ph.D. Dissertation, University of California, Davis.

Planas, J., Elices, M., Guinea, G. V., Gomez, F. J., Cendon, D. A., and Arbilla, I. (2003). "Generalizations and specializations of cohesive crack models." Engineering Fracture Mechanics, 70(14), 1759-1776.

Toumi, A., and Bascoul, A. (2002). "Mode I crack propagation in concrete under fatigue: microscopic observations and modelling." International Journal for Numerical and Analytical Methods in Geomechanics, 26(13), 1299-1312.

Wu, R., and Harvey, J. T. "Evaluation of the Effect of Wander on Rutting Performance in HVS Tests." *Proceedings of the 3rd International Conference on Accelerated Pavement Testing*, Madrid, Spain

Research on the Relationship between the Loading and the Conductivity of Smart Asphalt Concrete

Zhu Feng[1], Cheung Lam Wah[2]， Dong Zejiao[3]

[1]Doctor, the Harbin Institute of Technology, Harbin, Heilongjiang Province, China; Research Assistant, Department of Civil and Structural Engineering of the Hong Kong Polytechnic University, Hung Hom, Kowloon, Hong Kong, zf88482001@hotmail.com

[2] Research Fellow, Department of Civil and Structural Engineering of the Hong Kong Polytechnic University, Hung Hom, Kowloon, Hong Kong

[3]Associate Professor, the Harbin Institute of Technology, Harbin, Heilongjiang Province, China, dongzejiao79@163.com

ABSTRACT: Carbon fiber is used as the additive for the intelligent asphalt concrete. The relationship of the fiber volume and the concrete resistivity, and the relationship of the resistivity and the applied pressure were studied. The conductivity of asphalt concrete incorporating with carbon fiber changes with the magnitude of the applied pressure. This special characteristic of the material might be useful in the road engineering in two areas: (1) when pavement of this material are under loading, the change of the pressure can be reflected by measuring the resistivity of the material. The supervisor could monitor the loads of vehicle anywhere in the road network without the trouble of embedding sensors in the pavement. (2) If there are some defects that are difficult to be discover by visual method appear on the road, the supervisor could find them at the first time. According to the result of this paper, the conductivity of the asphalt concrete increases with the volume of fiber. The change is particularly prominent when the fiber volume is between the two mutant levels (with fibers of 4%-6%).

INTRODUCTION

In the last few decades, researches on intelligent concrete focused on cement concrete, and few studies gave their attention to asphalt concrete [1]. Research on intelligent asphalt concrete stays just at the level of “smart”, but not “intelligent”. The smart material tells what happen in its structural integrity by the change of its characteristics. The intelligent material can lower the environmental impact to the material performance by adjusting some of its characteristics.

In 1968, the Federation of Airport Authority and Super Graphite Company added graphite into asphalt concrete. They believed that when graphite was added into

asphalt concrete, the material would have the capacity to conduct electricity and could convert electricity power to heat up the pavement and, hence, reduced problems of low temperature cracking. They intended to use this kind of technology on airport runway to reduce shrinkage cracking problem in winter. In the 1990's, large scale trials on the use of graphite asphalt concrete were conducted on highways and airport runways in several U.S. states. The first test road in Canada making use of the electrical conductive asphalt concrete was at the Rocha Spur Bridge. In year 2002, similar research work on the intelligent concrete asphalt was carried out at Wuhan University of Technology of China. They added carbon black and graphite to asphalt concrete to remove snow and ice deposited on pavements [3].

It is noted that a high level of graphite was required to fulfill its role as the conductive material in a pavement system. The structural performance of the graphite asphalt concrete decreased with the increase of graphite volume. In year 2000, researchers of the Harbin Institute of Technology in China added carbon fiber to concrete and successfully changed the material to a conductor from an insulator [2].

Research on asphalt concrete incorporating with carbon fiber was conducted by the author. In this paper, finding observed from the study is presented. The conductivity characteristics of the carbon fiber asphalt concrete are discussed. It includes two aspects: 1) The relationship to the carbon fiber volume and the asphalt concrete conductivity characteristics; 2) The relationship to the additional loading and the asphalt concrete conductivity characteristics.

MATERIALS AND SPECIMEN'S PREPARATION

Three sizes of carbon fiber, with length of 3mm, 6mm and 9mm, were used. The grade Pen.110 bitumen and the aggregate gradation of AC20 in accordance with Chinese standard were chosen [4].

The fiber volume is defined as the volume ratio of the binder in percentage:

$$Vol(\%) = \frac{mc \cdot \rho a}{ma \cdot \rho c} \times 100\% \qquad 2\text{-}1$$

m_c and m_a are the weight of the fiber and the binder. ρ_c and ρ_a are the density of the fiber and the binder.

The specimens are prepared as these steps:

1) Mixing aggregates and the fibers for 30s;
2) Adding binder and mixing for 60s;
3) Adding filler and mixing for another 60s:
4) Making the specimens and the size is 300mm*300mm*50mm;
5) Waiting for 48h and then insert pole bars and the distance is 27cm;
6) Put the specimens in a invariable temperature room whose temperature is 20℃ for at least 4h;
7) Measure the resistivity with Wheatstone Bridge.

EFFECT OF LOAD PRESSURE ON CONDUCTIVITY

The electrical resistivity of the asphalt concrete at the three fiber lengths and at the different volumes was measured. The relationship between the resistivity and the volume of fiber in a semi-logarithm plot is shown in Figure 3-1.

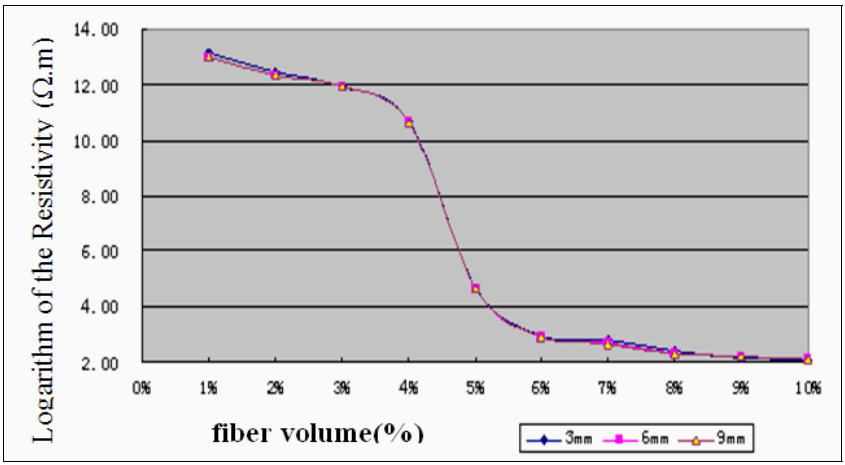

Figure 3-1: the relationship between resistivity and fiber volumes and lengths

The result indicates that before carbon fiber is added, the conductivity of the asphalt concrete is very low. Its resistivity is about $10^{13}\sim10^{15}\Omega$.m. When fiber is added, improvement in conductive capacity is obvious. There are two important volume fractions in the change of electricity resistivity. The first value, named "the down limit value", is at the location when the resistivity drops rapidly. It is about 4% of fiber volume. The second, named "the upper limit value", is at the location when the resistivity stops from mutating. The value is at about 6% of fiber volume. When the fiber volume is between the two limits values, the conductive capacity of the asphalt concrete improves significantly with the increase in fiber volume. When the volume is outside the limit, the improvement in conductive capacity reduces significantly.

The differences in the conductive capacity of the asphalt concrete brought by the length of the fiber are relatively small. In general, the longer is the fiber, the smaller is the resistivity. It is also noted that the difference in the conductivity between the asphalt concrete with 3mm fiber and 6mm fiber is large than those between 6mm fiber and 9mm fiber.

The following explanations are suggested to describe the phenomena:

(a) Leakage phenomenon: when the main component of a composite material is an insulator and the addition of the conductive fiber is very little, most fiber would remain as discrete elements, unable to connect to one another, and cannot effectively

conduct electricity through the composite material. The only conductive element in the composite material is moisture residual with its charged ions, which allow very limited electricity to leak through. This conductive process is termed “leakage phenomenon”.
(b) Conductivity of the material: When the fiber volume is plentiful, the fiber will connect to one another, and form many conductive pathways. These pathways allow electricity to get through the asphalt concrete efficiently.

EFFECT OF LOAD PRESSURE

The research results have revealed that when the fiber volume is between the two mutant limit values, resistivity of the asphalt concrete would be sensitive to the change of the fiber volume. For the study of the effect of pressure on the resistivity of asphalt concrete, 5.5% fiber volume was chosen. The relationship between the applied pressure and the electricity resistivity of the asphalt concrete is shown in figure 4-1.

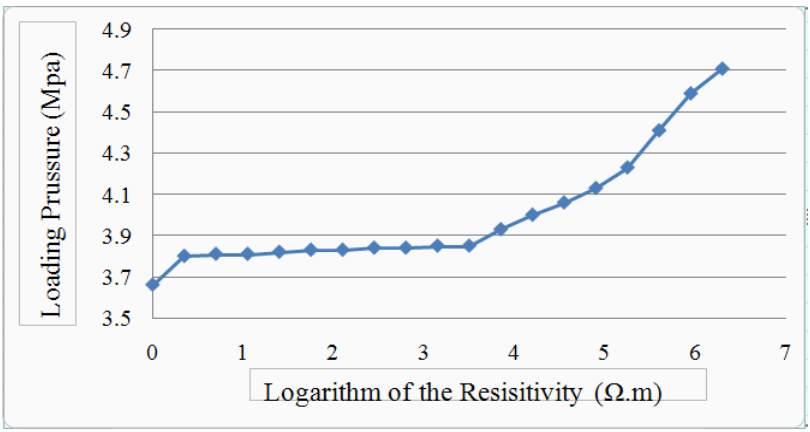

Figure 4-1: the relationship between load pressure and the asphalt concrete resistivity

As shown in figure 4-1, there is an immediate increase in the resistivity when external pressure is applied. It is followed by a steady increase in resistivity when the pressure is between 0.35MPa to 3.5MPa. In this region, the change of the resistivity is linear with the R2 of the linear relationship of 0.9989. When the pressure is beyond 3.5MPa, the resistivity accelerates, until the specimen is broken.

The following explanations are suggested to describe the behavior observed:

When the pressure is first loaded, the asphalt concrete is compressed. The asphalt concrete becomes denser with smaller voids, which diminish the conductive effect of the leakage phenomenon generated by any moisture in the asphalt concrete

structure. Therefore, there is an immediate increase in the resistivity of the asphalt concrete at the beginning of the loading.

Between the pressure of 0.35MPa and 3.5MPa, micro-cracks are developing in the asphalt concrete, which reduce the conductive capacity. With the pressure increasing, the internal stress and the related displacement between the aggregates in the asphalt concrete increase. The conductive network is gradually becoming less effective.

When the pressure is beyond 3.5MPa, the small micro-cracks expand to super micro-cracks. With the further increase of the pressure, the super micro-cracks merge to become small cracks and the small cracks into big cracks until the specimen is damaged. During the course of loading the asphalt concrete, the fibers are cut and drawn. The gap between the fibers grows. All these increase the resistivity of the asphalt concrete quickly.

CONCLUSIONS

(1) The conductivity asphalt concrete incorporating with carbon fiber changes with the magnitude of the applied pressure. This special characteristic of the material might be useful in road engineering in two areas: (a) Measure the Road loading. When pressure loading, by measuring the resistivity of the material, the computer could calculate the loading and the change of the pressure. Hence, axle loads of vehicle anywhere in a road network can be determined without the trouble of embedding sensors in the pavement. (b) When the material is overloaded or super micro-cracks have been developed in pavements, the defects, which are usually difficult to be discovered by visual inspection, can be revealed when high resistivity is noted. The technology can be used to monitor the health of the pavement in preventive maintenance.

(2) The length of the fiber has little effect on the conductivity of the asphalt concrete. However, the volume of the fiber plays a major role in changing the conductivity of the material.

(3) The conductivity of the asphalt concrete increases with the volume of fiber ascending. The change is particularly prominent when the fiber volume is between the two mutant levels (with fibers of 4%-6%).

(4) It is suggested that research is to be carried out to study the performance of the carbon fiber asphalt concrete and to study the application of the material on road pavement.

REFERENCES

Dai, Hongzhe; Wu, Sigang; and Wang, Wei (2004). "The research of the intelligent characters of the part steel reinforce concrete beam added carbon fiber. " the third China-Japan-U.S. Symposium on Structural Health Monitoring and Control, China.

Ministry of Communications of the People's Republic of China. (2004). "The Technical Specifications for Construction of Highway Asphalt Pavement-JTG F40-2004. " China.

Mo, Liantong. (2004). "MSc. Thesis: Preparation and research of electrically conductive asphalt concrete. " Wuhan University of Technology, China.

Zhang, Xiong; Xi, Zhizhen; Wang, Shengxian; and Yao, Wu. "The progress of the biomimetic self-heal concrete research." Concrete, China, 2001(3):10-13

Author Index

Page number refers to the first page of paper

An, Deok-Soon, 62

Cao, Wei-dong, 122
Chen, Bo-Ruei, 82
Chen, Chine-Ta, 32
Chen, Feicheng, 109
Chen, Hanli, 39
Chen, Hongxing, 55
Chen, Huaxin, 143
Chen, Shun-Hsing, 82
Cheng, Xiaoliang, 68
Chiang, Ziping, 32
Cui, Xin-zhuang, 122

Dong, Lin-lin, 122
Dong, Zejiao, 68, 165

Gao, Ying, 136

Harvey, John T., 158
He, Zhaoyi, 55
Huang, Wei-Hsing, 82
Huang, Xiaoming, 115, 136

Jönsthövel, T. B., 90
Ju Yun, Dong, 25

Kim, Seong-Min, 25
Kwon, Soo-Ahn, 62

Lan, Chao, 1
Li, Jiusu, 103
Li, Ming, 1
Li, Ningli, 143
Li, Tiehu, 143
Li, Y., 151
Li, Yuzhi, 47
Li, Zhenke, 47
Liao, Chi-Chou, 82
Lin, Du, 9
Lin, Jyh-Dong, 32
Liu, Shu-tang, 122
Liu, X., 90
Lu, Zhaofeng, 55

Mu, Hai-rui, 1

Nam, Jeong-Hee, 62

Park, Hee Beom, 25
Pi, Yuhui, 115

Qi, Xie, 109
Qi, Zhaohui, 136
Qian, Guoping, 96
Qin, Renjie, 47
Qin, Tao, 39

Rhee, Suk-Keun, 25

Scarpas, A., 90
Song, Jun-min, 1
Sung, Po-Hsun, 32

Tan, Yiqiu, 68
Tang, Li-min, 74
Tang, Ping-ying, 74
Tian, Xiaoge, 9

Vuik, C., 90

Wah, Cheung Lam, 165
Wei, Jian-guo, 129
Wu, C. Y., 151
Wu, JianLiang, 18
Wu, Luocheng, 18

Wu, Rongzong, 158
Wu, Wenbiao, 9

Yan, Kezhen, 18
Yuan, Jiang, 109

Zhang, Deng-pan, 74
Zhang, Honggang, 96
Zhang, Jinzhao, 18
Zhang, Jiupeng, 115, 136
Zhang, Zhengqi, 143
Zhao, Jian-san, 74
Zheng, Hao, 68
Zheng, Jianlong, 96, 129
Zhou, Liang, 109
Zhu, Feng, 165

Subject Index

Page number refers to the first page of paper

Aging, 143
Asphalt pavements, 1, 18, 47, 55, 68, 96, 109, 122, 129, 151
Asphalts, 115, 136, 143, 158, 165
Assessments, 1

Bridges, box girder, 151
Bridges, highway, 151
Bridges, steel, 151

China, 32, 39, 47
Concrete, 103, 158, 165
Concrete pavements, 9, 25, 55
Constitutive models, 90, 115
Coupling, 55
Cracking, 129, 158
Creep, 115, 136

Damage, 47, 115, 122
Deformation, 136
Dynamic loads, 25, 55
Dynamic response, 96

Fibers, 165
Financial management, 39
Finite element method, 151
Flexible pavements, 82
Fuzzy sets, 9

Infrastructure, 39

Korea, South, 62

Linear systems, 90

Load factors, 47, 96, 158

Maintenance, 9
Measurement, 82
Mixtures, 109, 115, 136, 143
Moisture, 109, 122

Neural networks, 1

Pavements, 18, 32, 62, 90, 136
Pore pressure, 122
Predictions, 74, 82, 136

Recycling, 103
Rehabilitation, 9
Risk management, 39
Roughness, 62

Settlement, 74
Simulation, 90
Stress, 129
Subgrades, 74

Taiwan, 82
Temperature effects, 68, 82, 143

United States, 32

Vehicles, 25, 55, 96
Viscoelasticity, 47

Warranties, 62
Weight, 32